

REGULARIZATIONS OF TWO-FOLD BIFURCATIONS IN PLANAR PIECEWISE SMOOTH SYSTEMS USING BLOWUP

K. ULDALL KRISTIANSEN AND S. J. HOGAN*

Abstract. We use blowup to study the regularization of codimension one two-fold singularities in planar piecewise smooth (PWS) dynamical systems. We focus on singular canards, pseudo-equilibria and limit cycles that can occur in the PWS system. Using the regularization of Sotomayor and Teixeira [30], we show rigorously how singular canards can persist and how the bifurcation of pseudo-equilibria is related to bifurcations of equilibria in the regularized system. We also show that PWS limit cycles are connected to Hopf bifurcations of the regularization. In addition, we show how regularization can create another type of limit cycle that does not appear to be present in the original PWS system. For both types of limit cycle, we show that the criticality of the Hopf bifurcation that gives rise to periodic orbits is strongly dependent on the precise form of the regularization. Finally, we analyse the limit cycles as locally unique families of periodic orbits of the regularization and connect them, when possible, to limit cycles of the PWS system. We illustrate our analysis with numerical simulations and show how the regularized system can undergo a canard explosion phenomenon.

Key words. Piecewise smooth systems, blowup, geometric singular perturbation theory, sliding bifurcations, canards, pseudo-equilibrium, limit cycles.

AMS subject classifications. 37G10, 34E15, 37M99

1. Introduction. Piecewise smooth (PWS) dynamical systems [15, 27] are of great significance in applications [8], ranging from problems in mechanics (friction, impact) and biology (genetic regulatory networks) to control engineering [32]. But, compared to smooth systems [16], the study of PWS systems is in its infancy. For example, notions of solution, trajectory, separatrix, topological equivalence and bifurcation, all need revision and extension [15]. Often PWS systems are used as caricatures of smooth systems [4, 28], especially if significant amounts of computation are expected. So one of the major challenges of PWS system theory is to see just how close the behaviour of a PWS system is to a suitable smooth system.

In this paper, we focus on PWS systems in the plane, of the form:

$$\dot{\mathbf{x}} = X^\pm(\mathbf{x}), \quad \mathbf{x} \in \Sigma_\pm \subset \mathbb{R}^2, \quad (1.1)$$

where the smooth vector fields X^\pm , defined on disjoint open regions Σ_\pm , are smoothly extendable to their common boundary Σ . The line Σ is called the *switching manifold* or *switching boundary*. The union $\Sigma_- \cup \Sigma_+$ covers the whole state space. When the normal components of the vector fields on either side of Σ are in *opposition*, a vector field needs to be defined *on* Σ . The precise choice is not unique and crucially depends on the nature of the problem under consideration. We adopt the widely-used Filippov convention [15], where a *sliding* vector field is defined on Σ . In this case, the dynamics is described as *sliding* and the PWS system (1.1), together with the sliding vector field, constitute a *Filippov system*. Such systems possess many phenomena that are not present in smooth systems; grazing and sliding bifurcations, period adding bifurcations and chattering are (almost) ubiquitous in and (virtually) unique to PWS systems.

Sotomayor and Teixeira [30] proposed a regularization of a planar PWS dynamical system, in which the switching manifold Σ is replaced by a boundary layer of width 2ϵ . Outside the boundary layer, the regularization agrees exactly with the PWS vector fields. Inside the boundary layer, a monotonic function is chosen such that the regularization is at least continuous everywhere. The regularization of PWS systems in \mathbb{R}^3 was considered by [26] and in \mathbb{R}^n by [24].

It is natural to ask whether bifurcations in PWS systems are close to bifurcations in a suitable smooth system. But for any regularization, there is a fundamental difficulty when dealing with bifurcations. Fenichel theory [12, 13, 14, 17], the main tool used to analyze regularization, requires hyperbolicity, which is lost at a PWS bifurcation. A widely used approach to deal with this loss of hyperbolicity is the *blowup method*, originally due to Dumortier and Roussarie [9, 10, 11], and subsequently developed by Krupa and Szmolyan [19] in the context of slow-fast systems.

*K. Uldall Kristiansen: Department of Applied Mathematics and Computer Science, Technical University of Denmark, 2800 Kgs. Lyngby, DK. S. J. Hogan: Department of Engineering Mathematics, University of Bristol, Bristol BS8 1UB, United Kingdom. S.J. Hogan wishes to thank both Danmarks Nationalbank and the Otto Mønstedts Fond for support. In addition, he is extremely grateful to Morten Brøns for hosting a very productive sabbatical at DTU, Lyngby, Denmark from January to September 2014.

Buzzi *et al.* [2] considered how different PWS phenomena¹ in the plane were affected by the regularization method of Sotomayor and Teixeira [30]. A similar study in \mathbb{R}^3 was carried out by Llibre *et al.* [23]. Regularization of PWS systems in \mathbb{R}^n was considered by Llibre *et al.* [24]. These three papers considered the case of one switching manifold separating two different smooth vector fields. Regularization in the case of two intersecting switching manifolds was considered by Llibre *et al.* [25], and in the case of surfaces of algebraic variety by Buzzi *et al.* [3]. Regularization of codimension one bifurcations in planar PWS systems was considered by De Carvalho and Tonon [6]. Common to all of these studies, however, is that they do not deal rigorously with the loss of hyperbolicity at a PWS bifurcation and hence they do not properly unfold the effect of the regularization.

Recently, Kristiansen and Hogan [18] successfully applied the blowup method of Krupa and Szmolyan [19] to study the regularization of both fold and two-fold singularities of PWS dynamical systems in \mathbb{R}^3 . For two-fold singularities, they showed that the regularized system only fully retains the features of the PWS singular canards when the sliding region does not include a full sector of singular canards. In particular, they showed that every locally unique singular canard persists the regularizing perturbation. For the case of a sector of singular canards, they showed that the regularized system contains a primary canard, provided a certain non-resonance condition holds and they provided numerical evidence for the existence of secondary canards near resonance. Other authors [29] have used asymptotic methods to analyze the regularization of a planar PWS fold bifurcation.

In this paper, we regularize planar codimension one two-fold singularities that occur as the result of collisions of folds (quadratic tangencies) in *both* X^- and X^+ . We seek to identify PWS bifurcations as smooth bifurcations through regularization. We will study the fate of singular canards, pseudo-equilibria and limit cycles that can occur in our PWS system. We illustrate our analytical results with numerical simulations and show how the regularized system can undergo a canard explosion phenomenon.

The paper is organized as follows. In section 2, we set up the problem, define the two-fold singularities we wish to regularize and present our PWS planar system in a normalized form such that the sliding regions retain their character under parameter variation. In section 3, we describe those properties of the PWS system that we wish to regularize, paying particular attention to singular canards, pseudo-equilibria and limit cycles. Then in section 4, we present a regularized version of our PWS system, using the approach of Sotomayor and Teixeira [30]. Before beginning our analysis, we collect together all our main results in section 5, giving the reader a concise summary of what is to come. In section 6, we carry out a blowup analysis [19] and show how singular canards persist the regularization. Our PWS system can also exhibit pseudo-equilibria, so in section 7, we consider how these unique PWS phenomena survive regularization. In section 8, we show how limit cycles that are present in the original PWS system behave when regularized. In addition, we show how regularization can create another type of limit cycle that does not appear to be present in the original PWS system. For both types of limit cycle, we show how that the criticality of the Hopf bifurcation that gives rise to periodic orbits is strongly dependent on the precise form of the regularization. Some numerical results are presented in section 9 to illustrate our analysis. Our conclusions are presented in section 10.

2. Preliminaries. In this section we set up the problem, define two-fold singularities and present our PWS planar system in a suitable normalized form. Let $\mathbf{x} = (x, y) \in \mathbb{R}^2$, $\mu \in \mathbb{R}$. Consider an open set $(\mathbf{x}, \mu) \in \mathcal{U} \times \mathcal{I}$ and a smooth function $f_\mu(\mathbf{x})$ having 0 as a regular value for all $\mu \in \mathcal{I}$. Then $\Sigma \subset \mathcal{U}$ defined by $\Sigma = f_\mu^{-1}(0)$ is a smooth $1D$ manifold. The manifold Σ is our switching boundary. It separates the set $\Sigma_+ = \{(x, y) \in \mathcal{U} | f_\mu(x, y) > 0\}$ from the set $\Sigma_- = \{(x, y) | f_\mu(x, y) < 0\}$. We introduce local coordinates so that $f_\mu(x, y) = y$ and so $\Sigma = \{(x, y) \in \mathcal{U} | y = 0\}$. From now on, we suppress the subscript μ .

We consider two smooth vector-fields X^+ and X^- that are smooth on $\overline{\Sigma}_+$ and $\overline{\Sigma}_-$, respectively, and define the PWS vector-field $X = (X^-, X^+)$ by

$$X(\mathbf{x}, \mu) = \begin{cases} X^-(\mathbf{x}, \mu) & \text{for } \mathbf{x} \in \Sigma_- \\ X^+(\mathbf{x}, \mu) & \text{for } \mathbf{x} \in \Sigma_+ \end{cases} \quad (2.1)$$

Then

- $\Sigma_{cr} \subset \Sigma$ is the *crossing region* where $(X^+ f(x, 0, \mu)(X^- f(x, 0, \mu)) = X_2^+(x, 0, \mu)X_2^-(x, 0, \mu) > 0$.

¹For example, they considered crossing, stable and unstable sliding, pseudo-saddle-nodes and two-folds.

• $\Sigma_{sl} \subset \Sigma$ is the *sliding region* where $(X^+f(x, 0, \mu))(X^-f(x, 0, \mu)) = X_2^+(x, 0, \mu)X_2^-(x, 0, \mu) < 0$. Here $X^\pm f(\cdot, \mu) = \nabla f \cdot X^\pm(\cdot, \mu)$ denotes the Lie-derivative of f along $X^\pm(\cdot, \mu)$. Since $f(x, y) = y$ in our coordinates we have that $X^\pm f = X_2^\pm$.

In the sliding region, the vector fields on either side of Σ_{sl} point either toward or away from Σ_{sl} . In this case, in order to have a solution to our system in forward or backward time, we need to define a vector field on Σ_{sl} . There are many possibilities, depending on the problem being considered. One of the most widely adopted definitions is the Filippov convention [15], in which the *sliding vector field* $X_{sl}(\mathbf{x}, \mu)$ is taken to be the convex combination of X^+ and X^- :

$$X_{sl}(\mathbf{x}, \mu) = \sigma X^+(\mathbf{x}, \mu) + (1 - \sigma)X^-(\mathbf{x}, \mu), \quad (2.2)$$

where $\sigma \in (0, 1)$ is such that $X_{sl}(\mathbf{x}, \mu)$ is tangent to Σ_{sl} . In this case,

$$\sigma = \frac{X^-f(x, 0, \mu)}{X^-f(x, 0, \mu) - X^+f(x, 0, \mu)}. \quad (2.3)$$

The sliding vector field $X_{sl}(\mathbf{x}, \mu)$ can have equilibria (*pseudo-equilibria*, or sometimes *quasi-equilibria* [15]). Unlike in smooth systems, it is possible for trajectories to reach these pseudo-equilibria in finite time. An orbit of a PWS system can be made up of a concatenation of arcs from Σ and Σ_\pm .

2.1. Two-fold singularities. The boundaries of Σ_{sl} and Σ_{cr} where $X^+f = X_2^+ = 0$ or $X^-f = X_2^- = 0$ are singularities called *tangencies*. The simplest tangency is the fold singularity, which is defined as follows.

DEFINITION 2.1. *A point $q \in \Sigma$ for $\mu \in \mathcal{I}$ is a fold singularity if*

$$X^+f(q, \mu) = 0, \quad X^+(X^+f)(q, \mu) \neq 0, \quad (2.4)$$

or if

$$X^-f(q, \mu) = 0, \quad X^-(X^-f)(q, \mu) \neq 0. \quad (2.5)$$

A fold singularity q with $X^\pm f(q, \mu) = 0$ is visible if

$$X^\pm(X^\pm f)(q, \mu) \geq 0, \quad (2.6)$$

and invisible if

$$X^\pm(X^\pm f)(q, \mu) \leq 0. \quad (2.7)$$

Note that, for μ sufficiently small, the inequalities in (2.4) and (2.5) are equivalent to the following

$$\partial_x X_2^+(q, 0)X_1^+(q, 0) \neq 0, \quad \partial_x X_2^-(q, 0)X_1^-(q, 0) \neq 0. \quad (2.8)$$

In this paper, we consider the case of the *two-fold* singularity, when there is a fold singularity in *both* X^\pm . In particular, we suppose that X^\pm have tangencies at $q^\pm = q^\pm(\mu) \in \Sigma$, respectively, which collide for $\mu = 0$ at $q = q^\pm(0)$ with non-zero velocity. Hence $(q^+ - q^-)'(0) \neq 0$.

DEFINITION 2.2. *We say that the two-fold singularity q is*

- visible if q^+ and q^- are both visible;
- visible-invisible if q^+ (q^-) is visible and q^- (q^+) is invisible;
- invisible if q^+ and q^- are both invisible.

The three different types of two-fold singularity are shown in Fig. 2.1. In the case of a single fold singularity, it is known that both the visible and invisible cases are structurally stable [15, p. 232]. The regularization of the visible case was studied in [29]. Filippov [15, Figs. 58, 59] also considered the case of a single *cusp* singularity, which can be either visible or invisible. The cusp singularity is known to be structurally unstable, bifurcating into two tangencies [15, Figs. 76, 77], which are on the *same* side of Σ . Kuznetsov *et al.* [22, Fig. 9] considered these bifurcations, which they label $DT_{1,2}$, together with the cases we consider here. But we feel that the cusp singularity is best left for future work, as part of the wider picture that includes cusp-fold and two-cusp singularities. The two-fold singularities that we consider are shown in

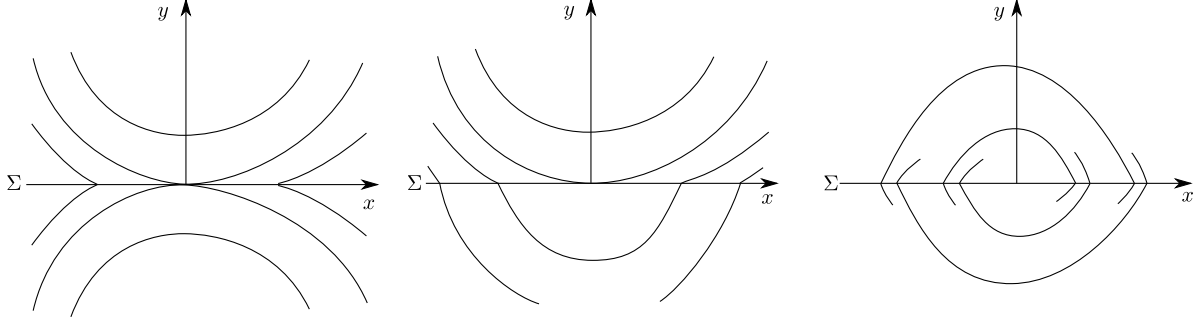


FIGURE 2.1. The three different types of two-fold singularity studied in this paper: (from L to R) visible, visible-invisible, invisible. Following Filippov [15], we show neither flow directions nor any sliding vector field.

Filippov [15, Figs. 64, 65, 67, 68], where they are termed *type 3 singularities*². There are 7 different generic cases. These were subsequently called $VV_{1,2}, VI_{1-3}, II_{1,2}$ by Kuznetsov *et al.* [22]; a notation that we will find useful to adopt. Other authors [2, 6] refer to two-fold singularities as *fold-fold singularities*, which can be *hyperbolic* (visible), *elliptic(al)* (invisible) or *parabolic* (visible-invisible). Two-folds in \mathbb{R}^3 were considered by the present authors in [18].

2.2. Normalized equations. In this section, we derive a normalized form for the equations near a two-fold singularity at $(q, \mu) = 0$ in \mathbb{R}^2 . By Taylor-expanding X^\pm , we have, for $y > 0$,

$$\begin{aligned}\dot{x} &= X_1^+(0) + \mathcal{O}(x + y + \mu), \\ \dot{y} &= \partial_y X_2^+(0)y + \partial_x X_2^+(0)x + \mathcal{O}(|(x, y)|^2 + \mu(x + y)),\end{aligned}$$

and, for $y < 0$,

$$\begin{aligned}\dot{x} &= X_1^-(0) + \mathcal{O}(x + y + \mu), \\ \dot{y} &= \partial_y X_2^-(0)y + \partial_x X_2^-(0)(x - \mu) + \mathcal{O}(|(x - \mu, y)|^2 + \mu(x - \mu + y)).\end{aligned}$$

We now introduce \tilde{x} and \tilde{t} where

$$\begin{aligned}x &= \sqrt{\left| \frac{X_1^+(0)}{\partial_y X_2^+(0)} \right|} \tilde{x}, \\ t &= \frac{\text{sign}(\partial_y X_2^+(0))}{\sqrt{|X_1^+(0)\partial_x X_2^+(0)|}} \tilde{t},\end{aligned}$$

which is well-defined, by virtue of (2.8). Then, on dropping tildes, we have, for $y > 0$:

$$\begin{aligned}\dot{x} &= \delta + \mathcal{O}(x + y + \mu), \\ \dot{y} &= x + \mathcal{O}(y + \mu x + x^2),\end{aligned}\tag{2.9}$$

and, for $y < 0$,

$$\begin{aligned}\dot{x} &= \alpha + \mathcal{O}(x + y + \mu), \\ \dot{y} &= -\beta(x - \mu) + \mathcal{O}(y + \mu(x - \mu) + (x - \mu)^2),\end{aligned}\tag{2.10}$$

where $\delta = \text{sign}(X_1^+(0)\partial_x X_2^+(0)) = \pm 1$. The constants

$$\begin{aligned}\alpha &= \text{sign}(\partial_y X_2^+(0)) \frac{X_1^-(0)}{|X_1^+(0)|}, \\ \beta &= \text{sign}(\partial_y X_2^+(0)) \frac{\partial_y X_2^-(0)}{\sqrt{|X_1^+(0)\partial_x X_2^+(0)|}},\end{aligned}$$

²Other type 3 singularities, shown in [15, Figs. 66, 69, 70, 71], have codimension greater than one (see [15, p. 239]). They include cusp-fold and two-cusp singularities.

are non-zero by (2.8). Later on, we will need to include higher order terms in our analysis. We introduce the following coefficients:

$$\zeta^\pm, \chi^\pm, \text{ and } \eta^\pm, \quad (2.11)$$

so that (2.9) becomes for $y > 0$:

$$\begin{aligned} \dot{x} &= \delta + \zeta^+ x + \mathcal{O}(x^2 + y + \mu), \\ \dot{y} &= x + \eta^+ x^2 + \chi^+ y + \mathcal{O}(xy + \mu(x + y) + x^3), \end{aligned} \quad (2.12)$$

and (2.10) becomes for $y < 0$:

$$\begin{aligned} \dot{x} &= \alpha + \zeta^- x + \mathcal{O}(x^2 + y + \mu), \\ \dot{y} &= -\beta(x - \mu) + \eta^-(x - \mu)^2 + \chi^- y + \mathcal{O}(xy + \mu y + \mu(x - \mu) + (x - \mu)^3). \end{aligned} \quad (2.13)$$

REMARK 2.3. *De Carvalho and Tonon [7] have given normal forms for codimension one planar PWS vector fields³. However, we need (2.9), (2.10) and (2.12), (2.13) in this form in order to unfold several of the phenomena studied in this paper.*

The sliding vector field (2.2) is given by

$$\begin{aligned} \dot{x} &= \sigma X_1^+(x, 0, \mu) + (1 - \sigma)X_1^-(x, 0, \mu), \\ \dot{y} &= 0, \end{aligned} \quad (2.14)$$

where σ , defined in (2.3), is given by

$$\sigma = \frac{(-\beta + \mathcal{O}(x + \mu))(x - \mu)}{(-\beta + \mathcal{O}(x + \mu))(x - \mu) - (1 + \mathcal{O}(x + \mu))x}. \quad (2.15)$$

The denominator in (2.15) is positive for *stable sliding* Σ_{sl}^- and negative for *unstable sliding* Σ_{sl}^+ . So if we multiply (2.14) by the modulus of this denominator, $|(-\beta + \mathcal{O}(x + \mu))(x - \mu) - (1 + \mathcal{O}(x + \mu))x|$, corresponding to a transformation of time, we find on $y = 0$ that, in Σ_{sl}^\pm ,

$$\begin{aligned} \dot{x} &= \pm(-\beta + \mathcal{O}(x + \mu))(x - \mu)(\delta + \mathcal{O}(x + \mu)) \pm (-1 + \mathcal{O}(x + \mu))x(\alpha + \mathcal{O}(x + \mu)), \\ \dot{y} &= 0, \end{aligned} \quad (2.16)$$

Equilibria of (2.16) are pseudo-equilibria, which we will study in section 3.2 below.

Within Σ_{sl}^- for $\mu = 0$ we find from (2.16) that

$$\dot{x} = (-\beta\delta + \mathcal{O}(x))x - (\alpha + \mathcal{O}(x))x = -(\beta\delta + \alpha)x + \mathcal{O}(x^2).$$

PROPOSITION 2.4. *The fold $q^+ = (0, 0)$ is visible (invisible) from above if $\delta = 1$ ($\delta = -1$), whereas the fold $q^- = (\mu, 0)$ is visible (invisible) from below if $\alpha\beta > 0$ ($\alpha\beta < 0$). Hence the two-fold $q = (0, 0)$ for $\mu = 0$ is*

- visible if $\delta = 1$ and $\alpha\beta > 0$;
- visible-invisible if $\delta = 1$ ($\delta = -1$) and $\alpha\beta < 0$ ($\alpha\beta > 0$);
- invisible if $\delta = -1$ and $\alpha\beta < 0$.

We also have that

$$\Sigma_{sl} : \beta x(x - \mu) > 0, \quad (2.17)$$

$$\Sigma_{cr} : \beta x(x - \mu) < 0, \quad (2.18)$$

for x and μ sufficiently small. The subset $\Sigma_{sl}^- = \Sigma_{sl} \cap \{x < 0\}$ of Σ_{sl} is the stable sliding region whereas the subset $\Sigma_{sl}^+ = \Sigma_{sl} \cap \{x > 0\}$ of Σ_{sl} is the unstable sliding region. The subset $\Sigma_{cr}^- = \Sigma_{cr} \cap \{x < 0\}$ of Σ_{cr} is crossing downwards whereas the subset $\Sigma_{cr}^+ = \Sigma_{cr} \cap \{x > 0\}$ of Σ_{cr} is crossing upwards.

³De Carvalho and Tonon (private communication) have indicated that they intend to publish a corrigendum to this paper, since their normal forms, as currently stated [7], can not distinguish between all the different planar PWS singularities.

Proof. These statements follow from simple computations. For example, to obtain the last part, we note that

$$X_2^+(x, 0, \mu)X_2^-(x, 0, \mu) = (1 + \mathcal{O}(x + \mu))x(-\beta + \mathcal{O}(x + \mu))(x - \mu),$$

and use the definition of Σ_{sl} in section 2 together with (2.8). \square

Henceforth, in the visible-invisible case, without loss of generality, we will focus on the case $\delta = 1$, $\alpha\beta < 0$ so that the fold $q^+ = (0, 0)$ is visible from above and $q^- = (\mu, 0)$ is invisible from below (as in Fig. 2.1).

Since we perform a local analysis, we restrict attention to x and μ sufficiently small so that statements (2.17) and (2.18) in Proposition 2.4, about Σ_{sl} and Σ_{cr} , apply. The advantage of the form (2.9) and (2.10) of the normalized equations is that the sliding regions Σ_{sl}^\pm retain their character (stable or unstable) under parameter variation.

For later convenience we introduce the parameter Ω defined by

$$\Omega \equiv \beta\delta + \alpha.$$

To conclude this section, we state the following assumptions, which we make throughout the rest of the paper.

ASSUMPTION 1. $\delta \neq 0$.

ASSUMPTION 2. $\alpha\beta \neq 0$.

ASSUMPTION 3. $\Omega \neq 0$.

Assumption 1 and Assumption 2 are the normalized form of (2.8), when combined with (2.9) and (2.10). In fact we have already set $\delta = \pm 1$. The significance of Assumption 3 will be explained in Remark 3.1 below.

3. Analysis of the PWS system. In this section, we analyze the planar PWS system (2.9) and (2.10), together with (2.14) and (2.15) whenever we have sliding. We pay particular attention to singular canards, pseudo-equilibria and limit cycles that can occur in our system. The fold at $q^+ = (0, 0)$ is fixed, whereas the fold at $q^- = (\mu, 0)$ varies with μ such that the two-fold at $\mu = 0$ bifurcates. Both pseudo-equilibria and sliding sections can appear, disappear or change character depending on whether q^\pm are visible or invisible. In addition, some of the two-folds at $\mu = 0$ possess singular canards, which disappear for $\mu \neq 0$, and at least one two-fold can have a limit cycle.

3.1. Singular canards. Trajectories can go from the attracting sliding region Σ_{sl}^- to the repelling sliding region Σ_{sl}^+ , or vice versa, for $\mu = 0$. These trajectories, which we call *singular canards* [18], resemble canards in slow-fast systems [1]. A singular canard is called a *vrai* singular canard if it goes from the attracting sliding region Σ_{sl}^- to the repelling sliding region Σ_{sl}^+ in forward time. Singular canards that go from the repelling sliding region Σ_{sl}^+ to the attracting sliding region Σ_{sl}^- are called *faux* singular canards. Singular canards can only exist for $\mu = 0$ and when there is sliding in both $x < 0$ and $x > 0$. From (2.17), we see that singular canards can only exist for $\beta > 0$.

For the existence of singular canards in our PWS system, it is important to note that, in terms of the original time used in (2.14), the two-fold on Σ_{sl} can be reached in finite time. A simple calculation using L'Hôpital's rule shows that on Σ_{sl} , for $\mu = 0$,

$$\lim_{x \rightarrow 0} \dot{x} = (1 + \beta)^{-1}\Omega. \quad (3.1)$$

There is no singularity at $1 + \beta = 0$ since we need $\beta > 0$ for sliding. So, by Assumption 3, we have a finite value of \dot{x} on Σ_{sl} for $x \rightarrow 0$ when $\mu = 0$. Hence it is possible to pass in finite time through $x = 0$ (the point separating attracting and repelling sliding regions, if they exist) at a two-fold.

REMARK 3.1. *The case $\Omega = 0$ is degenerate, since $\lim_{x \rightarrow 0} \dot{x}$ vanishes. Geometrically this case corresponds to the linearized trajectories of X^\pm having the same gradient on Σ_{sl} . We shall not consider this case further (cf. Assumption 3 above).*

Hence by (3.1) we conclude that singular canards exist in our PWS system. To decide whether they are *vrai* singular canards or *faux* singular canards, we need to consider the sign of \dot{x} in (3.1). We collect the results in the following proposition:

PROPOSITION 3.2. *Singular canards in our PWS system exist if and only if $\beta > 0$. If $\Omega > 0$ ($\Omega < 0$) then the singular canard is a *vrai* (*faux*) singular canard.*

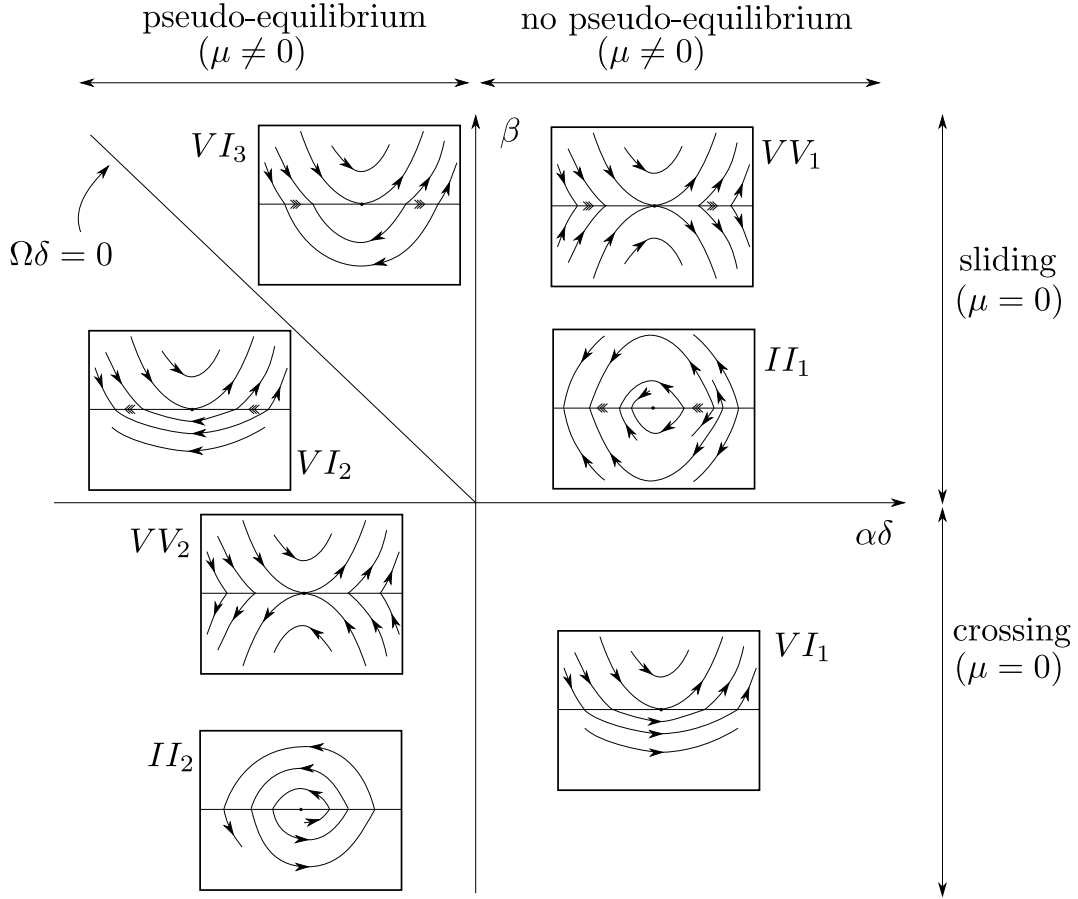


FIGURE 3.1. The different types of two-fold singularities. Sliding is indicated by triple headed arrows. Cases $II_{1,2}$ occur for $\delta = -1$, the other cases for $\delta = 1$.

One of the main objectives of this work is to establish persistence results of these singular canards under regularization. We will focus primarily on the persistence of *vrai* singular canards.

The different types of two-fold, together with their flow directions and any sliding regions are shown in Fig. 3.1. Note that the visible two-folds $VV_{1,2}$ and the visible-invisible two-folds VI_{1-3} exist for $\delta = 1$, whereas the invisible two-folds $II_{1,2}$ exist for $\delta = -1$.

3.2. Pseudo-equilibria. As mentioned in section 2, the sliding vector field $X_{sl}(\mathbf{x}, \mu)$ itself can have equilibria, called *pseudo-equilibria*⁴. These pseudo-equilibria are not necessarily equilibria of $X^\pm(\mathbf{x}, \mu)$. Instead they correspond to the case when $X^\pm(\mathbf{x}, \mu)$ on Σ_{sl} are linearly dependent. Filippov ([15], p. 218) terms them *type 1* singularities. They comprise three distinct topological classes; a pseudo-node, a pseudo-saddle and a pseudo-saddle-node. The following proposition describes the existence of pseudo-equilibria in (2.16).

PROPOSITION 3.3. *If*

$$\alpha\delta < 0, \tag{3.2}$$

⁴Hence there can be no pseudo-equilibria without a sliding vector field.

then, for μ sufficiently small, there exists a pseudo-equilibrium of (2.16) at $(x, y) = (x_{ps}, 0)$, where

$$x_{ps} = \beta\delta\Omega^{-1}\mu + \mathcal{O}(\mu^2). \quad (3.3)$$

Also if $\beta\delta\Omega^{-1}\mu < 0$ then $(x_{ps}, 0) \in \Sigma_{sl}^-$ and

- for $\Omega < 0$: $(x_{ps}, 0)$ is a pseudo-saddle with local repelling manifold coinciding with Σ_{sl}^- ;
- for $\Omega > 0$: $(x_{ps}, 0)$ is an attracting pseudo-node.

If $\beta\delta\Omega^{-1}\mu > 0$ then $(x_{ps}, 0) \in \Sigma_{sl}^+$ and

- for $\Omega < 0$: $(x_{ps}, 0)$ is a pseudo-saddle with local attracting manifold coinciding with Σ_{sl}^+ ;
- for $\Omega > 0$: $(x_{ps}, 0)$ is a repelling pseudo-node.

If $\alpha\delta > 0$, then $(x_{ps}, 0)$ is not a pseudo-equilibrium.

REMARK 3.4. From Assumption 3 we do not consider pseudo-saddle-nodes in our system.

Proof. To find pseudo-equilibria, we set $\dot{x} = 0$ in (2.16) to get

$$(-\beta\delta + \mathcal{O}(\mu + x))x + (-\alpha + \mathcal{O}(\mu + x))x - (-\beta\delta + \mathcal{O}(\mu))\mu = 0,$$

or

$$(1 + \beta^{-1}\delta\alpha + \mathcal{O}(\mu + x))x = (1 + \mathcal{O}(\mu))\mu.$$

Here we have used that $\delta = \pm 1$. Note that

$$1 + \beta^{-1}\delta\alpha = \beta^{-1}\delta^{-1}\Omega \neq 0,$$

by assumption. We can therefore solve this equation by the implicit function theorem to obtain

$$x = x_{ps} \equiv \beta\delta\Omega^{-1}\mu + \mathcal{O}(\mu^2).$$

This is a pseudo-equilibrium if and only if $(x_{ps}, 0) \in \Sigma_{sl}$. We determine Σ_{sl} as follows. Consider first $\beta > 0$. Then we have

$$\begin{aligned} \Sigma_{sl} : x < 0 \quad \text{or} \quad x > \mu \quad \text{for} \quad \mu > 0, \\ x = 0 \quad \text{for} \quad \mu = 0, \\ x < \mu \quad \text{or} \quad x > 0 \quad \text{for} \quad \mu < 0. \end{aligned}$$

Thus $\Sigma_{sl} : \text{sign}(\mu)x \notin (0, |\mu|)$. Then since

$$\text{sign}(\mu)x_{ps} = \beta\delta\Omega^{-1}|\mu| + \mathcal{O}(\mu^2),$$

we conclude that $(x_{ps}, 0) \in \Sigma_{sl}$ for μ sufficiently small, provided $\beta\delta\Omega^{-1} = (1 + \beta^{-1}\delta\alpha)^{-1} \notin (0, 1)$. Since $\beta > 0$, this condition is equivalent to $\alpha\delta < 0$. If, on the other hand $\beta\delta\Omega^{-1} = (1 + \beta^{-1}\delta\alpha)^{-1} \in (0, 1)$, then $\alpha\delta > 0$, for $\beta > 0$ and so $(x_{ps}, 0)$ is not a pseudo-equilibrium.

Next consider $\beta < 0$. Then

$$\Sigma_{sl} : \text{sign}(\mu)x \in (0, |\mu|).$$

Hence $(x_{ps}, 0) \in \Sigma_{sl}$ for $\mu \neq 0$ sufficiently small, provided $\beta\delta\Omega^{-1} = (1 + \beta^{-1}\delta\alpha)^{-1} \in (0, 1)$. For $\beta < 0$, this is equivalent to $\alpha\delta < 0$. If, on the other hand $\beta\delta\Omega^{-1} = (1 + \beta^{-1}\delta\alpha)^{-1} \notin (0, 1)$, then $\alpha\delta > 0$, for $\beta < 0$ and so $(x_{ps}, 0)$ is not a pseudo-equilibrium.

We conclude that $(x_{ps}, 0)$ is a pseudo-equilibrium, where x_{ps} is defined in (3.3), provided (3.2) holds.

If $x_{ps} < 0$ then $(x_{ps}, 0) \in \Sigma_{sl}^-$, the region of stable sliding, and if $x_{ps} > 0$ then $(x_{ps}, 0) \in \Sigma_{sl}^+$, the region of unstable sliding (see Proposition 2.4). Combining this with the linearization of (2.16) about $(x_{ps}, 0)$ gives the statements about stability. \square

These results are summarized in Fig. 3.2. As mentioned earlier, two-fold singularities occur in (2.9) and (2.10) when $\mu = 0$. From Proposition 3.3, it follows that the two-fold singularity can be accompanied by significant changes in the nature of pseudo-equilibria around $\mu = 0$. For example, if $\Omega < 0$ then x_{ps} is

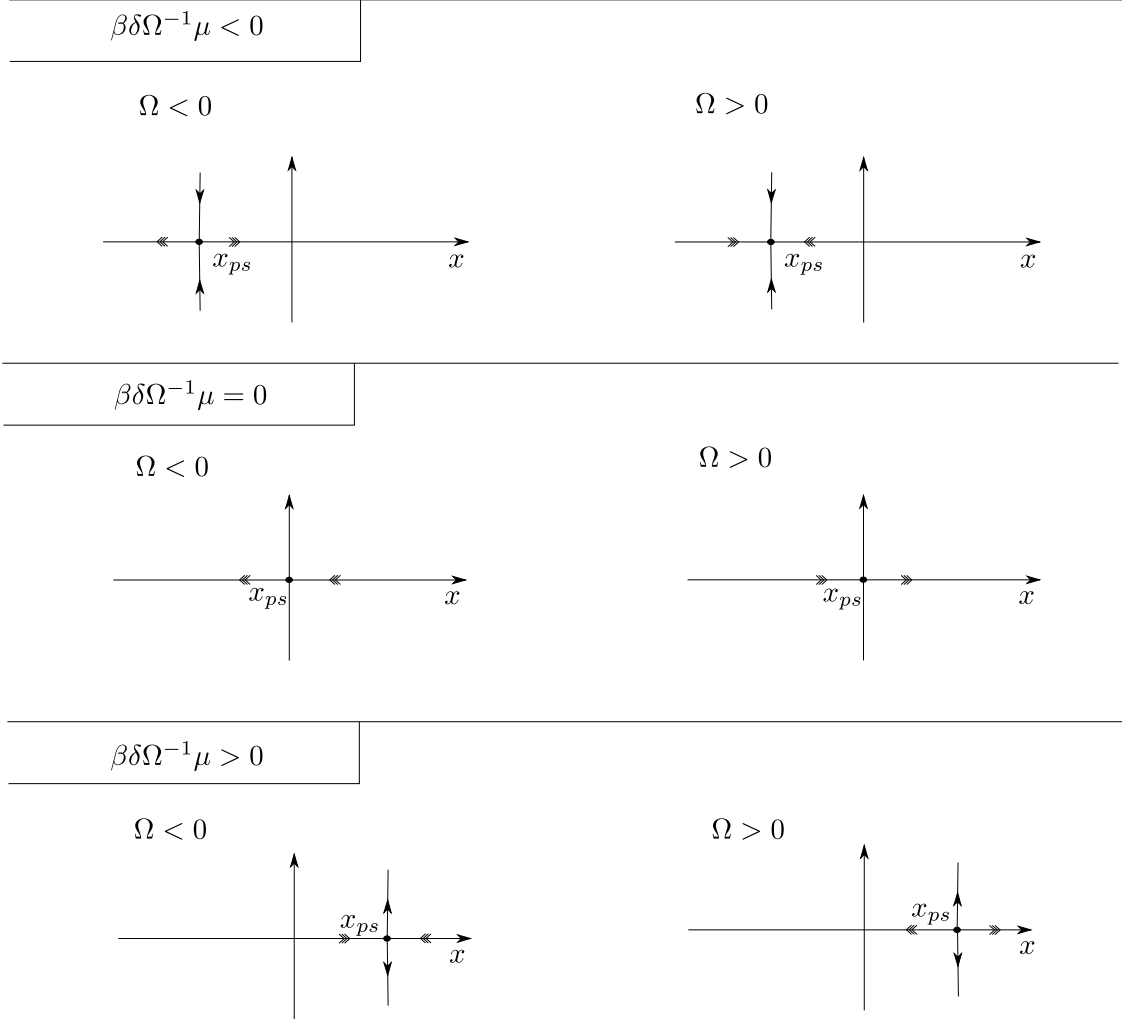


FIGURE 3.2. Results of Proposition 3.3. Here $\alpha\delta < 0$ and $x_{ps} = \beta\delta\Omega^{-1}\mu + \mathcal{O}(\mu^2)$.

a pseudo-saddle for all $\mu \neq 0$. The difference between $\mu > 0$ and $\mu < 0$ is, where $\beta\delta\Omega^{-1}\mu < 0$, the pseudo-saddle is in Σ_{sl}^- , which coincides with the associated repelling manifold of x_{ps} . But, where $\beta\delta\Omega^{-1}\mu > 0$, the pseudo-saddle is in Σ_{sl}^+ , which coincides with the associated attracting manifold of x_{ps} . Hence the attracting and repelling directions “switch” on passage through the two-fold at $\mu = 0$. We can see this behaviour in [22, Fig. 10], where Σ_{sl} is the attracting manifold of the pseudo-saddle of VV_2 on one side of the two-fold, whereas it is the repelling manifold on the other. Similarly, when $\Omega > 0$ a pseudo-equilibrium goes from being attracting on one side to repelling on the other side. We see this behaviour for example in [22, Fig. 11], for the VI_3 two-fold, where a repelling pseudo-node becomes an attracting pseudo-node.

Another main objective of this paper is to understand how the behaviour of these pseudo-equilibria is modified when our governing equations are regularized.

3.3. Limit cycles. A further phenomenon in the two-fold singularity is the existence of limit cycles. For our PWS system, it is clear from Fig. 3.1 (see also [22, Fig. 12]) that (local) limit cycles can occur in the invisible case II_2 where:

$$\delta = -1, \quad \alpha > 0, \quad \beta < 0. \quad (3.4)$$

To study periodic orbits in this case, one can introduce a Poincaré map P_0 which takes $\{(x, 0) | x > 0\}$ into $\{(x, 0) | x > \mu\}$ under the forward flow of X^+ and X^- (see Fig. 3.3 and [15, p. 236]). The map P_0 is composed of $\sigma_0^+ : x_0 \mapsto x_1$, the mapping from $(x_0, 0)$, $x_0 > 0$, to $(x_1(x_0), 0)$, $x_1(x_0) < 0$, under the forward flow of

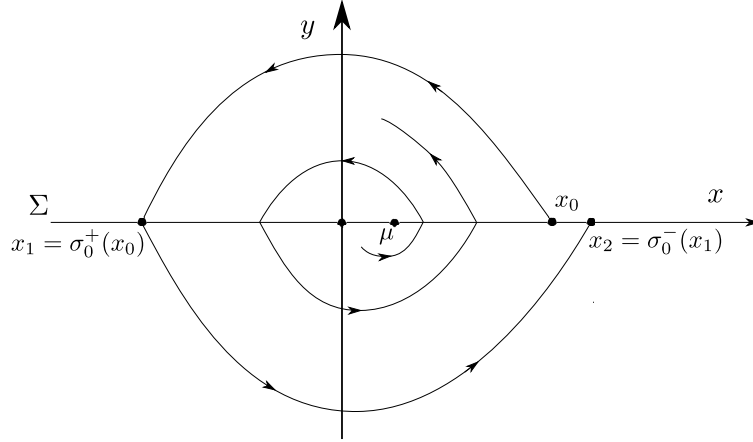


FIGURE 3.3. The Poincaré map $P_0 = \sigma_0^- \circ \sigma_0^+$ associated with the invisible two-fold singularity II_2 , where $\delta = -1$, $\alpha > 0$ and $\beta < 0$.

X^+ , and $\sigma_0^- : x_1 \mapsto x_2$, the mapping from $(x_1, 0)$, $x_1 < \mu$, to $(x_2(x_1), 0)$, $x_2(x_1) > \mu$, under the forward flow of X^- . Clearly P_0 is only defined for those x_0 for which $x_1 < \mu$. For X^- to map $x_1 < \mu$ into $x_2 > \mu$ we need $\dot{x} = \alpha + \mathcal{O}(x + y + \mu) > 0$. Therefore $\alpha > 0$. Hence we have the following lemma.

LEMMA 3.5. Consider (3.4). Then

$$\begin{aligned}\sigma_0^+(x_0) &= -x_0 + A^+ x_0^2 + \mathcal{O}(x_0(\mu + x_0^2)), \\ \sigma_0^-(x_1) &= -x_1 + 2\mu + A^- x_1^2 + \mathcal{O}(x_1(\mu + x_1^2)),\end{aligned}$$

where

$$\begin{aligned}A^- &= \frac{2}{3\alpha\beta}(\alpha\eta^- + \beta(\zeta^- + \chi^-)), \\ A^+ &= -\frac{2}{3}(\eta^+ + \zeta^+ + \chi^+).\end{aligned}\tag{3.5}$$

Proof. See [15, p. 236]. \square

The Poincaré mapping $P_0 = \sigma_0^- \circ \sigma_0^+$ therefore takes the following form:

$$P_0(x_0) = \sigma_0^-(\sigma_0^+(x_0)) = x_0 + 2\mu + (A^- - A^+)x_0^2 + \mathcal{O}(x_0^3 + \mu x_0),\tag{3.6}$$

for those x_0 which satisfy the inequality:

$$\sigma_0^+(x_0) = -x_0 + A^+ x_0^2 + \mathcal{O}(x_0^3 + x_0\mu) < \mu.\tag{3.7}$$

PROPOSITION 3.6. Consider (3.4) and suppose that

$$\Delta_{II_2} \equiv A^- - A^+ = \frac{2}{3\alpha\beta}(\alpha(\eta^- + \beta\eta^+) + \beta(\zeta^- + \chi^- + \alpha(\zeta^+ + \chi^+))),\tag{3.8}$$

is non-zero. Then, for $\mu\Delta_{II_2}^{-1} < 0$ sufficiently small, the PWS system has a family of periodic orbits. These periodic orbits correspond to fixed points of P_0 of the following form

$$x_0(\mu) = \sqrt{-2\mu\Delta_{II_2}^{-1}} + \mathcal{O}(\mu).\tag{3.9}$$

The periodic orbits are attracting for $\Delta_{II_2} < 0$ and repelling for $\Delta_{II_2} > 0$.

Proof. We obtain (3.9) by solving the equation $P_0(x_0) = x_0$ for $x_0 > 0$ using the implicit function theorem. For μ small, $x_0(\mu)$ is positive and satisfies the inequality (3.7). For stability we compute the derivative of (3.6) to get:

$$P_0'(x_0(\mu)) = 1 + 2\Delta_{II_2}x_0(\mu) + \mathcal{O}(\mu).$$

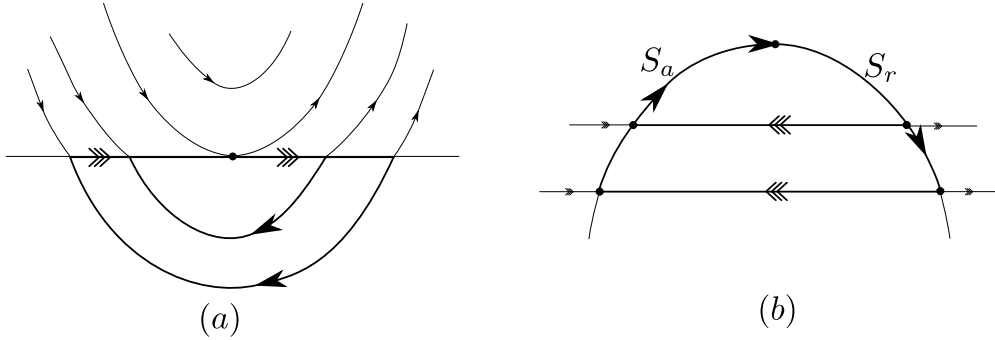


FIGURE 3.4. In (a): the VI_3 PWS two-fold bifurcation and in (b): the classical curved critical manifold e.g. appearing in the slow-fast van der Pol system. In (b) S_a and S_r denote the attracting and repelling part of the critical manifold. Note also the different use of triple-headed arrows. In (a) triple-headed arrows are used to indicate sliding whereas they in (b) are used to indicate fast orbit segments described by a set of layer equations. The thick curves illustrate singular closed curves which for case (a) will become periodic orbits upon regularization.

If $\Delta_{II_2} < 0$ ($\Delta_{II_2} > 0$) then $0 < P'(0) < 1$ ($P'(0) > 1$) for μ sufficiently small. The result follows. \square

Finally in this subsection, we note that the visible-invisible case VI_3 does not appear to have limit cycles. However, by straightening out the flow within Σ^- , so that Σ becomes curved and quadratic at the fold, the VI_3 case clearly resembles the classical slow-fast curved critical manifold with *singular cycles*. This similarity can be seen in Fig. 3.4 where we illustrate (a) the VI_3 two-fold and (b) the slow-fast equivalent as it appears, for example, in the van der Pol system (see also [21, Fig. 5]). There are two singular canard cycles in Fig. 3.4 (b), shown as thick curves, each composed of fast segments (with triple-headed arrows) and slow segments on the curved slow manifold. For ϵ sufficiently small, this slow-fast system is known to produce a *canard explosion phenomenon* [21], in which the singular cycles become limits of a family of rapidly increasing periodic orbits as $\epsilon \rightarrow 0$. However, when considering Fig. 3.4, it is important to highlight that there is no time scale separation in the PWS system. Nevertheless, we shall see that the *regularized* PWS system possesses a hidden slow-fast structure near the discontinuity set. This will allow us identify the *singular cycles* in Fig. 3.4 (a) as limits of periodic orbits of the regularization, and hence strengthen the connection between (a) and (b) further. The singular cycles in Fig. 3.4 (a) are also illustrated as thick curves, but in comparison to the cycles in (b), they are composed of an orbit segment of X^- , within Σ^- , and a sliding segment on Σ .

Another objective of this paper is to understand the existence of limit cycles under regularization. Further details are presented in section 8.

3.4. Summary of two-fold properties. We conclude this section with Table 3.1 which summarizes properties of the seven two-folds, for future reference.

Table 3.1: 1: type of two-fold singularity [visible (VV), visible-invisible (VI) and invisible (II), following [22]]. 2: value of δ . 3: sign of α . 4: sign of β . 5: sign of Ω . 6: type of singular canard (x=no canard). 7: type of pseudo-equilibrium after bifurcation (PS=pseudo-saddle, PN=pseudo-node, x=no pseudo-equilibrium). 8: possibility of limit cycle.

1	2	3	4	5	6	7	8
Two-fold type	δ	α	β	Ω	Singular canard	Pseudo-equilibrium	Limit cycle
VV_1	1	+	+	+	vrai	x	no
VV_2	1	-	-	-	x	PS	no
VI_1	1	+	-	\pm	x	x	no
VI_2	1	-	+	-	faux	PS	no

VI_3	1	-	+	+	vrai	PN	- ⁵
II_1	-1	-	+	-	faux	x	no
II_2	-1	+	-	+	x	PN	yes

4. Regularization. It is natural to ask how the results in section 3 are affected by regularization. For example, there is the question of the persistence of the singular canards (section 3.1). Then, of course, pseudo-equilibria (section 3.2) can not exist in a smooth system, so we will need to look at the existence and behaviour of equilibria in the regularization. Finally there is the need to understand both the fate of the limit cycles (section 3.3) in the invisible two-fold II_2 under regularization and the possibility of other limit cycles which may appear in the regularized system.

There is a number of ways that the original PWS vector field $X = (X^-, X^+)$ can be regularized. We follow the approach of Sotomayor and Teixeira [30]. We define a C^k -function ($1 \leq k \leq \infty$) $\phi(s)$ which satisfies:

$$\phi(s) = \begin{cases} 1 & \text{for } s \geq 1, \\ \in (-1, 1) & \text{for } s \in (-1, 1), \\ -1 & \text{for } s \leq -1, \end{cases} \quad (4.1)$$

where

$$\phi'(s) > 0 \quad \text{within } s \in (-1, 1). \quad (4.2)$$

Then for $\epsilon > 0$, the regularized vector-field $X_\epsilon(\mathbf{x}, \mu)$ is then given by

$$X_\epsilon(\mathbf{x}, \mu) = \frac{1}{2}X^+(\mathbf{x}, \mu)(1 + \phi(\epsilon^{-1}y)) + \frac{1}{2}X^-(\mathbf{x}, \mu)(1 - \phi(\epsilon^{-1}y)). \quad (4.3)$$

Note that

$$X_\epsilon(\mathbf{x}, \mu) = X^\pm(\mathbf{x}, \mu) \quad \text{for } y \gtrless \pm\epsilon. \quad (4.4)$$

The region $y \in (-\epsilon, \epsilon)$ is the *region of regularization*. The system (4.3) has a hidden slow-fast structure which is unfolded by the re-scaling (see also [29])

$$\hat{y} = \epsilon^{-1}y. \quad (4.5)$$

In terms of this re-scaling the region of regularization becomes $\hat{y} \in (-1, 1)$. Then, using (2.9) and (2.10), the regularized system (4.3) becomes

$$\begin{aligned} \dot{x} &= \frac{1}{2}((\delta + \mathcal{O}(x + \mu + \epsilon\hat{y}))(1 + \phi(\hat{y})) + (\alpha + \mathcal{O}(x + \mu + \epsilon\hat{y}))(1 - \phi(\hat{y}))), \\ \epsilon\dot{\hat{y}} &= \frac{1}{2}((x + \mathcal{O}(\mu x + x^2 + \epsilon\hat{y}))(1 + \phi(\hat{y})) + (-\beta(x - \mu) + \mathcal{O}(\mu(x - \mu) + (x - \mu)^2 + \epsilon\hat{y}))(1 - \phi(\hat{y}))). \end{aligned} \quad (4.6)$$

This is the *slow system* of a slow-fast system. The \hat{y} variable is fast with $\mathcal{O}(\epsilon^{-1})$ velocities and x is the slow variable with $\mathcal{O}(1)$ velocities. The limit $\epsilon = 0$:

$$\begin{aligned} \dot{x} &= \frac{1}{2}((\delta + \mathcal{O}(x + \mu))(1 + \phi(\hat{y})) + (\alpha + \mathcal{O}(x + \mu))(1 - \phi(\hat{y}))), \\ 0 &= \frac{1}{2}((x + \mathcal{O}(\mu x + x^2))(1 + \phi(\hat{y})) + (-\beta(x - \mu) + \mathcal{O}(\mu(x - \mu) + (x - \mu)^2))(1 - \phi(\hat{y}))). \end{aligned} \quad (4.7)$$

is called the *reduced problem*. When we re-scale time according to $\tau = \frac{1}{2\epsilon}t$, (4.6) becomes:

$$\begin{aligned} x' &= \epsilon((\delta + \mathcal{O}(x + \mu + \epsilon\hat{y}))(1 + \phi(\hat{y})) + (\alpha + \mathcal{O}(x + \mu + \epsilon\hat{y}))(1 - \phi(\hat{y}))), \\ \hat{y}' &= (x + \mathcal{O}(\mu x + x^2 + \epsilon\hat{y}))(1 + \phi(\hat{y})) + (-\beta(x - \mu) + \mathcal{O}(\mu(x - \mu) + (x - \mu)^2 + \epsilon\hat{y}))(1 - \phi(\hat{y})), \end{aligned} \quad (4.8)$$

⁵The regularized two-fold VI_3 does possess a limit cycle. See Theorem 8.8.

with $(\cdot)' = \frac{d}{d\tau}$. This is the *fast system* of a slow-fast system. The limit $\epsilon = 0$:

$$\begin{aligned} x' &= 0, \\ \hat{y}' &= (x + \mathcal{O}(\mu x + x^2))(1 + \phi(\hat{y})) + (-\beta(x - \mu) + \mathcal{O}(\mu(x - \mu) + (x - \mu)^2))(1 - \phi(\hat{y})). \end{aligned} \quad (4.9)$$

is called the *layer problem*. Time τ is the *fast time* and time t is the *slow time*.

REMARK 4.1. *The re-scaling used in (4.5) is necessary to identify the slow-fast structure hidden in (4.3). It is not due to loss of hyperbolicity and so the use of (4.5) is different from the scaling used later in section 6 in connection with the blowup of a nonhyperbolic line. We use (4.5) to cover $\hat{y} \in (-1, 1)$. Outside this region we will use (4.4) and the exact PWS analysis to describe the dynamics.*

In [23, 24, 25], the re-scaling (4.5) is replaced by a transformation $y = r\bar{y}$, $\epsilon = r\bar{\epsilon}$, $(\bar{y}, \bar{\epsilon}) \in S^1$, making it possible to illustrate, in one diagram, the dynamics of X^\pm outside the region of regularization and the slow-fast dynamics within (by inserting the cylinder $(x, (\bar{y}, \bar{\epsilon})) \in \mathbb{R} \times S^1$ at $y = 0$). However it does nothing to address any loss of hyperbolicity that may occur.

In this paper, we apply and extend Fenichel theory [12, 13, 14, 17] of singular perturbations to study these regularized equations (4.6)-(4.9), allowing us to go from a description of the singular limit $\epsilon = 0$ to a description for $\epsilon > 0$. This approach has the advantage that it is geometric so, for example, we are able to solve persistence problems by invoking transversality. It will also be important to identify the singular limit $\epsilon = 0$ with the original PWS system.

The key to the subsequent analysis in this paper is the following result (a related result is given in [24, Theorem 1.1], in a slightly different form):

THEOREM 4.2. *There exist critical manifolds $S_{a,r}$ and \tilde{q} , given by*

$$S_a : \frac{1 - \phi(\hat{y})}{1 + \phi(\hat{y})} = \frac{x + \mathcal{O}(x^2 + \mu x)}{\beta(x - \mu) + \mathcal{O}(\mu(x - \mu) + (x - \mu)^2)}, \quad (x, 0) \in \Sigma_{sl}^-, \quad (4.10)$$

$$S_r : \frac{1 - \phi(\hat{y})}{1 + \phi(\hat{y})} = \frac{x + \mathcal{O}(x^2 + \mu x)}{\beta(x - \mu) + \mathcal{O}(\mu(x - \mu) + (x - \mu)^2)}, \quad (x, 0) \in \Sigma_{sl}^+,$$

$$\tilde{q} : x = 0, \mu = 0, \hat{y} \in (-1, 1), \quad (4.11)$$

which are normally attracting, normally repelling and normally non-hyperbolic, respectively. On the critical manifolds $S_{a,r}$, the motion of the slow variable x is described by the reduced problem (4.7), which coincides with the sliding equations (2.14) and (2.15).

Proof. This follows from simple computations. Recall that the critical manifolds are fixed points of the layer equations (4.9). Each manifold is normally hyperbolic if the linearization has one non-zero eigenvalue. Otherwise it is non-hyperbolic. \square

REMARK 4.3. *The non-hyperbolic line \tilde{q} of the regularized system corresponds to the two-fold q of the PWS system.*

As in our previous paper [18] it is useful to introduce the following function $w = w(\hat{y})$:

$$w(\hat{y}) = \frac{1 - \phi(\hat{y})}{1 + \phi(\hat{y})}, \quad (4.12)$$

which appears on the left hand side of (4.10), since this reduces the complexity of subsequent expressions. For $\hat{y} \in (-1, 1)$ we have $w \in (0, \infty)$. Also

$$w'(\hat{y}) = -\frac{2\phi'(\hat{y})}{(1 + \phi(\hat{y}))^2} < 0, \quad (4.13)$$

within $\hat{y} \in (-1, 1)$, and the critical manifolds $S_{a,r}$ are therefore graphs of \hat{y} over Σ_{sl}^\mp :

$$S_a : \hat{y} = w^{-1} \left(\frac{x + \mathcal{O}(x^2 + \mu x)}{\beta(x - \mu) + \mathcal{O}(\mu(x - \mu) + (x - \mu)^2)} \right), \quad (x, 0) \in \Sigma_{sl}^-,$$

$$S_r : \hat{y} = w^{-1} \left(\frac{x + \mathcal{O}(x^2 + \mu x)}{\beta(x - \mu) + \mathcal{O}(\mu(x - \mu) + (x - \mu)^2)} \right), \quad (x, 0) \in \Sigma_{sl}^+,$$

where

$$w^{-1}(z) = \phi^{-1}\left(\frac{1-z}{1+z}\right), \quad z \in (0, \infty)$$

is the inverse of w .

In the sequel, we will also need the *extended problem*, which is given by

$$\begin{aligned} x' &= \epsilon \left((\delta + \zeta^+ x + \mathcal{O}(x^2 + \mu + \epsilon \hat{y}))(1 + \phi(\hat{y})) + (\alpha + \zeta^- x + \mathcal{O}(x^2 + \mu + \epsilon \hat{y}))(1 - \phi(\hat{y})) \right), \\ \hat{y}' &= (x + \eta^+ x^2 + \epsilon \chi^- \hat{y} + \mathcal{O}(\epsilon x \hat{y} + \mu(x + \epsilon \hat{y}) + x^3))(1 + \phi(\hat{y})) \\ &\quad + (-\beta(x - \mu) + \eta^-(x - \mu)^2 + \epsilon \chi^- \hat{y} + \mathcal{O}(\epsilon x \hat{y} + \mu \epsilon \hat{y} + \mu(x - \mu) + (x - \mu)^3))(1 - \phi(\hat{y})), \\ \epsilon' &= 0, \\ \mu' &= 0. \end{aligned} \tag{4.14}$$

Here we have used (2.12) and (2.13).

Finally, when studying canards in section 6, it will also be useful to introduce a new time $\tilde{\tau}$, defined by

$$d\tilde{\tau} = (1 + \phi(\hat{y}))d\tau, \tag{4.15}$$

so that our extended problem (4.14), now only defined within $\hat{y} \in (-1, 1)$, becomes:

$$\begin{aligned} x' &= \epsilon \left(\delta + \zeta^+ x + \mathcal{O}(x^2 + \mu + \epsilon \hat{y}) + (\alpha + \zeta^- x + \mathcal{O}(x^2 + \mu + \epsilon \hat{y}))w(\hat{y}) \right), \\ \hat{y}' &= x + \eta^+ x^2 + \epsilon \chi^- \hat{y} + \mathcal{O}(\epsilon x \hat{y} + \mu(x + \epsilon \hat{y}) + x^3) \\ &\quad + (-\beta(x - \mu) + \eta^-(x - \mu)^2 + \chi^- y + \mathcal{O}(\epsilon x \hat{y} + \mu \epsilon \hat{y} + \mu(x - \mu) + (x - \mu)^3))w(\hat{y}), \\ \epsilon' &= 0, \\ \mu' &= 0. \end{aligned} \tag{4.16}$$

where, by abuse of notation, we take $(\cdot)' = \frac{d}{d\tilde{\tau}}$ in section 6 only. Note that $w(\hat{y})$ appears on the right hand sides of equations (4.16).

REMARK 4.4. *If we return to our original y variable using (4.5) then the critical manifolds $S_{a,r}$ become graphs $y = \epsilon h(x, \mu)$ which, for $\epsilon = 0$, collapse to $\bar{\Sigma}_{sl}$.*

REMARK 4.5. *The critical manifolds $S_{a,r}$ and \tilde{q} are shown in Fig. 4.1 for $\beta > 0$. It is clear that a singular canard exists for $\mu = 0$ only.*

4.1. Fenichel theory. Consider compact sets I^\pm contained within Σ_{sl}^\pm , respectively. Then according to Fenichel theory [12, 13, 14, 17], there exist slow manifolds of (4.3) of the form

$$S_{a,\epsilon} : \hat{y} = w^{-1}\left(\frac{x + \mathcal{O}(x^2 + \mu x)}{\beta(x - \mu) + \mathcal{O}(\mu(x - \mu) + (x - \mu)^2)}\right) + \mathcal{O}(\epsilon), \quad (x, 0) \in I^- \subset \Sigma_{sl}^-, \tag{4.17}$$

$$S_{r,\epsilon} : \hat{y} = w^{-1}\left(\frac{x + \mathcal{O}(x^2 + \mu x)}{\beta(x - \mu) + \mathcal{O}(\mu(x - \mu) + (x - \mu)^2)}\right) + \mathcal{O}(\epsilon), \quad (x, 0) \in I^+ \subset \Sigma_{sl}^+. \tag{4.18}$$

The flow on $S_{a,\epsilon}$ and $S_{r,\epsilon}$ is therefore $\mathcal{O}(\epsilon)$ -close to the flow of the sliding equations. The potential non-uniqueness of $S_{a,\epsilon}$ and $S_{r,\epsilon}$ only manifests itself in $\mathcal{O}(e^{-c/\epsilon})$ small deviations. Henceforth we shall fix copies of $S_{a,\epsilon}$ and $S_{r,\epsilon}$.

4.2. Loss of hyperbolicity. From Theorem 4.2, it follows that the analysis in section 3 can be directly applied to singular canards on the critical manifold for the limiting regularized system. In contrast, a (maximal) canard of the regularized system (4.8) appears as an intersection of the extension by the flow of the Fenichel slow manifolds $S_{a,\epsilon}$ and $S_{r,\epsilon}$ to a vicinity of the non-hyperbolic line \tilde{q} . A canard of the regularized system is called a *vrai (faux) canard* if it goes from $S_{a,\epsilon}$ ($S_{r,\epsilon}$) to $S_{r,\epsilon}$ ($S_{a,\epsilon}$) in forward time.

REMARK 4.6. *Our focus is mainly on vrai canards, usually referred to as canards [19, 31], a convention we shall adopt.*

To study the extensions of $S_{a,\epsilon}$ and $S_{r,\epsilon}$ near \tilde{q} , we will use the blowup method of Dumortier and Roussarie [9, 10, 11], in the formulation of Krupa and Szmolyan [19].

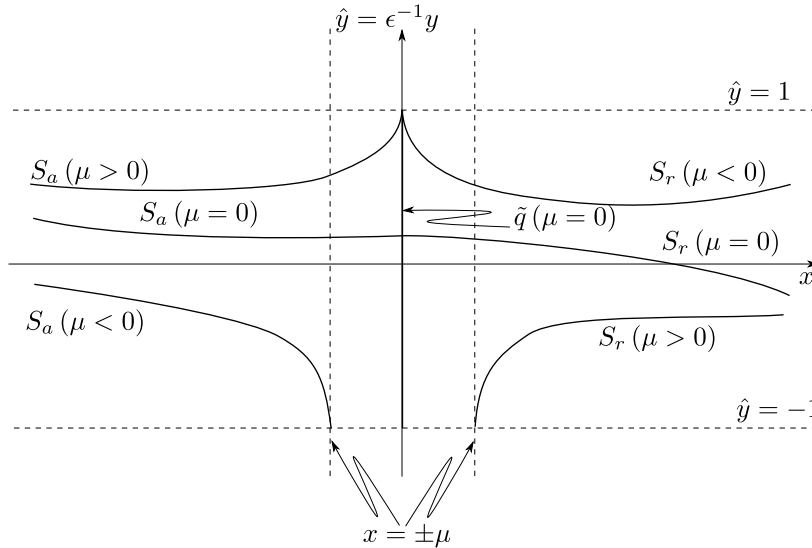


FIGURE 4.1. The critical manifolds $S_{a,r}$ for different values of μ together with the non-hyperbolic line \tilde{q} for $\beta > 0$. The critical manifolds agree with the sliding regions of the PWS smooth system. In particular, stable (unstable) sliding becomes an attracting (repelling) critical manifold of the regularization carrying slow dynamics described by the sliding equations.

Consider the following sections:

$$\Lambda^\mp : x = \mp \rho, \quad (4.19)$$

where ρ is a small positive constant. Then Fenichel's slow manifolds $S_{a,\epsilon}$ and $S_{r,\epsilon}$ intersect Λ^\mp , respectively, in

$$\hat{y} = w^{-1}(\beta^{-1}) + \mathcal{O}_{a,r}(\rho + \mu + \epsilon), \quad (4.20)$$

from (4.17) and (4.18). This will become useful later when extending $S_{a,\epsilon}$ and $S_{r,\epsilon}$.

We are also interested in studying the regularization of pseudo-equilibria and limit cycles. The non-hyperbolicity of the line \tilde{q} defined in (4.11) will again complicate the analysis and we will also use the blowup method to obtain an accurate and complete description of the regularization of these phenomena.

5. Main results. In this section, we anticipate our main regularization results, in a form convenient for the reader. The connection between sections of the paper devoted to PWS results and to regularization results is shown in Table 5.1:

TABLE 5.1
Connection between phenomena in the PWS and regularized systems

PWS phenomenon	Regularized phenomenon
Singular canards (section 3.1)	Canards (section 6)
Pseudo-equilibria (section 3.2)	Equilibria (section 7)
Limit cycles (section 3.3)	Limit cycles (section 8)

5.1. Canards. From section 3.1, singular canards of the PWS system can only exist for $\mu = 0$. From Proposition 3.2, singular canards exist for

$$\beta > 0 \quad \text{and} \quad \Omega > 0. \quad (5.1)$$

Canards of the regularized system (4.3) are considered in section 6. The main result of that section is that singular canards survive the regularization in the following sense:

THEOREM 6.4 *Assuming (5.1), the regularized system (4.3) has a maximal canard at*

$$\mu = \sqrt{\epsilon}\mu_{2,c}(\sqrt{\epsilon}) = \mathcal{O}(\epsilon),$$

where $\mu_{2,c}$ is given by (6.22), which is $\mathcal{O}(\sqrt{\epsilon})$ -close to the singular canard.

REMARK 5.1. *Canards are non-unique because the slow manifolds are non-unique. But often in the literature, any solution following $S_{r,\epsilon}$ for an $\mathcal{O}(1)$ -distance is called a canard. Hence the canard in Theorem (6.4), which is obtained geometrically as the transverse intersection of fixed copies of $S_{a,\epsilon}$ and $S_{r,\epsilon}$, is referred to as the maximal canard.*

5.2. Equilibria. From section 3.2, pseudo-equilibria of the PWS system can only exist for

$$\alpha\delta < 0. \tag{5.2}$$

Equilibria of the regularized system (4.3) are considered in section 7. We have two main results. Our first result is Theorem 7.5, which shows that, for $\Omega < 0$, the equilibria are saddles and, for $\Omega > 0$, there is a Hopf bifurcation at $\mu = \mathcal{O}(\sqrt{\epsilon})$, after which the equilibria become foci, and then nodes, as μ varies.

THEOREM 7.5 *Assuming (5.2), the regularized system (4.3) has a smooth and locally unique family of equilibria*

$$(x, y) = (x^*, y^*)(\mu, \sqrt{\epsilon}) \equiv \left(\frac{\mu}{1 + \beta^{-1}\delta\alpha} + \mathcal{O}(\mu^2 + \epsilon), \mathcal{O}(\epsilon) \right)$$

where $(x^*(\mu, 0), y^*(\mu, 0)) = (x^*(\mu, 0), 0)$ agrees with the family of pseudo-equilibria for the PWS system (see Proposition 3.3) and, in particular, $\partial_\mu x^*(\mu, 0) \neq 0$. For

$\Omega < 0$: *The family of equilibria consists of saddles and does not undergo any bifurcation.*

$\Omega > 0$: *The family of equilibria undergoes a Hopf bifurcation at $\mu = \sqrt{\epsilon}\mu_{2,H}(\sqrt{\epsilon}) = \mathcal{O}(\epsilon)$, where $\mu_{2,H}$ is given by (7.14). The first Lyapunov coefficient is given by $a = a_2\sqrt{\epsilon} + \mathcal{O}(\epsilon)$ where a_2 , given by (7.15), depends upon the regularization function ϕ .*

Our second result for equilibria of the regularized system (4.3), Theorem 7.6, is perhaps surprising, in that it shows that the criticality of the Hopf bifurcation depends on the regularization function ϕ .

THEOREM 7.6 *Suppose that $\Omega > 0$ so that, from Theorem 7.5, there exists a Hopf bifurcation. Then for ϵ sufficiently small, provided*

$$\delta(\zeta^- + \chi^-) - \alpha(\zeta^+ + \chi^+) \neq 0, \tag{7.19}$$

where ζ^\mp, χ^\mp are the higher order coefficients in (2.11), the first Lyapunov coefficient a can be positive, zero or negative, depending on the regularization function ϕ .

5.3. Limit cycles. From section 3.3, limit cycles of the PWS system can exist for the case II_2 , which occurs when

$$\delta = -1, \quad \alpha > 0, \quad \beta < 0. \tag{5.3}$$

Limit cycles of the regularized system (4.3) are considered in section 8 where, following Theorem 7.5 above, we find limit cycles provided:

$$\Omega > 0 \quad \text{and} \quad \alpha\delta < 0. \tag{5.4}$$

This leads to the regularization of II_2 and of VI_3 , which we denote by II_2^ϵ and VI_3^ϵ , respectively. We have two main results for limit cycles of the regularized system. The first main result Theorem 8.8 shows how small amplitude periodic orbits due the Hopf bifurcation in Theorem 7.5 can be connected to $\mathcal{O}(1)$ (with respect to ϵ) amplitude periodic orbits.

THEOREM 8.8 *For ϵ sufficiently small:*

II_2^ϵ : *There exists a C^k -smooth family of locally unique periodic orbits of the regularized system (4.3) that is due to the Hopf bifurcation in Theorem 7.5. If $a_2 < 0$ ($a_2 > 0$) where a_2 is the first Lyapunov*

coefficient as defined in (7.15), then the periodic orbits are attracting (repelling) near the Hopf bifurcation. If

$$\Delta_{II_2} = \frac{2}{3\alpha\beta} (\alpha(\eta^- + \beta\eta^+) + \beta(\zeta^- + \chi^- + \alpha(\zeta^+ + \chi^+))), \quad (3.8)$$

is negative (positive) then the periodic orbits for $\Delta_{II_2}^{-1}\mu \leq -c\sqrt{\epsilon}$, $c > 0$ sufficiently large, are attracting (repelling). The periodic orbits for $\mu = \mathcal{O}(1)$ (with respect to ϵ) are continuously $\mathcal{O}(\epsilon)$ -close to the PWS periodic orbits in Proposition 3.6.

VI_3^ϵ : There exists a C^k -smooth family of small periodic orbits of the regularized system (4.3) that is due to the Hopf bifurcation in Theorem 7.5. There also exists a C^k -smooth family of periodic orbits that are $\mathcal{O}(1)$ (with respect to ϵ) in amplitude and which undergo a canard explosion, where the amplitude changes by $\mathcal{O}(1)$ within an exponentially small parameter regime around the canard value $\mu = \sqrt{\epsilon}\mu_{2,c}(\sqrt{\epsilon})$ (see Theorem 6.4). If $a_2 < 0$ ($a_2 > 0$) where a_2 is the first Lyapunov coefficient as defined in (7.15), then the periodic orbits are attracting (repelling) near the Hopf bifurcation. If

$$\Delta_{VI_3} = \frac{2}{3\alpha\beta} (\alpha(\eta^- + \beta\eta^+) + \beta(\beta + 1)(\zeta^- + \chi^-)) \quad (8.11)$$

is negative (positive) then the $\mathcal{O}(1)$ -periodic orbits are attracting (repelling).

We conjecture on the connection of the two families of periodic orbits in VI_3^ϵ :

CONJECTURE 1 *The two families of periodic orbits in VI_3^ϵ belong to the same family of locally unique periodic orbits.*

The second main result for limit cycles of the regularized system (4.3) shows how an open set of regularization functions can induce at least one saddle-node bifurcation in the periodic orbits of Theorem 8.8.

THEOREM 8.18 *Suppose (7.19) and (5.4). Then for ϵ sufficiently small:*

II_2^ϵ : *There exists an open set of regularization functions such that the periodic orbits in Theorem 8.8, case II_2^ϵ , undergo at least one saddle-node bifurcation.*

VI_3^ϵ : *Suppose, in addition, that Conjecture 1 holds. Then there exists an open set of regularization functions such that the periodic orbits in Theorem 8.8, case VI_3^ϵ , undergo at least one saddle-node bifurcation.*

In section 9, we illustrate the results in Theorem 8.18 by applying two different regularization functions to two model systems of II_2^ϵ and VI_3^ϵ . The regularization functions are such that each case, II_2^ϵ or VI_3^ϵ , will have a saddle-node bifurcation for only one of the regularization functions.

6. On the existence of canards. In section 3.1, Proposition 3.2, we showed that our PWS system (2.9) and (2.10) together with the sliding vector field (2.14) and (2.15) contains singular canards for $\beta > 0$. In this section, we aim to discover the fate of these singular canards in the regularized system. To do this, we focus on dynamics in the region of regularization $y \in (-\epsilon, \epsilon)$, or $\hat{y} \in (-1, 1)$, as described by equations (4.16), which are written in terms of the new time $\tilde{\tau}$, defined in (4.15). We work with $\tilde{\tau}$ in this section only.

As discussed in section 4.2, Fenichel theory breaks down on the non hyperbolic line \tilde{q} , defined in (4.11). We use the blowup method [9, 10, 11] to deal with this line. We introduce the *quasi-homogeneous blowup*, given by

$$(x, \epsilon, \mu) = (r^{a_1}\bar{x}, r^{a_2}\bar{\epsilon}, r^{a_3}\bar{\mu}),$$

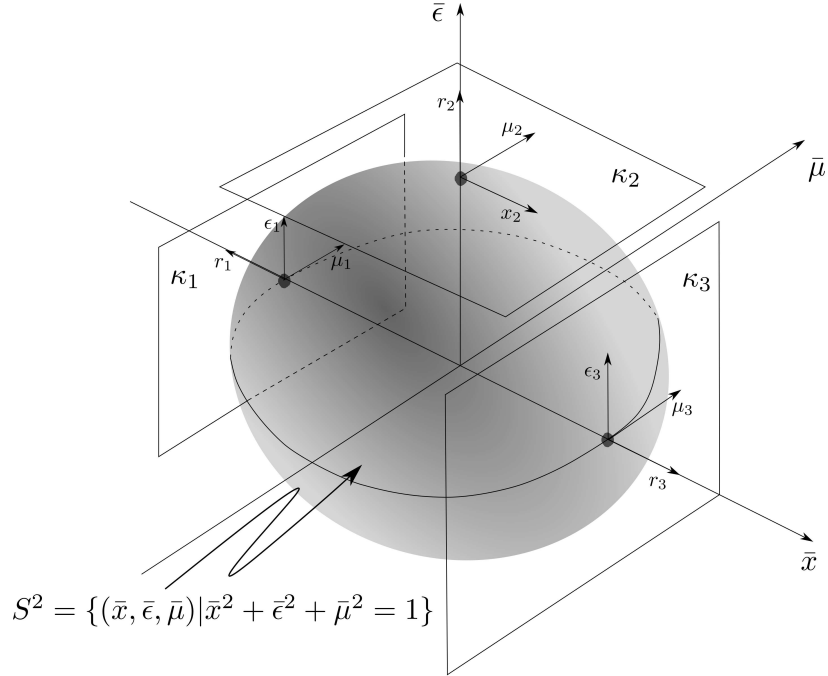
where the number r is called the *exceptional divisor*. By this transformation, the line \tilde{q} is blown up to a cylinder

$$S^2 \times (-1, 1) = \{((\bar{x}, \bar{\epsilon}, \bar{\mu}), \hat{y}) | \bar{x}^2 + \bar{\epsilon}^2 + \bar{\mu}^2 = 1, \hat{y} \in (-1, 1)\}.$$

When $r = 0$, the blown-up coordinates collapse to the non-hyperbolic line \tilde{q} .

The weights (a_1, a_2, a_3) are chosen so that the vector field written as a function of the blowup coordinates has a power of the exceptional divisor as a common factor. By transforming time using this common factor, it is then possible to remove the exceptional divisor and so de-trivialize the vector-field on \tilde{q} . By substituting the quasi-homogeneous blowup into (4.16) and removing the exceptional divisor, it turns out that $(a_1, a_2, a_3) = (1, 2, 1)$. So we have the following blowup of \tilde{q} :

$$x = r\bar{x}, \quad \epsilon = r^2\bar{\epsilon}, \quad \mu = r\bar{\mu}$$

FIGURE 6.1. The two-sphere S^2 and the charts κ_{1-3} .

with $r \geq 0$, $(\bar{x}, \bar{\epsilon}, \bar{\mu}) \in S^2$. Note that this blowup does not depend on \hat{y} . The new phase space is therefore

$$((\bar{x}, \bar{\epsilon}, \bar{\mu}), r, \hat{y}) \in S^2 \times \overline{\mathbb{R}}_+ \times (-1, 1).$$

To describe the dynamics on the blowup space we consider the following charts:

$$\text{chart } \kappa_1 : \bar{x} = -1, x = -r_1, \epsilon = r_1^2 \epsilon_1, \mu = r_1 \mu_1 \quad (6.1)$$

$$\text{chart } \kappa_2 : \bar{\epsilon} = 1, x = r_2 x_2, \epsilon = r_2^2, \mu = r_2 \mu_2, \quad (6.2)$$

$$\text{chart } \kappa_3 : \bar{x} = 1, x = r_3, \epsilon = r_3^2 \epsilon_3, \mu = r_3 \mu_3. \quad (6.3)$$

The chart κ_2 is called the scaling chart or *family rescaling* chart [9, 10, 11]. The charts $\kappa_{1,3}$ are called *phase directional* charts. The point $(x, \epsilon, \mu) = (0, 0, 0)$ has been blown up into the planes $r_i = 0 : i = 1, 2, 3$. The two-sphere S^2 and the charts κ_{1-3} are shown in Fig. 6.1. We adopt the convention that the subscript n of each quantity is used when we are working in chart κ_n .

The following coordinate change between charts κ_1 and κ_2 will be important in what follows:

$$\kappa_{21} : (r_1, \hat{y}, \epsilon_1, \mu_1) \mapsto (x_2, \hat{y}, \mu_2, r_2) = (-\epsilon_1^{-1/2}, \hat{y}, \epsilon_1^{-1/2} \mu_1, r_1 \sqrt{\epsilon_1}), \quad (6.4)$$

$$\kappa_{12} : (x_2, \hat{y}, r_2, \mu_2) \mapsto (r_1, \hat{y}, \epsilon_1, \mu_1) = (-r_2 x_2, \hat{y}, x_2^{-2}, -x_2^{-1} \mu_2), \quad (6.5)$$

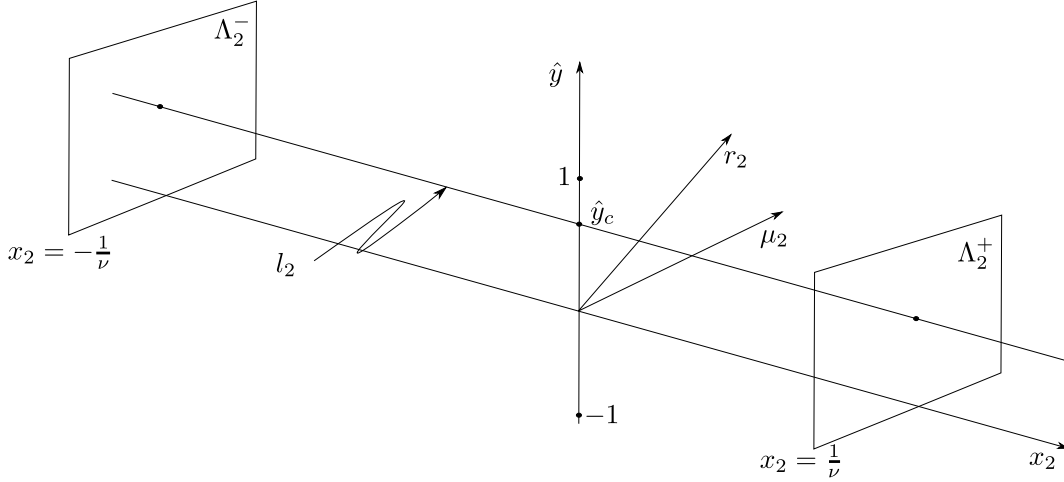
defined for $x_2 < 0$ and $\epsilon_1 > 0$ respectively. The change between charts κ_2 and κ_3 is given by:

$$\kappa_{32} : (x_2, \hat{y}, r_2, \mu_2) \mapsto (r_3, \hat{y}, \epsilon_3, \mu_3) = (r_2 x_2, \hat{y}, x_2^{-2}, x_2^{-1} \mu_2), \quad (6.6)$$

$$\kappa_{23} : (r_3, \hat{y}, \epsilon_3, \mu_3) \mapsto (x_2, \hat{y}, \mu_2, r_2) = (\epsilon_3^{-1/2}, \hat{y}, \epsilon_3^{-1/2} \mu_3, r_3 \sqrt{\epsilon_3}), \quad (6.7)$$

defined for $x_2 > 0$ and $\epsilon_3 > 0$ respectively.

We now describe the dynamics in each chart, beginning with the chart κ_2 . Sections 6.2 and 6.3 describe the dynamics in charts $\kappa_{1,3}$. Finally, section 6.4 combines the results from charts κ_{1-3} to prove Theorem 6.4.

FIGURE 6.2. The line l_2 and the sections Λ_2^\pm .

6.1. Chart κ_2 . The extended problem (4.16) written in chart κ_2 becomes

$$\begin{aligned} \dot{x}_2 &= \delta + \alpha w(\hat{y}) + r_2(\zeta^+ x_2 + \zeta^- x_2 w(\hat{y})) + \mathcal{O}(r_2(\mu_2 + r_2)), \\ \dot{\hat{y}} &= x_2 + r_2(\eta^+ x_2^2 + \chi^+ \hat{y}), \\ &\quad + (-\beta(x_2 - \mu_2) + r_2(\eta^-(x_2 - \mu_2)^2 + \chi^- \hat{y})) w(\hat{y}) + \mathcal{O}(r_2(\mu_2 + r_2)), \\ \dot{r}_2 &= 0, \\ \dot{\mu}_2 &= 0, \end{aligned} \tag{6.8}$$

where we have multiplied time by r_2 . For $\beta > 0$ there is an invariant line l_2 given by:

$$l_2 : x_2 \in \mathbb{R}, \hat{y} = \hat{y}_c, r_2 = 0, \mu_2 = 0, \tag{6.9}$$

where

$$\hat{y}_c = w^{-1}(\beta^{-1}) = \phi^{-1}\left(\frac{\beta - 1}{\beta + 1}\right) \in (-1, 1), \tag{6.10}$$

carrying the *special* solution:

$$x_2 = \beta^{-1} \Omega t_2, \hat{y} = \hat{y}_c, r_2 = 0, \mu_2 = 0,$$

where t_2 is the time used in (6.8).

Consider the following sections

$$\Lambda_2^\mp = \{(x_2, \hat{y}, r_2, \mu_2) | x_2 = \mp \nu^{-1}\}, \tag{6.11}$$

where ν is small and positive. The line l_2 intersects Λ_2^\mp in

$$l_2 \cap \Lambda_2^\mp : x_2 = \mp \nu^{-1}, \hat{y} = \hat{y}_c, r_2 = 0, \mu_2 = 0. \tag{6.12}$$

The line l_2 and the sections Λ_2^\mp are shown in Fig. 6.2.

6.2. Chart κ_1 . We now describe the dynamics in chart κ_1 and relate them to the dynamics in chart κ_2 . The extended problem (4.16) written in chart κ_1 becomes

$$\begin{aligned} \dot{r}_1 &= -r_1 \epsilon_1 F_1(r_1, \hat{y}, \epsilon_1, \mu_1), \\ \dot{\hat{y}} &= -1 + \beta(1 + \mu_1) w(\hat{y}) + \mathcal{O}(r_1), \\ \dot{\epsilon}_1 &= 2\epsilon_1^2 F_1(r_1, \hat{y}, \epsilon_1, \mu_1), \\ \dot{\mu}_1 &= \epsilon_1 \mu_1 F_1(r_1, \hat{y}, \epsilon_1, \mu_1), \end{aligned} \tag{6.13}$$

where we have divided the vector-field by r_1 and set $F_1(r_1, \hat{y}, \epsilon_1, \mu_1) = \delta + \alpha w(\hat{y}) + \mathcal{O}(r_1)$. The $\mathcal{O}(r_1)$ -terms include the constants $\zeta^\pm, \eta^\pm, \chi^\pm$ from (2.11) but they will not play a role in this section and we therefore suppress them. The line $r_1 = 0, \hat{y} = w^{-1}\left(\frac{1}{\beta(1+\mu_1)}\right), \epsilon_1 = 0$ is a line of fixed points, provided $\beta(1+\mu_1) > 0$, since $w(\hat{y}) \in (0, \infty)$. In particular, this line includes the point $r_1 = 0, \hat{y} = \hat{y}_c, \epsilon_1 = 0, \mu_1 = 0$ because we focus on $\beta > 0$. There exists an attracting center manifold $M_{a,1}$ of this line, given by:

$$M_{a,1} : \hat{y} = w^{-1}\left(\frac{1}{\beta(1+\mu_1)}\right) + \mathcal{O}(r_1 + \epsilon_1)$$

and, within $r_1 = 0$, a center manifold $C_{a,1}$, given by:

$$C_{a,1} : \hat{y} = w^{-1}\left(\frac{1}{\beta(1+\mu_1)}\right) + \mathcal{O}(\epsilon_1).$$

Within $C_{a,1}$, there exists an invariant line:

$$l_{a,1} : r_1 = 0, \hat{y} = \hat{y}_c, \epsilon_1 \geq 0, \mu_1 = 0.$$

Recall (6.10). The center manifold $C_{a,1}$ is overflowing and hence unique near $l_{a,1}$ if $\dot{\epsilon}_1 > 0$ for $\epsilon_1 > 0$. From (6.13), we therefore have

$$\dot{\epsilon}_1 = 2\epsilon_1^2(\delta + \alpha w(\hat{y})) = 2\epsilon_1^2\beta^{-1}\Omega + \mathcal{O}(\epsilon_1),$$

with $r_1 = 0$ and $w(\hat{y}) = \beta^{-1} + \mathcal{O}(\epsilon_1)$ near $l_{a,1}$. Hence since $\beta > 0$, $\dot{\epsilon}_1 > 0$ for $\epsilon_1 > 0$ if $\Omega > 0$. For $\Omega < 0$, we have $\dot{\epsilon}_1 < 0$ and so $C_{a,1}$ is non-unique near $l_{a,1}$ in this case.

The manifold $M_{a,1}$ has invariant foliations, which we denote by $M_{a,1}(\epsilon)$, with $\epsilon = r_1^2\epsilon_1 = \text{const}$. The sub-manifold $M_{a,1}(\epsilon)$ intersects the section $r_1 = \rho$, corresponding to Λ^- (4.19), in

$$\hat{y} = w^{-1}(\beta^{-1}) + \mathcal{O}(\rho + \mu + \epsilon) = \hat{y}_c + \mathcal{O}(\rho + \mu + \epsilon),$$

which agrees with (4.20) since $\mu = r_1\mu_1 = \rho\mu_1$. Hence $M_{a,1}(\epsilon)$ is the extension of $S_{a,\epsilon}$ into chart κ_1 near the line \tilde{q} (ignoring exponentially small terms).

In order to relate the dynamics in chart κ_1 to the dynamics in chart κ_2 , we use the coordinate change κ_{21} in (6.5). The section Λ_2^- defined in (6.11) then becomes

$$\Lambda_1^- : \epsilon_1 = \nu^2. \tag{6.14}$$

The manifold $C_{a,1}$ intersects Λ_1^- in

$$C_{a,1} \cap \Lambda_1^- : \epsilon_1 = \nu^2, r_1 = 0, \hat{y} = \hat{y}_c + \mathcal{O}(\nu^2 + \mu_1)$$

and hence, by the conservation of ϵ , we conclude that the intersection of $M_{a,1}(\epsilon)$ with Λ_1^- is $\mathcal{O}(\sqrt{\epsilon})$ -close to $C_{a,1}$.

The line $l_{a,1}$ and the section Λ_1^- are shown in Fig. 6.3.

6.3. Chart κ_3 . The extended problem (4.16) written in chart κ_3 becomes

$$\begin{aligned} \dot{r}_3 &= r_3\epsilon_3 F_3(r_3, \hat{y}, \epsilon_3, \mu_3), \\ \dot{\hat{y}} &= 1 - \beta(1 - \mu_3)w(\hat{y}) + \mathcal{O}(r_3), \\ \dot{\epsilon}_3 &= -2\epsilon_3^2 F_3(r_3, \hat{y}, \epsilon_3, \mu_3), \\ \dot{\mu}_3 &= -\epsilon_3\mu_3 F_3(r_3, \hat{y}, \epsilon_3, \mu_3), \end{aligned} \tag{6.15}$$

where we have divided the vector-field by r_3 and set $F_3(r_3, \hat{y}, \epsilon_3, \mu_3) = \delta + \alpha w(\hat{y}) + \mathcal{O}(r_3)$. The analysis of the dynamics in this chart is very similar to the analysis in chart κ_1 . Therefore we state the main results only.

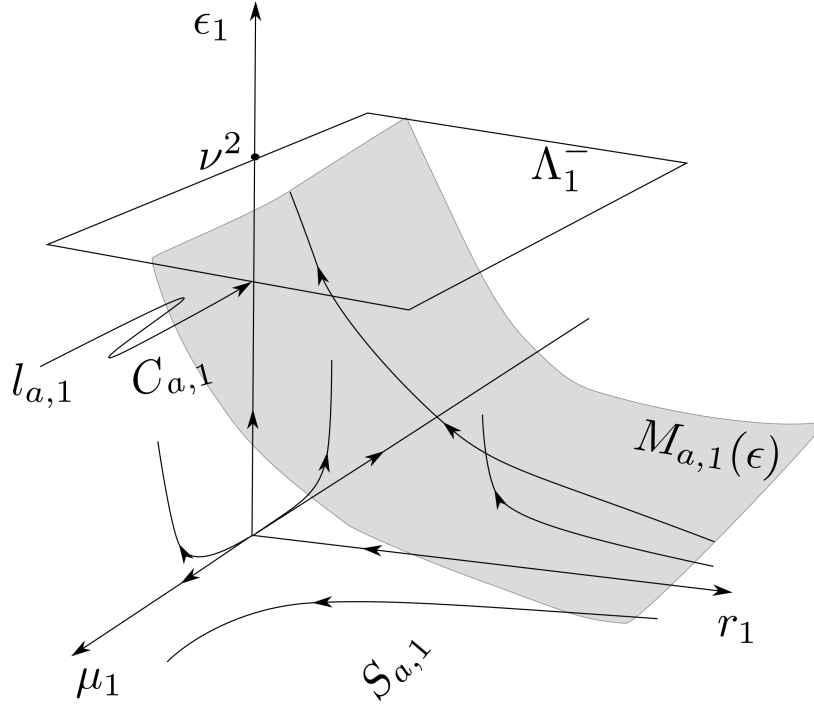


FIGURE 6.3. The line $l_{a,1}$ and the section Λ_1^- .

There exists a repelling center manifold $M_{r,3}$ of $r_3 = 0$, $\hat{y} = w^{-1}\left(\frac{1}{\beta(1-\mu_3)}\right)$, $\epsilon_3 = 0$ given by

$$M_{r,3} : \hat{y} = w^{-1}\left(\frac{1}{\beta(1-\mu_3)}\right) + \mathcal{O}(r_3 + \epsilon_3)$$

and a center manifold $C_{r,3}$ within $r_3 = 0$ which takes the form

$$C_{r,3} : \hat{y} = w^{-1}\left(\frac{1}{\beta(1-\mu_3)}\right) + \mathcal{O}(\epsilon_3).$$

Within $C_{r,3}$ there exists an invariant line

$$l_{r,3} : r_3 = 0, \hat{y} = \hat{y}_c, \epsilon_3 \geq 0, \mu_3 = 0.$$

The center manifold $C_{r,3}$ is overflowing and hence unique near $l_{r,3}$ for $\Omega > 0$. If $\Omega < 0$ then $C_{r,3}$ is non-unique near $l_{a,3}$. The sub-manifold $M_{r,3}(\epsilon) = M_{r,3} \cap \{r_3^2 \epsilon_3 = \epsilon\}$ is the extension of $S_{r,\epsilon}$ into chart κ_3 near the line \tilde{q} . Also $M_{r,3}(\epsilon)$ intersects

$$\Lambda_3^+ : \epsilon_3 = \nu^2, \tag{6.16}$$

which corresponds to Λ_2^+ through the coordinate change κ_{23} in (6.6), $\mathcal{O}(\sqrt{\epsilon})$ -close to the intersection of $C_{r,3}$ with (6.16)

$$C_{r,3} \cap \Lambda_3^+ : \epsilon_3 = \nu^2, r_3 = 0, \hat{y} = \hat{y}_c + \mathcal{O}(\nu^2 + \mu_3).$$

The line $l_{r,3}$ and the section Λ_3^+ are shown in Fig. 6.4.

6.4. Persistence of canards. In this section, we combine results from the three charts κ_{1-3} to show how singular canards in our PWS system can survive the regularization. For singular canards, there were two cases to consider: $\Omega > 0$ (vrai singular canards) and $\Omega < 0$ (faux singular canards). We now consider the same two cases for canards in the regularized system.

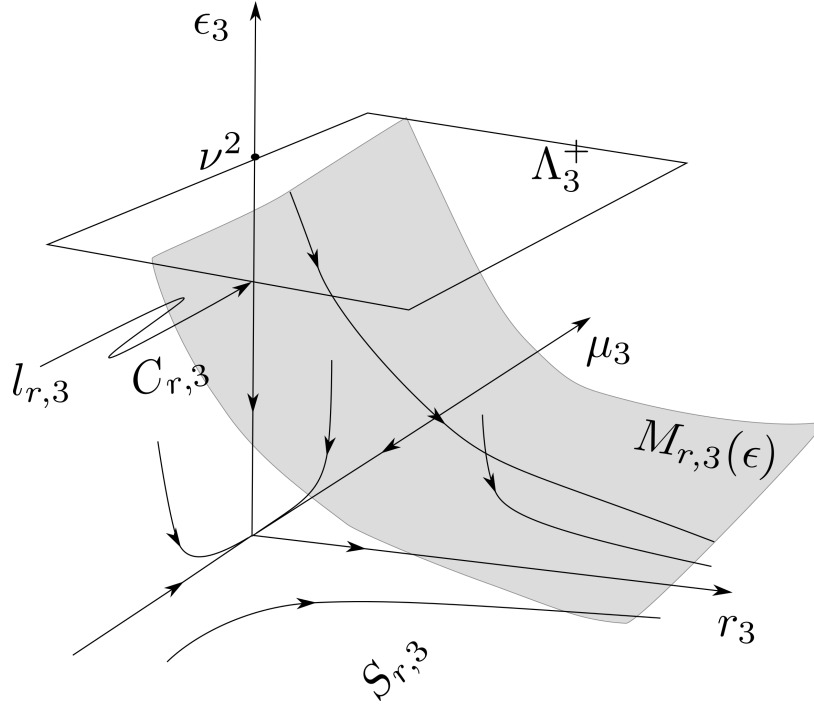


FIGURE 6.4. The line $l_{r,3}$ and the section Λ_3^+ .

For $\Omega > 0$, $C_{a,1}$ and $C_{r,3}$ are unique as center manifolds. By transforming $l_2 \cap \Lambda_2^\mp$ of (6.12) into charts κ_1 and κ_3 we conclude that $\kappa_{12}(l_2) = l_{a,1} \subset C_{a,1}$ for $x_2 \ll 0$ and $\kappa_{32}(l_2) = l_{r,3} \subset C_{r,3}$ for $x_2 \gg 0$. It is therefore possible to extend $C_{a,1}$ and $C_{r,3}$ into κ_2 as invariant manifolds $C_{a,2}$ and $C_{r,2}$ by using the invariant line l_2 as a guide. Then from the analyses in section 6.2 and section 6.3, we conclude that the manifolds $M_{a,2}(\epsilon) = \kappa_{21}(M_{a,1}(\epsilon))$ and $M_{r,2}(\epsilon) = \kappa_{23}(M_{r,3}(\epsilon))$ intersect Λ_2^\mp a distance $\mathcal{O}(r_2)$ -close to the intersections of $C_{a,2}$ and $C_{r,2}$, respectively, where $r_2 = \sqrt{\epsilon}$ by (6.2). By applying regular perturbation theory in chart κ_2 the manifolds $M_{a,2}(\epsilon)$ and $M_{r,2}(\epsilon)$ can be continued all the way up to $x_2 = 0$ where they remain $\mathcal{O}(r_2)$ -close to $C_{a,2}$ and $C_{r,2}$, respectively.

The manifolds $C_{a,2}$ and $C_{r,2}$ intersect along l_2 . We now investigate whether the intersection is transverse. If so, we can conclude that $M_{a,2}(\epsilon)$ and $M_{r,2}(\epsilon)$ also intersect transversally $\mathcal{O}(r_2)$ -close to l_2 , since $M_{a,2}(\epsilon)$ and $M_{r,2}(\epsilon)$ are $\mathcal{O}(r_2)$ -close to $C_{a,2}$ and $C_{r,2}$, respectively. We first eliminate time from (6.8) by division with \dot{x}_2 and re-writing our equations in terms of w instead of \hat{y} using (4.12). Then we let $(u(x_2), \tilde{\mu}_2(x_2), \tilde{r}_2(x_2))$ denote the variations of (w, μ_2, r_2) about $l_2 : (w, \mu_2, r_2) = (\beta^{-1}, 0, 0)$. This gives

$$\begin{aligned} \frac{du}{dx_2} &= \lambda(\beta x_2 u - \tilde{\mu}_2 + \tilde{r}_2 G_2(x_2, u)), \\ \frac{d\tilde{\mu}_2}{dx_2} &= 0, \\ \frac{d\tilde{r}_2}{dx_2} &= 0, \end{aligned} \tag{6.17}$$

where

$$\lambda = \frac{(\beta + 1)^2 \phi_{1,c}}{2\beta\Omega}, \quad G_2(x_2) = \beta^{-1} (x_2^2(\eta^- + \beta\eta^+) - \hat{y}_c(\chi^- + \beta\chi^+)), \tag{6.18}$$

and

$$\phi_{1,c} \equiv \phi'(\hat{y}_c) > 0.$$

For simplicity we now drop the tildes from μ_2 and r_2 . We will apply the following lemma to (6.17).

LEMMA 6.1. ([31, Proposition 4.2]) $C_{a,2}$ and $C_{r,2}$ intersect transversally along l_2 if and only if there exists no non-zero solution of (6.17) $_{r_2=0}$ which has algebraic growth for both $x_2 \rightarrow \pm\infty$.

Proof. Variations within the tangent spaces $T_0C_{a,2}$ and $T_0C_{r,2}$ are characterized by algebraic growth in the past ($x_2 \rightarrow -\infty$) and in the future ($x_2 \rightarrow \infty$), respectively. Since $C_{a,2}$ and $C_{r,2}$ are unique, variations normal to $T_0C_{a,2}$ and $T_0C_{r,2}$ will be characterized by exponential growth in the past and in the future, respectively. \square

The following lemma describes the properties of the solutions of (6.17) $_{r_2=0}$ necessary to invoke Lemma 6.1.

LEMMA 6.2. If $\Omega > 0$ then (6.17) $_{r_2=0}$ has two linearly independent solutions

$$\gamma^- = (u^-, \mu_2^-) = \left(\sqrt{\frac{\pi\lambda}{2\beta}} (1 - \operatorname{erf}\left(\sqrt{\frac{\lambda\beta}{2}} x_2\right)) e^{-\frac{\lambda\beta x_2^2}{2}}, 1 \right),$$

and

$$\gamma^+ = (u^+, \mu_2^+) = \left(\sqrt{\frac{\pi\lambda}{\beta}} (1 + \operatorname{erf}\left(\sqrt{\frac{\lambda\beta}{2}} x_2\right)) e^{-\frac{\lambda\beta x_2^2}{2}}, 1 \right).$$

The solutions γ^\mp grow exponentially as $x_2 \rightarrow \pm\infty$ but the growth is only algebraic as $x_2 \rightarrow \mp\infty$, respectively. If $\Omega < 0$, then neither of the solutions of (6.17) $_{r_2=0}$ grows exponentially as $x_2 \rightarrow \pm\infty$.

Proof. For $\Omega > 0$ the result follows from the asymptotic behaviour of the error-function:

$$\operatorname{erf}(z) = \frac{2}{\sqrt{\pi}} \int_0^z e^{-t^2} dt.$$

For $\Omega < 0$ we use that $\int_0^z e^{t^2 - z^2} dt = \mathcal{O}(z^{-1})$ for $z \rightarrow \pm\infty$. \square

Therefore by Lemma 6.1, the manifolds $C_{a,2}$ and $C_{r,2}$ intersect transversally for $\Omega > 0$ along l_2 . Hence $M_{a,2}(\epsilon)$ and $M_{r,2}(\epsilon)$ intersect transversally $\mathcal{O}(\sqrt{\epsilon})$ -close to r_2 for $\mu_2 = \mu_{2,c}$ where

$$\mu_{2,c} = \mathcal{O}(r_2) \tag{6.19}$$

and $r_2 = \sqrt{\epsilon}$ sufficiently small. In fact, the following lemma allow us to calculate $\mu_{2,c}$ to lowest order:

LEMMA 6.3. Consider $\Omega > 0$, then the only solution of (6.17) which has algebraic growth for $x_2 \rightarrow \pm\infty$ is

$$u(x_2) = -r_2\beta^{-2}(\eta^- + \beta\eta^+)x_2,$$

for

$$\mu_2 = - \left(\frac{2\Omega}{(\beta+1)^2\phi_{1,c}} (\eta^- + \beta\eta^+) + \hat{y}_c(\chi^- + \beta\chi^+) \right) \beta^{-1}r_2. \tag{6.20}$$

Proof. The complete solution of (6.17) is

$$\begin{aligned} u(x_2) = & \left(- (r_2\beta^{-2} (\eta^- + \beta\eta^+) + \lambda(\mu_2 + r_2\beta^{-1}\hat{y}_c(\chi^- + \beta\chi^+))) \sqrt{\frac{\pi}{2\lambda\beta}} \operatorname{erf}\left(\sqrt{\frac{\lambda\beta}{2}} x_2\right) + u(0) \right) e^{\frac{\lambda\beta x_2^2}{2}} \\ & - r_2\beta^{-2}(\eta^- + \beta\eta^+)x_2. \end{aligned} \tag{6.21}$$

Setting $u(0) = 0$ and (6.20) the result follows from Lemma 6.2. \square

Then following [20, Prop. 3.1] and using (6.20) we obtain

$$\mu_{2,c} = - \left(\frac{2\Omega}{(\beta+1)^2\phi_{1,c}} (\eta^- + \beta\eta^+) + \hat{y}_c(\chi^- + \beta\chi^+) \right) \beta^{-1}r_2 + \mathcal{O}(r_2^2), \tag{6.22}$$

and hence we have the following main theorem.

THEOREM 6.4. *Assuming (5.1), the regularized system (4.3) has a maximal canard at*

$$\mu = \sqrt{\epsilon}\mu_{2,c}(\sqrt{\epsilon}) = \mathcal{O}(\epsilon),$$

where $\mu_{2,c}$ is given by (6.22), which is $\mathcal{O}(\sqrt{\epsilon})$ -close to the singular canard.

Proof. The statements follow from the analysis above. \square

In the case where $\Omega < 0$ then $C_{a,1}$ and $C_{r,3}$ are both non-unique and there exists a faux canard. The proof of this is very similar to the proof of faux canards in \mathbb{R}^3 [18, 31].

7. Equilibria of the regularized system. We now revert to describing the dynamics in terms of the fast time τ in (4.15) for the remainder of the paper. In section 3.2, pseudo-equilibria of the PWS system were shown to exist for $\alpha\delta < 0$ only. In Theorem 4.2, we showed that the equations of the reduced problem (4.7) agree with the sliding equations (2.14) and (2.15). Hence, as a consequence of the implicit function theorem, pseudo-equilibria of the sliding vector field $X_{sl}(\mathbf{x}, \mu)$ for $|\mu| > \mu_0 > 0$ perturb to locally unique equilibria on the slow manifold of the regularized problem for $0 < \epsilon \leq \epsilon_0(\mu_0)$ sufficiently small. Indeed, from our fast system (4.16), we find an equilibrium at

$$\begin{aligned} x^* &= \beta\delta\Omega^{-1}\mu + \mathcal{O}(\mu^2 + \epsilon), \\ \hat{y}^* &= w^{-1}(-\alpha^{-1}\delta) + \mathcal{O}(\mu + \epsilon). \end{aligned} \tag{7.1}$$

Since we require $w(\hat{y}) > 0$ by (4.12), (x^*, \hat{y}^*) is an equilibrium provided $\alpha\delta < 0$. This is in accordance with equation (3.2) for the PWS system. The stability of this equilibrium is described by Proposition 3.3. However, for $\mu = 0$, $\epsilon = 0$, the equilibrium lies on the non-hyperbolic line \tilde{q} , defined in (4.11), of the critical manifold. Hence Fenichel theory can not give a description of the equilibrium for $\epsilon \neq 0$. To accurately follow the equilibria near $\mu = 0$ we need to consider the extended equations in chart κ_2 , equations (6.8).

7.1. Chart κ_2 . From (6.8), we find the following equilibrium:

$$(x_2^*, \hat{y}^*) = (\beta\delta\Omega^{-1}\mu_2, w^{-1}(-\alpha^{-1}\delta)) + \mathcal{O}(r_2). \tag{7.2}$$

The equilibrium (x_2^*, \hat{y}^*) intersects the section Λ_2^- , defined in (6.11), when

$$\begin{aligned} \hat{y}^* &= w^{-1}(-\alpha^{-1}\delta) + \mathcal{O}(r_2), \\ \mu_2 &= -\beta^{-1}\delta\Omega\nu^{-1} + \mathcal{O}(r_2). \end{aligned} \tag{7.3}$$

Consider $r_2 = 0$. The linearization of (6.8) about (x_2^*, \hat{y}^*) is then given by

$$\dot{z} = Az, \quad A = \begin{pmatrix} 0 & \alpha w'(-\alpha^{-1}\delta) \\ \alpha^{-1}\Omega & \alpha\beta\Omega^{-1}w'(-\alpha^{-1}\delta)\mu_2 \end{pmatrix}, \tag{7.4}$$

where z is the variation of (x_2, \hat{y}) about (x_2^*, \hat{y}^*) and

$$w'(-\alpha^{-1}\delta) = -\frac{2\phi'(\hat{y}^*)}{(1 + \phi(\hat{y}^*))^2} = -\frac{1}{2}(1 - \alpha^{-1}\delta)^2\phi'(\hat{y}^*),$$

using (4.13) and the fact that

$$\phi(\hat{y}^*) = \frac{1 + \alpha^{-1}\delta}{1 - \alpha^{-1}\delta}.$$

The determinant of the coefficient matrix A is independent of μ_2 :

$$\det A = -\Omega w'(-\alpha^{-1}\delta) \tag{7.5}$$

and the trace of A is given by

$$\text{tr } A = \alpha\beta\Omega^{-1}w'(-\alpha^{-1}\delta)\mu_2 \tag{7.6}$$

which vanishes for $\mu_2 = 0$. Since $w' < 0$ from (4.13), the sign of $\det A$ is determined by the sign of Ω . Therefore we conclude the following:

LEMMA 7.1. *Consider $r_2 = 0$ and suppose $\alpha\delta < 0$.*

- For $\Omega < 0$ we have:
 - The equilibrium (x_2^*, \hat{y}^*) , defined in (7.2), is a neutral saddle for $\mu_2 = \mu_{2,N} \equiv 0$ and a generic saddle for $\mu_2 \neq \mu_{2,N}$.
 - The stable (unstable) eigenspace associated with (x_2^*, \hat{y}^*) and the linearization (7.4) is asymptotically vertical for $\beta\delta\Omega^{-1}\mu_2 \rightarrow \mp\infty$.
 - The unstable (stable) eigenspace associated with (x_2^*, \hat{y}^*) and the linearization (7.4) is asymptotically horizontal for $\beta\delta\Omega^{-1}\mu_2 \rightarrow \mp\infty$.
- For $\Omega > 0$ we have:
 - A Hopf bifurcation at $\mu_2 = \mu_{2,H} \equiv 0$.
 - The equilibrium (x_2^*, \hat{y}^*) is attracting (repelling) for $\beta\delta\Omega^{-1}\mu_2 \leq 0$.
 - For $|\mu_2| \in (\mu_{2,H}, \mu_{2,F})$, where

$$\mu_{2,F} \equiv \frac{2\Omega^{3/2}}{\sqrt{-w'(-\alpha^{-1}\delta)|\alpha\beta|}}, \quad (7.7)$$

- the equilibrium (x_2^*, \hat{y}^*) is a focus.
- For $|\mu_2| \geq \mu_{2,F}$, (x_2^*, \hat{y}^*) is a node.
- The strong eigenspace is asymptotically vertical for $\beta\delta\Omega^{-1}\mu_2 \rightarrow \pm\infty$.
- The weak eigenspace is asymptotically horizontal for $\beta\delta\Omega^{-1}\mu_2 \rightarrow \pm\infty$.

The quantities $\mu_{2,N}$, $\mu_{2,H}$ and $\mu_{2,F}$ perturb by an amount of $\mathcal{O}(r_2)$ for $r_2 \neq 0$ by the implicit function theorem.

Proof. From (7.4) we find the following eigenvalues and eigenvectors:

$$\lambda_{\pm} = \frac{\text{tr } A}{2} \pm \frac{1}{2}\sqrt{\text{tr}^2 A - 4\det A}, \quad (7.8)$$

$$v_{\pm} = \begin{pmatrix} \frac{\alpha}{\lambda_{\pm}} \\ 1 \end{pmatrix}. \quad (7.9)$$

For $\mu_2 = 0$ we have a neutral saddle for $\Omega < 0$ and a center for $\Omega > 0$, since $\text{tr } A = 0$ from (7.6) and the sign of $\det A$ is determined by the sign of Ω . Also, since $\frac{d}{d\mu_2}\text{tr } A \neq 0$, we have a Hopf bifurcation at $\mu_2 = \mu_{2,H} \equiv 0$ when $\Omega > 0$.

For $\Omega > 0$ we note that when

$$\text{tr } A = \pm 2\sqrt{\det A},$$

that is, when $\mu_2 = \mp\mu_{2,F}$ from (7.7), then the equilibrium (x_2^*, \hat{y}^*) is a node. It is attracting (repelling) for those μ_2 for which $\text{tr } A \leq 0$. So from (7.6), we conclude that (x_2^*, \hat{y}^*) is attracting (repelling) for $\beta\delta\Omega^{-1}\mu_2 \leq 0$.

For either sign of Ω we have, for $\beta\delta\Omega^{-1}\mu_2 \rightarrow \pm\infty$, that

$$\begin{aligned} \lambda_+ &\rightarrow \pm\infty, \\ \lambda_- &\rightarrow 0. \end{aligned}$$

So, for $\Omega < 0$, using (7.9), this means that the stable (unstable) eigenspace associated with (x_2^*, \hat{y}^*) and the linearization (7.4) is asymptotically vertical for $\beta\delta\Omega^{-1}\mu_2 \rightarrow \mp\infty$. On the other hand the unstable (stable) eigenspace is asymptotically horizontal for $\beta\delta\Omega^{-1}\mu_2 \rightarrow \mp\infty$.

Similarly for $\Omega > 0$ we find that the strong (weak) eigenspace⁶ associated with (x_2^*, \hat{y}^*) and the linearization (7.4) is asymptotically vertical (horizontal) for $\beta\delta\Omega^{-1}\mu_2 \rightarrow \pm\infty$. \square

The results of Lemma 7.1 are shown in Fig. 7.1, which can be compared with Fig. 3.2.

7.2. Charts $\kappa_{1,3}$. The results in Lemma 7.1 are in accordance with Proposition 3.3 in the limits $\mu_2 \rightarrow \pm\infty$. But they occur within chart κ_2 and everything collapses to $\mu = 0$ for $r_2 = 0$, see (6.2). To connect the results in chart κ_2 with the case $\mu = \mathcal{O}(1)$, we can consider charts $\kappa_{1,3}$. We obtain the following:

⁶The strong (weak) eigenspace is the eigenspace associated with the eigenvalue representing the stronger (weaker) contraction or expansion.

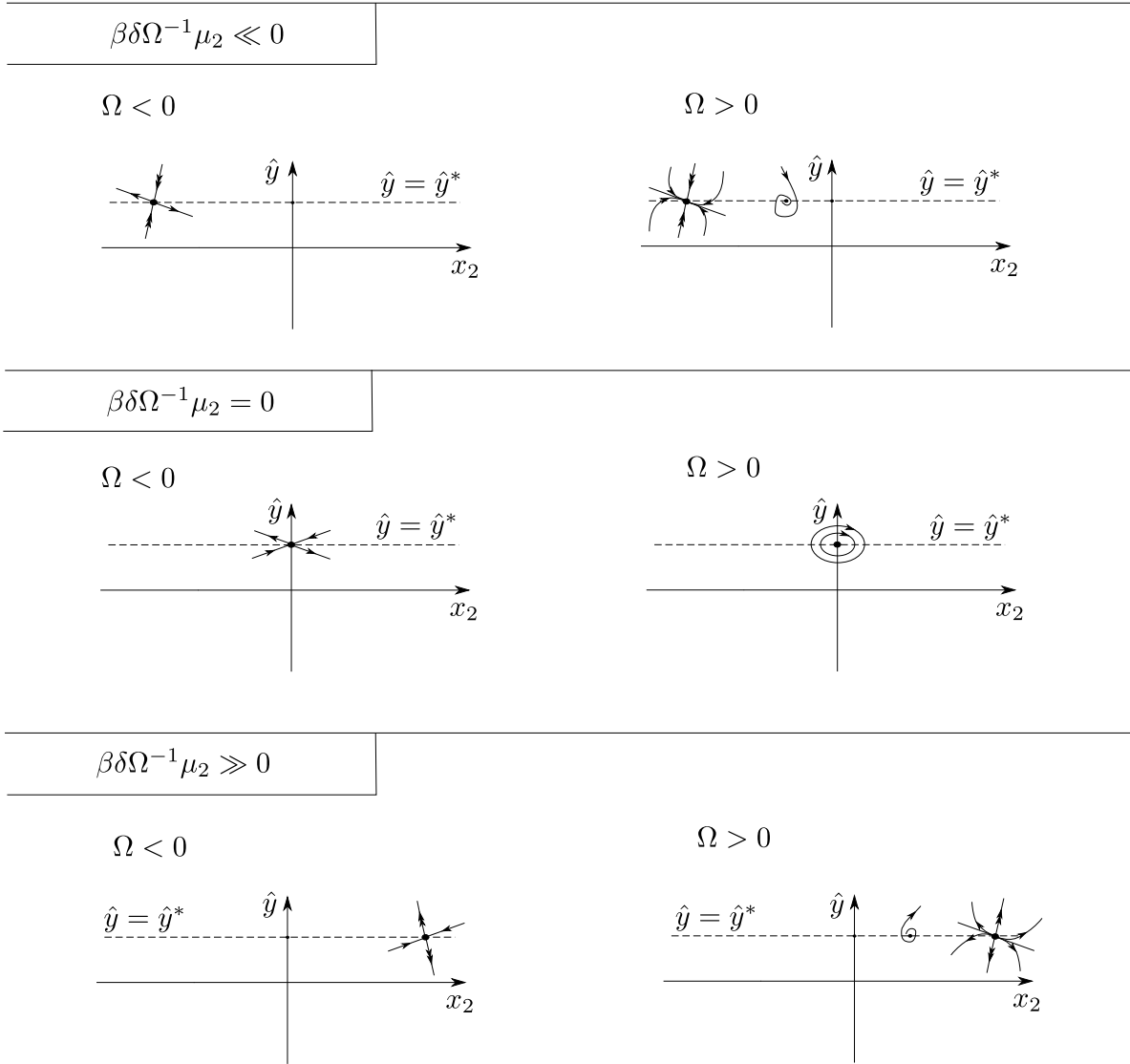


FIGURE 7.1. Results of Lemma 7.1. The dashed line corresponds to $\hat{y}^* = w^{-1}(-\alpha^{-1}\delta)$, from (7.2). This figure can be compared with Fig. 3.2.

LEMMA 7.2. The equilibria described in Lemma 7.1 belong to the same smooth, locally unique family of equilibria as those in (7.1). The equilibria do not undergo any further bifurcations in passing from Λ_2^\pm to Λ^\pm .

Proof. In chart κ_1 , we find the following family of equilibria:

$$\begin{aligned}\hat{y} &= w^{-1}(-\alpha^{-1}\delta) + \mathcal{O}(r_1 + \epsilon_1), \\ \mu_1 &= -\beta\delta\Omega^{-1} + \mathcal{O}(r_1 + \epsilon_1),\end{aligned}$$

within $M_{a,1}$. Using the conservation of ϵ and μ it is straightforward to trace this family of equilibria from Λ_1^- to Λ^- and connect them to the equilibria described in chart κ_2 with the $\mathcal{O}(1)$ equilibria described in (7.1). The analysis in chart κ_3 is identical. \square

7.3. The Hopf bifurcation for $\Omega > 0$. We now describe in further detail the Hopf bifurcation for $\Omega > 0$ in Lemma 7.1 and the resulting birth of limit cycles. As mentioned at the start of this section, we return to the time τ , since time $\tilde{\tau}$ defined in (4.15) and used in section 6 leads to difficulties when the periodic orbits leave the region of regularization $y \in (-\epsilon, \epsilon)$, or $\hat{y} \in (-1, 1)$ (whereas canards do not suffer this fate).

To proceed, we write the extended problem (4.14) in chart κ_2 to obtain

$$\begin{aligned} \dot{x}_2 &= (\delta + r_2\zeta^+ x_2 + \mathcal{O}(r_2(\mu_2 + r_2)))(1 + \phi(\hat{y})) + (\alpha + r_2\zeta^- x_2 + \mathcal{O}(r_2(\mu_2 + r_2)))(1 - \phi(\hat{y})), \\ \dot{\hat{y}} &= (x_2 + r_2\eta^+ x_2^2 + \mathcal{O}(r_2(\mu_2 + r_2)))(1 + \phi(\hat{y})) \\ &\quad + (-\beta(x_2 - \mu_2) + r_2\eta^-(x_2 - \mu_2)^2 + \mathcal{O}(r_2(\mu_2 + r_2)))(1 - \phi(\hat{y})). \end{aligned} \quad (7.10)$$

where we have multiplied time τ by r_2 . The equilibrium in (7.2) for $\alpha\delta < 0$ then becomes

$$(x_2^*, \hat{y}^*) \equiv \left(\beta\delta\Omega^{-1}\mu_2, \phi^{-1}\left(\frac{1 + \alpha^{-1}\delta}{1 - \alpha^{-1}\delta}\right) \right) + \mathcal{O}(r_2). \quad (7.11)$$

This equilibrium undergoes a Hopf bifurcation at $\mu_2 = \mu_{2,H} = \mathcal{O}(r_2)$ when $\Omega > 0$ (compare with Lemma 7.1). Let

$$\phi_{i,H} \equiv \phi^{(i)}(\hat{y}_0^*), \quad i = 1, 2, 3, \quad (7.12)$$

where

$$\hat{y}_0^* = \phi^{-1}\left(\frac{1 + \alpha^{-1}\delta}{1 - \alpha^{-1}\delta}\right), \quad (7.13)$$

and

$$\phi^{(i)} \equiv \frac{d^i \phi}{d\hat{y}^i}.$$

The subscript 0 in (7.13) is used to emphasize that \hat{y}^* has been obtained from (7.11) with $\mu_2 = r_2 = 0$. By assumption $\phi_{1,H} > 0$ and so we obtain

PROPOSITION 7.3. *System (7.10) has an equilibrium at (x_2^*, \hat{y}^*) , as defined in (7.11), which undergoes a Hopf bifurcation at*

$$\mu_2 = \mu_{2,H}(r_2)$$

where

$$\mu_{2,H}(r_2) \equiv \left(\frac{2(\alpha(\zeta^+ + \chi^+) - \delta(\zeta^- + \chi^-))\Omega}{(\alpha - \delta)^2 \phi_{1,H}} - (\chi^- + \beta\chi^+) \hat{y}_0^* \right) \beta^{-1} r_2 + \mathcal{O}(r_2^2). \quad (7.14)$$

The first Lyapunov coefficient is given by

$$a = a_2 r_2 + \mathcal{O}(r_2^2),$$

where

$$\begin{aligned} a_2 &= \frac{(\alpha - \delta)\phi_{1,H}^2}{16\Omega^2} \left((\beta + 1)^2 (\delta\zeta^- - \alpha\zeta^+) - (\alpha - \delta)^2 (\eta^- + \beta\eta^+) \right) + \frac{(\beta + 1)\phi_{2,H}}{16\Omega} (\delta\chi^- - \alpha\chi^+) \\ &\quad + \frac{1}{8} \left(\frac{\phi_{3,H}}{\phi_{1,H}(\alpha - \delta)} - \frac{\phi_{2,H}^2}{\phi_{1,H}^2(\alpha - \delta)} - \frac{(\beta + 1)\phi_{2,H}}{\Omega} \right) (\delta(\zeta^- + \chi^-) - \alpha(\zeta^+ + \chi^+)). \end{aligned} \quad (7.15)$$

If $a_2 \neq 0$ then for ϵ sufficiently small there exists a family of unique periodic solutions bifurcating from (x_2^*, \hat{y}^*) for

$$\begin{aligned} \beta\delta\Omega^{-1}\mu_2 &> \beta\delta\Omega^{-1}\mu_{2,H} \quad \text{when } a_2 < 0, \\ \beta\delta\Omega^{-1}\mu_2 &< \beta\delta\Omega^{-1}\mu_{2,H} \quad \text{when } a_2 > 0, \end{aligned}$$

with amplitude $\mathcal{O}\left(\sqrt{|\mu_2 - \mu_{2,H}|r_2^{-1}}\right)$. The periodic orbits are attracting for $a_2 < 0$ and repelling for $a_2 > 0$, for r_2 sufficiently small.

Proof. The calculation of a_2 is based on classical Hopf bifurcation theory [5]. \square

Note that the Hopf bifurcation is degenerate within $r_2 = 0$ since $a \equiv 0$ there. The reason for this is that the system (7.10) with $\mu_2 = 0$ and $r_2 = 0$ is Hamiltonian, as we shall now demonstrate. In this case, (7.10) becomes:

$$\begin{aligned} \dot{x}_2 &= \delta(1 + \phi(\hat{y})) + \alpha(1 - \phi(\hat{y})), \\ \dot{\hat{y}} &= (1 + \phi(\hat{y}) - \beta(1 - \phi(\hat{y})))x_2, \end{aligned} \quad (7.16)$$

The Hamiltonian function $H = H(x_2, \hat{y})$ is given by

$$H(x_2, \hat{y}) = \frac{1}{2}x_2^2 + \int_{\hat{y}_0^*}^{\hat{y}} \frac{\delta(1 + \phi(s)) + \alpha(1 - \phi(s))}{\beta(1 - \phi(s)) - (1 + \phi(s))} ds. \quad (7.17)$$

The symplectic structure matrix $J(x_2, \hat{y})$ is non-canonical:

$$J(x_2, \hat{y}) = (\beta(1 - \phi(\hat{y})) - (1 + \phi(\hat{y}))) \begin{pmatrix} 0 & 1 \\ -1 & 0 \end{pmatrix}, \quad (7.18)$$

which is regular and non-zero near $\hat{y} = \hat{y}_0^*$ since $\phi(\hat{y}_0^*) = \frac{1+\alpha^{-1}\delta}{1-\alpha^{-1}\delta}$, $\alpha\delta < 0$ and Assumption 3. Hence the system with $\mu_2 = 0$ and $r_2 = 0$ has a whole family of periodic orbits in the vicinity of (7.11) $_{\mu_2=r_2=0}$. The Hamiltonian system is not well-defined for $\hat{y} = \hat{y}_c$ (6.10), $\beta > 0$, since $J(x_2, \hat{y}_c) = 0$.

REMARK 7.4. *The periodic orbits within the (x_2, \hat{y}) -plane rotate about (7.11) in the counter clockwise (clockwise) direction if $\alpha > 0$ ($\alpha < 0$).*

Combining the results in Lemma 7.1, Lemma 7.2, and Proposition 7.3 we obtain one of our main results, Theorem 7.5, as follows:

THEOREM 7.5. *Assuming (5.2), the regularized system (4.3) has a smooth and locally unique family of equilibria*

$$(x, y) = (x^*, y^*)(\mu, \sqrt{\epsilon}) \equiv (\beta\delta\Omega^{-1}\mu + \mathcal{O}(\mu^2 + \epsilon), \mathcal{O}(\epsilon))$$

where $(x^*(\mu, 0), y^*(\mu, 0)) = (x^*(\mu, 0), 0)$ agrees with the family of pseudo-equilibria for the PWS system (see Proposition 3.3) and, in particular, $\partial_\mu x^*(\mu, 0) \neq 0$. For

$\Omega < 0$: *The family of equilibria consists of saddles and does not undergo any bifurcation.*

$\Omega > 0$: *The family of equilibria undergoes a Hopf bifurcation at $\mu = \sqrt{\epsilon}\mu_{2,H}(\sqrt{\epsilon}) = \mathcal{O}(\epsilon)$, where $\mu_{2,H}$ is given by (7.14). The first Lyapunov coefficient is given by $a = a_2\sqrt{\epsilon} + \mathcal{O}(\epsilon)$ where a_2 , given by (7.15), depends upon the regularization function ϕ .*

Note that a_2 , as given in (7.15), depends upon the regularization function ϕ , through $\phi_{1,H}$, $\phi_{2,H}$ and $\phi_{3,H}$ as defined in (7.12), and hence that the criticality of the Hopf bifurcation depends on ϕ . This observation leads to another one of our main results:

THEOREM 7.6. *Suppose that $\Omega > 0$ and $\alpha\delta < 0$ so that there exists a Hopf bifurcation. Then, provided*

$$\delta(\zeta^- + \chi^-) - \alpha(\zeta^+ + \chi^+) \neq 0, \quad (7.19)$$

all cases $a_2 < 0$, $a_2 = 0$ and $a_2 > 0$ can be attained by varying ϕ .

Proof. We are free to choose $\phi_{1,H} > 0$, $\phi_{2,H}$ and $\phi_{3,H}$ in (7.15). Note, from (7.15), that the equation $a_2 = 0$ is linear in $\phi_{3,H}$ and that the coefficient of $\phi_{3,H}$:

$$\frac{\delta(\zeta^- + \chi^-) - \alpha(\zeta^+ + \chi^+)}{8\phi_{1,H}(\alpha - \delta)}$$

is non-zero by assumption (7.19). Hence $a_2 = 0$ can be solved for $\phi_{3,H}$. The statement of the proposition therefore follows. \square

REMARK 7.7. *It seems natural to insist that ϕ should be an odd function. If ϕ were not odd, then one of the vector-fields X^\pm would be favoured over the other by the regularization. The functions ϕ that we used to*

prove Theorem 7.6 can be odd, at least if $\hat{y}_0^* \neq 0$. If $\hat{y}_0^* = 0$ and ϕ is odd, then $\phi_{2,H} = 0$. Hence, the equation $a_2 = 0$ should have a solution with $\phi_{3,H} < 0$ for ϕ to be odd and for Theorem 7.6 to apply.

REMARK 7.8. Another natural condition appears to be that ϕ' should be strictly increasing within $(-1, 0)$ and strictly decreasing within $(0, 1)$. The functions used in the proof of Theorem 7.6 may also be chosen to satisfy these conditions, at least when $\hat{y}_0^* \neq 0$. The functions then just have $\phi_{2,H} \geq 0$ for $\hat{y}_0^* \leq 0$. For $\hat{y}_0^* = 0$ we have $\phi_{2,H} = 0$ and the equation $a_2 = 0$ should have a solution with $\phi_{3,H} < 0$ to ensure $\phi''(\hat{y}) \geq 0$ for $\hat{y} \leq 0$ and that Theorem 7.6 apply.

8. Limit cycles of the regularized system. From section 3.3, limit cycles of the PWS system can exist for the case II_2 , which occurs when

$$\delta = -1, \quad \alpha > 0, \quad \beta < 0. \quad (8.1)$$

See also Table 3.1. Limit cycles can also occur in the regularized version of case VI_3 . This case occurs for

$$\delta = 1, \quad \beta > -\alpha > 0. \quad (8.2)$$

Note that $\beta > 0$ in (8.2) and hence from Theorem 6.4 the regularization of VI_3 also possesses a canard which is $\mathcal{O}(\sqrt{\epsilon})$ -close to the singular canard of the PWS system.

The regularization of II_2 and VI_3 , denoted by II_2^ϵ and VI_3^ϵ respectively, exhibit significant differences. In case II_2^ϵ , the limit cycles eventually (for μ_2 large enough) cross the region of regularization $\hat{y} \in (-1, 1)$ from $\hat{y} > 1$ to $\hat{y} < -1$ and back again. There is no sliding and hence no singular canards in the corresponding PWS case II_2 . Thus there are no canards in the regularized case II_2^ϵ . However, for VI_3^ϵ , the resulting limit cycles interact with the slow manifolds and the maximal canard to produce a scenario almost identical to the canard explosion phenomenon in classical slow-fast theory [21].

In this section we present a comprehensive study of the regularized limit cycles that are due to the Hopf bifurcation in chart κ_2 (see Proposition 7.3). In section 8.1, these limit cycles are followed, beyond the validity of the classical Hopf bifurcation theory, into large limit cycles in chart κ_2 . In terms of the original (x, y) -variables, from (6.2), these periodic orbits are, however, still small, only extending $\mathcal{O}(\sqrt{\epsilon})$ in the x -direction and $\mathcal{O}(\epsilon)$ in the y -direction. To follow these orbits to $\mathcal{O}(1)$ -size, and obtain a connection to the PWS system, we must use charts $\kappa_{1,3}$.

In doing so, we use different techniques for cases II_2^ϵ and VI_3^ϵ . We split the analysis into separate parts. In section 8.2.1 we study limit cycles of $\mathcal{O}(1)$ -size for case II_2^ϵ while section 8.2.2 contains the corresponding analysis for case VI_3^ϵ . The connection of these $\mathcal{O}(1)$ -limit cycles with the limit cycles in chart κ_2 for cases II_2^ϵ and VI_3^ϵ is shown in sections 8.3.1 and 8.3.2, respectively.

8.1. Chart κ_2 . Proposition 7.3 only guarantees the existence of small periodic orbits for μ_2/r_2 small within chart κ_2 . To follow these periodic orbits within chart κ_2 for larger values of μ_2/r_2 we follow the Melnikov-based approach of Krupa and Szmolyan [21]. We will consider both II_2^ϵ and VI_3^ϵ in this section.

First we define \hat{y}_0^h , \hat{y}_1^h and \hat{y}_2^h as follows. Consider the forward solution $\sigma = (x_2, \hat{y})(t)$ with initial condition $(0, \hat{y}_0^h)$ where the Hamiltonian H in (7.17) takes the value $H(0, \hat{y}_0^h) = h > 0$ and

$$\hat{y}_0^h < \hat{y}_0^*. \quad (8.3)$$

The point $(0, \hat{y}_2^h)$ is then the second return of σ to $x_2 = 0$ where

$$\hat{y}_2^h < \hat{y}_0^*.$$

Similarly, we let $(0, \hat{y}_1^h)$ denote the first return of σ to $x_2 = 0$ where

$$\hat{y}_1^h > \hat{y}_0^*.$$

The relevant quantities are shown in Fig. 8.1 for the case VI_3^ϵ . Notice that by (8.2) and $\Omega > 0$ it follows from (6.9) and (7.2) that the singular canard for $\mu_2 = r_2 = 0$ is above the bifurcating equilibrium. This is illustrated in Fig. 8.1 by letting the continuation of $S_{a,\epsilon}$ and $S_{r,\epsilon}$ lie above \hat{y}_0^* . The case II_2^ϵ is similar but there are no slow manifolds in this case.

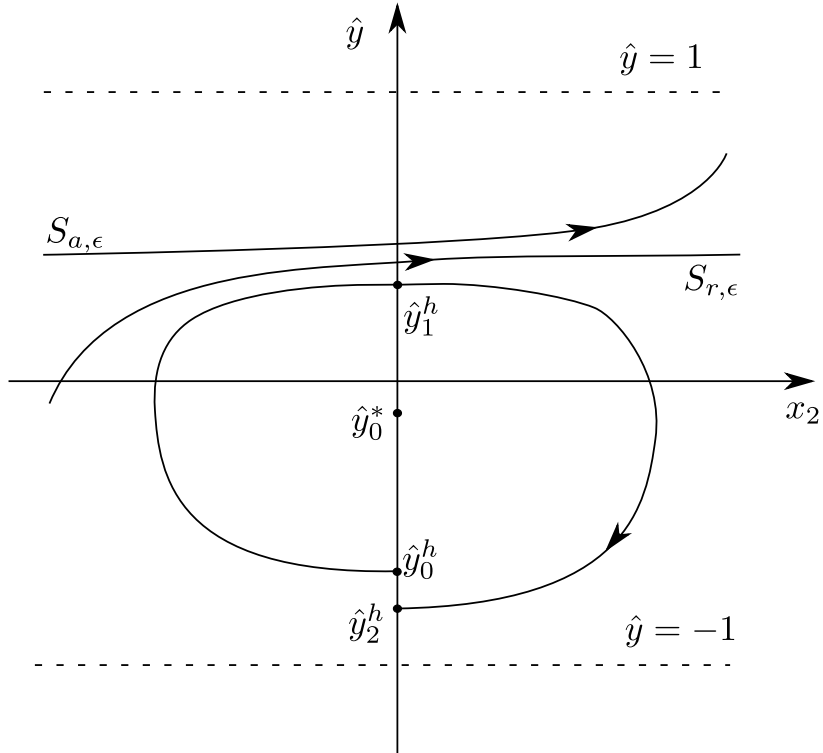


FIGURE 8.1. Illustration of \hat{y}_0^h , \hat{y}_1^h and \hat{y}_2^h for the case VI_3^ϵ . Here $S_{a,\epsilon}$ and $S_{r,\epsilon}$ are in fact the continuation $M_{a,2}(\epsilon)$ and $M_{r,2}(\epsilon)$ of the Fenichel slow manifolds into chart κ_2 . The case III_2^ϵ is similar but there are no slow manifolds in this case.

Following Proposition 7.3 there exists an $h_0 > 0$ independent of r_2 so that for $0 \leq h \leq h_0$ there exists a locally unique family of limit cycles parametrized by μ_2 whose stability is determined by the sign of a_2 given in (7.15). We therefore take $h \geq h_0 > 0$ and consider the following distance function

$$D(r_2, \mu_2, h) = H(0, \hat{y}_2^h) - H(0, \hat{y}_0^h). \quad (8.4)$$

From the analysis preceding Proposition 7.3, the system with $\mu_2 = r_2 = 0$ is Hamiltonian and hence $D(0, 0, h) = 0$ for all $h \geq 0$. Also since

$$\partial_{\hat{y}} H = \frac{\delta(1 + \phi(\hat{y})) + \alpha(1 - \phi(\hat{y}))}{\beta(1 - \phi(\hat{y})) - (1 + \phi(\hat{y}))} \neq 0,$$

for $\hat{y} < \hat{y}_0^*$ (in accordance with (8.3)), roots of the equation $D = 0$ correspond to periodic orbits.

Let T^h denote the period of the orbit σ of the Hamiltonian system with $\mu_2 = r_2 = 0$ satisfying $H(\sigma) = h$. We have the following lemma, similar to [21, Proposition 4.1]:

LEMMA 8.1. *For $h \geq h_0$ we have*

$$D(r_2, \mu_2, h) = D_{r_2}(h)r_2 + D_{\mu_2}(h)\mu_2 + \mathcal{O}((r_2 + \mu_2)^2), \quad (8.5)$$

where

$$D_{r_2}(h) = 2 \int_0^{T^h/2} (\zeta^+(1 + \phi(\hat{y})) + \zeta^-(1 - \phi(\hat{y})))x_2^2 + \frac{\delta(1 + \phi(\hat{y})) + \alpha(1 - \phi(\hat{y}))}{\beta(1 - \phi(\hat{y})) - (1 + \phi(\hat{y}))} ((\eta^+x_2^2 + \chi^+\hat{y})(1 + \phi(\hat{y})) + (\eta^-x_2^2 + \chi^-\hat{y})(1 - \phi(\hat{y})))dt, \quad (8.6)$$

$$D_{\mu_2}(h) = -4 \int_{\hat{y}_0^h}^{\hat{y}_1^h} \frac{\beta\phi'(y)}{(\beta(1 - \phi(\hat{y})) - (1 + \phi(\hat{y})))^2} x_2 d\hat{y}, \quad (8.7)$$

where $(x_2, \hat{y})(t)$ satisfies (7.16) with $(x_2, \hat{y})(0) = (0, \hat{y}_0^h)$, $H(x_2, \hat{y}) = h$ and $(x_2, \hat{y})(T^h/2) = (0, \hat{y}_1^h)$.

Proof. Similar calculations to those in [21, Proposition 4.1] lead to

$$\begin{aligned} D_{r_2}(h) &= \int_0^{T^h} \nabla H(x_2(t), \hat{y}(t)) \cdot G_{r_2}(x_2(t), \hat{y}(t)) dt, \\ D_{\mu_2}(h) &= \int_0^{T^h} \nabla H(x_2(t), \hat{y}(t)) \cdot G_{\mu_2}(x_2(t), \hat{y}(t)) dt, \end{aligned}$$

where

$$\begin{aligned} G_{r_2}(x_2, \hat{y}) &= \begin{pmatrix} (\zeta^+(1 + \phi(\hat{y})) + \zeta^-(1 - \phi(\hat{y})))x_2 \\ (\eta^+x_2^2 + \chi^+\hat{y})(1 + \phi(\hat{y})) + (\eta^-x_2^2 + \chi^-\hat{y})(1 - \phi(\hat{y})) \end{pmatrix}, \\ G_{\mu_2}(x_2, \hat{y}) &= \begin{pmatrix} 0 \\ (1 - \phi(\hat{y}))\beta \end{pmatrix}. \end{aligned}$$

The Hamiltonian system possesses a time-reversible symmetry $(x_2, \hat{y}, t) \mapsto (-x_2, \hat{y}, -t)$ so:

$$\begin{aligned} D_{r_2}(h) &= 2 \int_0^{T^h/2} \nabla H(x_2(t), \hat{y}(t)) \cdot G_{r_2}(x_2(t), \hat{y}(t)) dt, \\ D_{\mu_2}(h) &= 2 \int_0^{T^h/2} \nabla H(x_2(t), \hat{y}(t)) \cdot G_{\mu_2}(x_2(t), \hat{y}(t)) dt. \end{aligned}$$

For $D_{\mu_2}(h)$ we then use integration by parts. \square

REMARK 8.2. If $|\hat{y}_0^h|, |\hat{y}_1^h| > 1$ then D_{μ_2} can be simplified further:

$$D_{\mu_2}(h) = -4 \int_{-1}^1 \frac{\beta x_2}{(\beta(1 - \phi) - (1 + \phi))^2} d\phi. \quad (8.8)$$

This is only relevant for case II_2^ϵ . In the case VI_3^ϵ the maximal canard prevents the local limit cycles from entering $\hat{y} \geq 1$ (see Fig. 8.1).

Since $D_{\mu_2}(h) \neq 0$ we can apply the implicit function theorem to conclude the following:

PROPOSITION 8.3. Fix $\nu > 0$ small. The family of limit cycles from the Hopf bifurcation, described in Proposition 7.3, can be continued into periodic orbits corresponding to roots of $D(r_2, \mu_2, h)$ for $h \leq 2\nu^{-2}$ and $r_2 \leq r_{20}(\nu)$ sufficiently small. The orbits are $\mathcal{O}(r_2)$ -close to the periodic orbits of the Hamiltonian system $H = H(x_2, \hat{y})$ defined in (7.17).

Proof. From (8.5) and the implicit function theorem we obtain

$$\mu_2 = -\frac{D_{r_2}(h)}{D_{\mu_2}(h)} r_2 + \mathcal{O}(r_2^2). \quad (8.9)$$

\square

REMARK 8.4. The periodic orbit with $h = 2\nu^{-2}$ intersects $\hat{y} = \hat{y}_0^*$ in $x_2 = \mp 2\nu^{-1}$ for $\mu_2 = r_2 = 0$. By Proposition 8.3 we are therefore able to continue periodic orbits beyond the sections Λ_2^\mp in chart κ_2 . These orbits belong to a C^k -smooth and locally unique family because they are obtained using an argument based on the implicit function theorem for $\mu_2 = r_2 = 0$.

8.2. $\mathcal{O}(1)$ limit cycles. We now wish to consider limit cycles of the regularized system with amplitudes that are $\mathcal{O}(1)$ with respect to ϵ . As mentioned above, the analysis is divided into two cases: II_2^ϵ and VI_3^ϵ .

8.2.1. $\mathcal{O}(1)$ -limit cycles for case II_2^ϵ . We start by obtaining $\mathcal{O}(1)$ -periodic orbits in the original (x, y) -variables by following fixed points of a Poincaré map:

$$P_\epsilon : \{y = \epsilon, x > 0\} \rightarrow \{y = \epsilon, x > 0\}, \quad (8.10)$$

where defined under the flow of the regularized system. Since these orbits are $\mathcal{O}(1)$ with respect to ϵ and only involve crossing (see Fig. 3.3 case II_2), the mapping P_ϵ is smoothly $\mathcal{O}(\epsilon)$ -close to P_0 , as defined in (3.6) for the PWS system. We therefore obtain the following proposition.

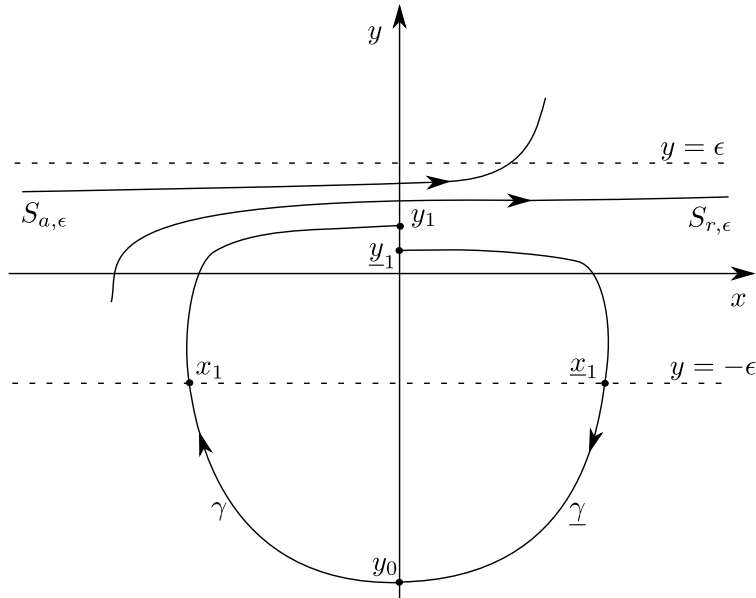


FIGURE 8.2. Important quantities for case VI_3^ϵ , relevant to Proposition 8.6. The region of regularization $y \in (-\epsilon, \epsilon)$ is exaggerated for illustrative purposes.

PROPOSITION 8.5. Fix μ_0 small and consider (8.1). Suppose that $|\mu| \geq \mu_0 > 0$ and $\Delta_{II_2} \neq 0$, where Δ_{II_2} is defined in (3.8). Then for $\epsilon \leq \epsilon_0(\mu_0)$ sufficiently small, the regularized system has a family of periodic orbits corresponding to fixed points of P_ϵ of the following form

$$x_\epsilon(\mu) = x_0(\mu) + \mathcal{O}(\epsilon),$$

with $x_0(\mu)$ given by (3.9), and $\mu \Delta_{II_2}^{-1} < -\mu_0 |\Delta_{II_2}|^{-1} < 0$. The periodic orbits are attracting for $\Delta_{II_2} < 0$ and repelling for $\Delta_{II_2} > 0$. Moreover, they are continuously $\mathcal{O}(\epsilon)$ -close to periodic orbits of the PWS system.

Proof. Proposition 8.5 gives non-degenerate fixed points $x_0(\mu)$ of P_0 for $\mu \Delta_{II_2}^{-1} < -\mu_0 |\Delta_{II_2}|^{-1} < 0$. Since $P_\epsilon = P_0 + \mathcal{O}(\epsilon)$ we can apply the implicit function theorem to obtain fixed points $x_\epsilon(\mu) = x_0(\mu) + \mathcal{O}(\epsilon)$ of P_ϵ . The stability of the fixed points $x_\epsilon(\mu)$ is also determined by the stability of $x_0(\mu)$ as a fixed point of P_0 . \square

8.2.2. $\mathcal{O}(1)$ -limit cycles for case VI_3^ϵ . This case has a canard at $\mu = r_2 \mu_{2,c}$ and a Hopf bifurcation at $\mu = r_2 \mu_{2,H}$. The co-existence of a Hopf bifurcation and a canard leads to the canard explosion phenomenon in which the amplitude of limit cycles undergo $\mathcal{O}(1)$ variations within an exponentially small parameter regime. In order to prove this statement, we follow the proof of a related assertion in [21, Proposition 5.1] for classical planar slow-fast systems.

Let $\mu = r_2 \mu_2 = \sqrt{\epsilon} \mu_2$ and consider the original (x, y) -variables, in which the region of regularization is $y \in (-\epsilon, \epsilon)$, and let γ be the forward orbit with initial condition $(x, y)(0) = (0, y_0)$ where $y_0 < 0$ small but independent of ϵ . The situation is illustrated in Fig. 8.2. Since the fold of the associated PWS system is invisible from below (see (8.1) and Proposition 2.4) we know that the first return of γ with $x = 0$ is a point $(0, y_1)$ with $y_1 = \mathcal{O}(\epsilon)$. Let $\underline{\gamma}$ be the backward orbit with initial condition $(x, y)(0) = (0, y_0)$. Denote by $(0, \underline{y}_1)$ the first return of $\underline{\gamma}$ with $x = 0$. Here $\underline{y}_1 = \mathcal{O}(\epsilon)$. Let $(x_1(y_0, \epsilon), -\epsilon)$ and $(\underline{x}_1(y_0, \epsilon), -\epsilon)$ denote the first intersections of γ and $\underline{\gamma}$, respectively, with $y = -\epsilon$. The functions $x_1(y_0, \epsilon)$ and $\underline{x}_1(y_0, \epsilon)$ are smooth in y_0 and ϵ . In particular, $x_1(y_0, 0)$ and $\underline{x}_1(y_0, 0)$ can be obtained from the associated PWS system.

We consider the distance function:

$$\mathcal{D}(y_0, \mu_2) = y_1 - \underline{y}_1.$$

Roots of \mathcal{D} correspond to periodic orbits. As in [21] we solve $\mathcal{D}(y_0, \mu_2) = 0$ by noting, from Fenichel theory, that

$$\mathcal{D}(y_0, \mu_{2,c}) = \mathcal{O}(e^{-c/\epsilon}), \quad c = c(y_0) > 0.$$

Since $S_{r,\epsilon}$ and $S_{a,\epsilon}$ are transverse for $\mu_2 = \mu_{2,c}$ this then effectively implies the existence of a $\mu_2 = \mu_{2,p}(y_0)$ solving $\mathcal{D}(y_0, \mu_2) = 0$ and satisfying $\mu_{2,p} = \mu_{2,c} + \mathcal{O}(e^{-c/\epsilon})$. Since x_1 and \underline{x}_1 are increasing functions of y_0 for y_0 small, it also follows that $\mu_{2,p}(y_0)$ approaches $\mu_{2,c}$ monotonically as y_0 increases, at least for y_0 sufficiently small. The stability of the periodic orbits is determined by the sign of a *way-in/way-out* function $R = R(y_0)$, see [21, Proposition 5.4], that measures the contraction and expansion along $S_{a,r}$. In our case the contraction and expansion is determined by the following function

$$(X_2^+(x, 0, 0) - X_2^-(x, 0, 0))\phi'(\hat{y}).$$

Inserting $\hat{y} = \hat{y}_c = \phi^{-1}\left(\frac{\beta-1}{\beta+1}\right)$ from (6.10), which corresponds to $S_{a,r}$ for $\mu_2 = r_2 = 0$, we obtain the function $R = R(y_0)$:

$$R(y_0) = \phi_{1,c} \int_{x_1(y_0,0)}^{\underline{x}_1(y_0,0)} (X_2^+(x, 0, 0) - X_2^-(x, 0, 0))dx.$$

Since $\phi_{1,c} = \phi'(\hat{y}_c) > 0$, the sign of R coincides with the sign of

$$\tilde{R}(y_0) = \int_{x_1(y_0,0)}^{\underline{x}_1(y_0,0)} (X_2^+(x, 0, 0) - X_2^-(x, 0, 0))dx.$$

We obtain the following proposition:

PROPOSITION 8.6. *Consider a point $p = (0, y_0)$ with $y_0 \in [-c_1^{-1}, -c_2^{-1}]$ with $c_2 > c_1$ sufficiently large but fixed. Then for $\epsilon \leq \epsilon_0(c_1, c_2)$ sufficiently small there exists a unique periodic orbit through p for $\mu = \mu_p(r_2, y_0)$ where*

$$\mu_p(r_2, y_0) \equiv \mu_c + \mathcal{O}(e^{-c/\epsilon}).$$

The function $\mu_p(r_2, \cdot)$ is monotonic so that $\mu_p(r_2, y_0)$ approaches $\mu_c(r_2)$ as y_0 increases.

The periodic orbits are attracting if

$$\Delta_{VI_3} \equiv \frac{2}{3\alpha\beta} (\alpha(\eta^- + \beta\eta^+) + \beta(\beta + 1)(\zeta^- + \chi^-)), \quad (8.11)$$

is negative. They are repelling if Δ_{VI_3} is positive.

Proof. To verify the statement about stability we need to compute $\tilde{R}(y_0)$. To do this we invert $x_1 = x_1(y_0, 0)$ for y_0 and parametrize \underline{x}_1 in terms of x_1 rather than y_0 . Then $\underline{x}_1(x_1)$ is obtained from the map σ_0^- in Lemma 3.5 with $\mu = 0$:

$$\underline{x}_1 = \sigma_0^-(x_1) = -x_1 + A^-x_1^2 + \mathcal{O}(x_1^3),$$

using the backward flow of X^- , where A^- is given by (3.5). We therefore consider the following integral

$$\begin{aligned} \tilde{R}(x_1) &= \int_{x_1}^{\underline{x}_1(x_1)} (X_2^+(x, 0, 0) - X_2^-(x, 0, 0))dx \\ &= \int_{x_1}^{\underline{x}_1(x_1)} ((1 + \beta)x + (\eta^+ - \eta^-)x^2 + \mathcal{O}(x^3))dx \\ &= \left(A^-(1 + \beta) + \frac{2}{3}(\eta^+ - \eta^-) \right) |x_1|^3 + \mathcal{O}(x_1^4). \end{aligned}$$

Hence the sign of $\tilde{R}(x_1)$ is determined by

$$A^-(1 + \beta) + \frac{2}{3}(\eta^+ - \eta^-) = \frac{2}{3\alpha\beta} (\alpha(\eta^- + \beta\eta^+) + \beta(\beta + 1)\zeta^-),$$

where we have used (3.5). The right hand side is (8.11). Since $\tilde{R} < 0$ implies stability while $\tilde{R} > 0$ implies instability the result follows for x_1 (and hence y_0) sufficiently small. \square

REMARK 8.7. *In classical planar slow-fast systems [21], a canard is generically associated with a Hopf bifurcation and a canard explosion. This is not necessarily the case here. For example the PWS case VV_1*

has a singular canard but no local limit cycles in either the PWS system or its regularization. Conversely, the regularized system can undergo a Hopf bifurcation without the presence of a canard. This is demonstrated by case II_2^ϵ .

We conclude this subsection with Table 8.1 which summarizes properties of the seven regularized two-folds (compare with Table 3.1).

Table 8.1: 1: type of regularized two-fold singularity. 2: value of $\alpha\delta$. 3: equilibrium (x = no, \checkmark = yes). 4: sign of Ω . 5: Hopf (x = no, \checkmark = yes, n.a. = not applicable). 6: value of β . 7: canard (x = no, \checkmark = yes).

1	2	3	4	5	6	7
Type	$\alpha\delta$	Equilibrium	Ω	Hopf	β	Canard
VV_1^ϵ	+	x	+	n.a.	+	\checkmark
VV_2^ϵ	-	\checkmark	-	x	-	x
VI_1^ϵ	+	x	\pm	n.a.	-	x
VI_2^ϵ	-	\checkmark	-	x	+	\checkmark
VI_3^ϵ	-	\checkmark	+	\checkmark	+	\checkmark
II_1^ϵ	+	x	-	n.a.	+	\checkmark
II_2^ϵ	-	\checkmark	+	\checkmark	-	x

8.3. Connecting limit cycles. Having obtained $\mathcal{O}(1)$ limit cycles in the two cases II_2^ϵ and VI_3^ϵ , we now analyze the connection between these limit cycles and those described by Proposition 8.3 that are due to the Hopf bifurcation. The results are summarized in one of our main results:

THEOREM 8.8. *For ϵ sufficiently small:*

II_2^ϵ : *There exists a C^k -smooth family of locally unique periodic orbits of the regularized system (4.3) that is due to the Hopf bifurcation in Theorem 7.5. If $a_2 < 0$ ($a_2 > 0$) where a_2 is the first Lyapunov coefficient as defined in (7.15), then the periodic orbits are attracting (repelling) near the Hopf bifurcation. If*

$$\Delta_{II_2} = \frac{2}{3\alpha\beta} (\alpha(\eta^- + \beta\eta^+) + \beta(\zeta^- + \chi^- + \alpha(\zeta^+ + \chi^+))), \quad (3.8)$$

is negative (positive) then the periodic orbits for $\Delta_{II_2}^{-1}\mu \leq -c\sqrt{\epsilon}$, $c > 0$ sufficiently large, are attracting (repelling). The periodic orbits for $\mu = \mathcal{O}(1)$ (with respect to ϵ) are continuously $\mathcal{O}(\epsilon)$ -close to the PWS periodic orbits in Proposition 3.6.

VI_3^ϵ : *There exists a C^k -smooth family of small periodic orbits of the regularized system (4.3) that is due to the Hopf bifurcation in Theorem 7.5. There also exists a C^k -smooth family of periodic orbits that are $\mathcal{O}(1)$ (with respect to ϵ) in amplitude and which undergo a canard explosion, where the amplitude changes by $\mathcal{O}(1)$ within an exponentially small parameter regime around the canard value $\mu = \sqrt{\epsilon}\mu_{2,c}(\sqrt{\epsilon})$ (see Theorem 6.4). If $a_2 < 0$ ($a_2 > 0$) where a_2 is the first Lyapunov coefficient as defined in (7.15), then the periodic orbits are attracting (repelling) near the Hopf bifurcation. If*

$$\Delta_{VI_3} = \frac{2}{3\alpha\beta} (\alpha(\eta^- + \beta\eta^+) + \beta(\beta + 1)(\zeta^- + \chi^-)) \quad (8.11)$$

is negative (positive) then the $\mathcal{O}(1)$ -periodic orbits are attracting (repelling).

The proof of Theorem 8.8 is divided into two cases: II_2^ϵ and VI_3^ϵ .

8.3.1. Connecting limit cycles for case II_2^ϵ using charts $\kappa_{1,3}$. To connect the periodic orbits described in chart κ_2 by Proposition 8.3 with the $\mathcal{O}(1)$ periodic orbits in Proposition 8.5 we first return to the original (x, y) variables in which the region of regularization is $y \in (-\epsilon, \epsilon)$ and consider the mappings σ_ϵ^\pm taking (x_0, ϵ) to $(\sigma_\epsilon^+(x_0), \epsilon)$ and $(x_1, -\epsilon)$ to $(\sigma_\epsilon^-(x_1), -\epsilon)$, respectively. See Fig. 8.3. We have:

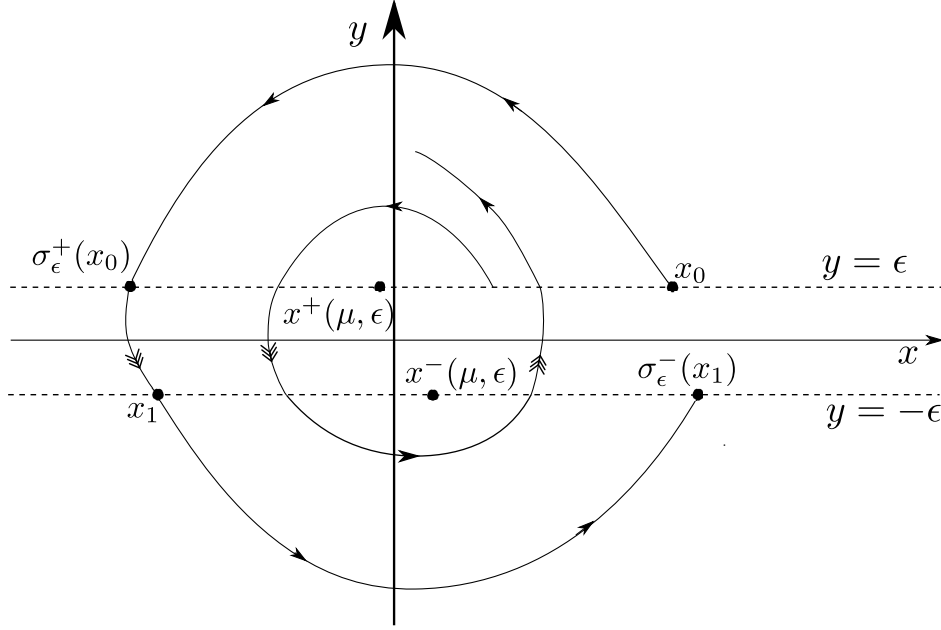


FIGURE 8.3. The mappings σ_ϵ^\pm associated with the regularization of the invisible two-fold singularity II_2 , where $\delta = -1$, $\alpha > 0$ and $\beta < 0$. The points $(x, y) = (x^\pm, \pm\epsilon)$ are points where $X_2^\pm(x, \pm\epsilon, \mu) = 0$. Note that the mappings ξ_1^- and ξ_3^+ in (8.16) and (8.17) describe the fast transitions indicated in the figure by the triple-headed arrows, using the charts κ_1 and κ_3 . These transitions would appear nearly vertical in the stretched coordinate system (x, \hat{y}) .

LEMMA 8.9. Fix $c > 0$ large. The maps σ_ϵ^\pm are defined for

$$x \in (x_f^+(\mu, \epsilon), c^{-1}] \quad \text{where} \quad x_f^+(\mu, \epsilon) \equiv -\chi^+\epsilon + \mathcal{O}(\epsilon(\mu + \epsilon)), \quad (8.12)$$

and

$$x \in [-c^{-1}, x_f^-(\mu, \epsilon)) \quad \text{where} \quad x_f^-(\mu, \epsilon) \equiv \mu - \beta^-\chi^-\epsilon + \mathcal{O}(\epsilon(\mu + \epsilon)), \quad (8.13)$$

respectively and for those x the maps σ_ϵ^\pm satisfy

$$\sigma_\epsilon^\pm = \sigma_0^\pm + \mathcal{O}(\epsilon), \quad (8.14)$$

where σ_0^\pm are described in Lemma 3.5.

Proof. The mappings σ_0^\pm map $\{y = 0\}$ to itself by the forward flow of X^\pm for $x > 0$ and $x < \mu$, respectively. The mappings σ_ϵ^\pm , on the other hand, map $\{y = \pm\epsilon\}$ to itself by the forward flow of X^\pm , respectively. Here σ_ϵ^+ is defined for $x > x_f^+(\mu, \epsilon)$ where $X_2^+(x_f^+(\mu, \epsilon), \epsilon, \mu) = 0$ while σ_ϵ^- is defined for $x < x_f^-(\mu, \epsilon)$ where $X_2^-(x_f^-(\mu, \epsilon), -\epsilon, \mu) = 0$. Using (2.12) and (2.13) and the implicit function theorem gives (8.12) and (8.13), respectively, for c sufficiently large. Equation (8.14) therefore follows by standard regular perturbation theory. \square

REMARK 8.10. The mappings σ_ϵ^\pm do not depend upon the regularization. They are due to (4.4) determined by X^\pm .

We now write these mappings σ_ϵ^\mp in terms of the charts $\kappa_{1,3}$. The resulting mappings will be denoted by

$$\sigma_{31}^- = \kappa_3 \circ \sigma_\epsilon^- \circ \kappa_1^{-1},$$

and

$$\sigma_{13}^+ = \kappa_1 \circ \sigma_\epsilon^+ \circ \kappa_3^{-1},$$

respectively, using the subscripts to highlight that these mappings are from κ_1 (κ_3) to κ_3 (κ_1), respectively.

LEMMA 8.11. Consider (8.1). In terms of the charts $\kappa_{1,3}$ the mappings σ_ϵ^\mp take the following forms:

$$\begin{aligned}\sigma_{31}^- : \quad & \kappa_1 \cap \{\hat{y} = -1\} \rightarrow \kappa_3 \cap \{\hat{y} = -1\}, \\ & r_3 = r_1(1 + 2\mu_1 + A^- r_1 + \mathcal{O}(r_1(\epsilon_1 + \mu_1 + r_1))), \\ & \epsilon_3 = \epsilon_1(1 - 2(2\mu_1 + A^- r_1) + \mathcal{O}(r_1(\epsilon_1 + \mu_1 + r_1) + \mu_1^2)), \\ & \mu_3 = \mu_1(1 - (2\mu_1 + A^- r_1) + \mathcal{O}(r_1(\epsilon_1 + \mu_1 + r_1) + \mu_1^2)),\end{aligned}$$

and

$$\begin{aligned}\sigma_{13}^+ : \quad & \kappa_3 \cap \{\hat{y} = 1\} \rightarrow \kappa_1 \cap \{\hat{y} = 1\}, \\ & r_1 = r_3(1 - A^+ r_3 + \mathcal{O}(r_3(\epsilon_3 + \mu_3 + r_3))), \\ & \epsilon_1 = \epsilon_3(1 + 2A^+ r_3 + \mathcal{O}(r_3(\epsilon_3 + \mu_3 + r_3))), \\ & \mu_1 = \mu_3(1 + A^+ r_3 + \mathcal{O}(r_3(\epsilon_3 + \mu_3 + r_3))),\end{aligned}$$

respectively, for r_1 , ϵ_1 and μ_1 sufficiently small.

Proof. Consider the case σ_ϵ^- (the case σ_ϵ^+ is identical). We then use (8.14) and Lemma 3.5 and set $x_1 = -r_1$ and $x_3 = r_3$ as described by the charts $\kappa_{1,3}$, respectively. The expressions for ϵ_3 and μ_3 then follow from the conservation of ϵ and μ , respectively. The condition (8.12) and (8.13) are satisfied for r_3 , ϵ_3 , μ_3 and r_1 , ϵ_1 , μ_1 , respectively, sufficiently small. \square

We then consider the Poincaré mapping P_ϵ from (8.10) used in Proposition 8.5 and write this mapping in chart κ_3 . The resulting mapping is given by

$$\begin{aligned}P_3 = \kappa_3 \circ P_\epsilon \circ \kappa_3^{-1} : \quad & \kappa_3 \cap \{\hat{y} = 1\} \rightarrow \kappa_3 \cap \{\hat{y} = 1\}, \\ & (r_3, \epsilon_3, \mu_3) \mapsto (r_3^+, \epsilon_3^+, \mu_3^+),\end{aligned}\tag{8.15}$$

We will compose P_3 into four different mappings σ_{13}^+ , ξ_1^- , σ_{31}^- and ξ_3^+ so that:

$$P_3 = \xi_3^+ \circ \sigma_{31}^- \circ \xi_1^- \circ \sigma_{13}^+.$$

The mappings σ_{13}^+ and σ_{31}^- are described in Lemma 8.11 while ξ_1^- and ξ_3^+ are given in terms of the forward flow associated with the differential equations in charts κ_1 and κ_3 (see (6.13) and (6.15)) and map $\{y = \pm\epsilon\}$ ($\{\hat{y} = \pm 1\}$) to $\{y = \mp\epsilon\}$ ($\{\hat{y} = \mp 1\}$), respectively. Hence the mappings:

$$\begin{aligned}\xi_1^- : \quad & \{\hat{y} = 1\} \rightarrow \{\hat{y} = -1\}, \\ & (r_1, \epsilon_1, \mu_1) \mapsto (r_1^-, \epsilon_1^-, \mu_1^-),\end{aligned}\tag{8.16}$$

and

$$\begin{aligned}\xi_3^+ : \quad & \{\hat{y} = -1\} \rightarrow \{\hat{y} = 1\}, \\ & (r_3, \epsilon_3, \mu_3) \mapsto (r_3^+, \epsilon_3^+, \mu_3^+),\end{aligned}\tag{8.17}$$

are defined by the forward flow of the following equations:

$$\dot{r}_1 = -r_1 \epsilon_1 \tilde{F}_1(r_1, \hat{y}, \epsilon_1, \mu_1),\tag{8.18}$$

$$\dot{\hat{y}} = (-1 + \mathcal{O}(r_1))(1 + \phi(\hat{y})) + (\beta(1 + \mu_1) + \mathcal{O}(r_1))(1 - \phi(\hat{y})),$$

$$\dot{\epsilon}_1 = 2\epsilon_1^2 \tilde{F}_1(r_1, \hat{y}, \epsilon_1, \mu_1),$$

$$\dot{\mu}_1 = \epsilon_1 \mu_1 \tilde{F}_1(r_1, \hat{y}, \epsilon_1, \mu_1),\tag{8.19}$$

and

$$\dot{r}_3 = r_3 \epsilon_3 \tilde{F}_3(r_3, \hat{y}, \epsilon_3, \mu_3),$$

$$\dot{\hat{y}} = (1 + \mathcal{O}(r_3))(1 + \phi(\hat{y})) + (-\beta(1 - \mu_3) + \mathcal{O}(r_3))(1 - \phi(\hat{y})),$$

$$\dot{\epsilon}_3 = -2\epsilon_3^2 \tilde{F}_3(r_3, \hat{y}, \epsilon_3, \mu_3),$$

$$\dot{\mu}_3 = -\epsilon_3 \mu_3 \tilde{F}_3(r_3, \hat{y}, \epsilon_3, \mu_3),$$

respectively. These equations are equations (6.13) and (6.15), respectively, written in terms of \hat{y} rather than w , where

$$\begin{aligned}\tilde{F}_1(r_1, \hat{y}, \epsilon_1, \mu_1) &= (-1 + \mathcal{O}(r_1))(1 + \phi(\hat{y})) + (\alpha + \mathcal{O}(r_1))(1 - \phi(\hat{y})), \\ \tilde{F}_3(r_3, \hat{y}, \epsilon_3, \mu_3) &= (-1 + \mathcal{O}(r_3))(1 + \phi(\hat{y})) + (\alpha + \mathcal{O}(r_3))(1 - \phi(\hat{y})).\end{aligned}$$

LEMMA 8.12. *Consider (8.1) and let*

$$E = \int_{-1}^1 \frac{-(1 + \phi(\hat{y})) + \alpha(1 - \phi(\hat{y}))}{1 + \phi(\hat{y}) - \beta(1 - \phi(\hat{y}))} d\hat{y}.$$

Then the mappings ξ_1^-, ξ_3^+ in (8.16) and (8.17) take the following form:

$$\begin{aligned}\xi_1^- : r_1^- &= r_1(1 - E\epsilon_1 + \mathcal{O}(r_1\epsilon_1)), \\ \epsilon_1^- &= \epsilon_1(1 + 2E\epsilon_1 + \mathcal{O}(r_1\epsilon_1)), \\ \mu_1^- &= \mu_1(1 + E\epsilon_1 + \mathcal{O}(r_1\epsilon_1)),\end{aligned}$$

and

$$\begin{aligned}\xi_3^+ : r_3^+ &= r_3(1 + E\epsilon_3 + \mathcal{O}(r_3\epsilon_3)), \\ \epsilon_3^+ &= \epsilon_3(1 - 2E\epsilon_3 + \mathcal{O}(r_3\epsilon_3)), \\ \mu_3^+ &= \mu_3(1 - E\epsilon_3 + \mathcal{O}(r_3\epsilon_3)).\end{aligned}$$

Proof. Consider ξ_1^- and (8.18) (the analysis for ξ_3^+ is identical). Since $\beta < 0$ we have that $\dot{\hat{y}} < 0$ for $\hat{y} \in [-1, 1]$ for $r_1 = \mu_1 = 0$ and hence we can replace time by \hat{y} by dividing the equations for $\dot{r}_1, \dot{\epsilon}_1$ and $\dot{\mu}_1$ by $\dot{\hat{y}}$. The point $(r_1, \epsilon_1, \mu_1) = 0$ is a fixed point of these equations. Solving the second order variational equations gives the desired result. \square

We then have:

LEMMA 8.13. *Consider (8.1). The Poincaré map $P_3 : (r_3, \epsilon_3, \mu_3) \mapsto (r_3^+, \epsilon_3^+, \mu_3^+)$ takes the following form:*

$$\begin{aligned}P_3 : r_3^+ &= r_3(1 + 2\mu_3 + \Delta_{II_2}r_3 + \mathcal{O}(r_3(\epsilon_3 + \mu_3 + r_3))), \\ \epsilon_3^+ &= \epsilon_3(1 - 2(2\mu_3 + \Delta_{II_2}r_3) + \mathcal{O}(r_3(\epsilon_3 + \mu_3 + r_3))), \\ \mu_3^+ &= \mu_3(1 - (2\mu_3 + \Delta_{II_2}r_3) + \mathcal{O}(r_3(\epsilon_3 + \mu_3 + r_3))),\end{aligned}\tag{8.20}$$

where Δ_{II_2} is given by (3.8).

Proof. We use Lemma 8.12 and Lemma 8.11. \square

REMARK 8.14. *Note that to leading order (8.20) is independent of E and hence of ϕ , the regularization function. Hence ϕ does not induce bifurcations in the transition from sufficiently large limit cycles (meaning ν sufficiently small) in chart κ_2 to the $\mathcal{O}(1)$ limit cycles.*

Next, we solve for fixed points of P_3 and obtain:

PROPOSITION 8.15. *Suppose that Δ_{II_2} in (3.8) is non-zero. Then for μ_3, ϵ_3 sufficiently small and $\mu_3\Delta_{II_2}^{-1} < 0$, the mapping P_3 has a locally unique family of fixed points:*

$$r_3 = -2\mu_3\Delta_{II_2}^{-1} + \mathcal{O}(\mu_3(\epsilon_3 + \mu_3)).\tag{8.21}$$

The family of fixed point of P_3 corresponds to a C^k -smooth family of periodic orbits which are attracting (repelling) for $\Delta_{II_2} < 0$ ($\Delta_{II_2} > 0$).

Proof. Suppose that (r_3, μ_3, ϵ_3) is a fixed point of P_3 . Then since $\mu = r_3\mu_3$ and $\epsilon = r_3\epsilon_3$ we solve for $r_3 = r_3(\mu_3, \epsilon_3)$ by setting $r_3^+ = r_3$ in (8.20). This gives

$$2\mu_3 + \Delta_{II_2}r_3 + \mathcal{O}(r_3(\epsilon_3 + \mu_3 + r_3)) = 0.$$

We solve this equation by the implicit function theorem and obtain (8.21). The statement about stability follows from the fact that the sign of Δ_{II_2} determines the sign of $\partial_{r_3} r_3^+ = r_3(\Delta_{II_2} + \mathcal{O}(\epsilon_3 + \mu_3 + r_3))$. \square

The periodic orbits in chart κ_2 , described by Proposition 8.3, that are due to the Hopf bifurcation, are locally unique since they are obtained by the implicit function theorem for $\mu_2 = r_2 = 0$. These orbits can be continued all the way up to the section Λ_2^+ , defined in (6.11) (see also Remark 8.4). The periodic orbits that are $\mathcal{O}(1)$ with respect to $\mathcal{O}(\epsilon)$, described by Proposition 8.5, are also locally unique by virtue of the implicit function theorem. Therefore by setting $\epsilon_3 = \nu^2$, corresponding to the section Λ_2^+ (6.11), and taking ν sufficiently small, we obtain:

$$x_2 = \nu^{-1}, \hat{y} = 1, \mu_2 = -\frac{\Delta_{II_2}}{2\nu^2} r_2 + \mathcal{O}(r_2^2), \quad (8.22)$$

using (6.7) and (8.21). Therefore we can conclude that the periodic orbits described by (8.21) coincide with the locally unique ones in chart κ_2 described by Proposition 8.3. Similarly, setting $r_3 = \rho$, corresponding to section Λ^+ (4.19), shows that the periodic orbits in (8.21) coincide with those in Proposition 8.5, where these are defined. This gives a C^k -smooth and locally unique family of periodic orbits as described by Theorem 8.8, case II_2^ϵ .

REMARK 8.16. *We believe that the application of the directional charts $\kappa_{1,3}$ in this section to describe the Poincaré-mapping P_ϵ is a novelty. The coordinates of $\kappa_{1,3}$ enabled us to connect the periodic orbits in chart κ_2 with the larger periodic orbits without the need for careful estimation. This is a general advantage of the blowup method and the phase directional charts $\kappa_{1,3}$. Having said that, it might be possible to prove the connection of the limit cycles in κ_2 with the larger limit cycles in Proposition 8.5 by working in chart κ_2 alone. To do this one would, however, have to perform a careful estimation of the function D in (8.4). The following remark, Remark 8.17, contains a discussion of this issue.*

REMARK 8.17. *By (6.7) it follows that the family of fixed points of P_3 described in Proposition 8.15 intersects Λ_2^+ in (8.22). By Theorem 8.8, case II_2^ϵ , this fixed point of P_3 corresponds to a periodic orbit obtained from Proposition 8.3 for a corresponding value of the energy constant h . Hence the value of μ_2 in (8.22) must agree with the value given in (8.9). This is a corollary of Theorem 8.8, case II_2^ϵ . One may expect that there could be a more direct way of showing this. We now outline a formal derivation of the result by approximation the integrals in D_{r_2} and D_{μ_2} in (8.9).*

Since $x_2 = \nu^{-1}$ in (8.22) we take $h = \frac{1}{2\nu^2}$. To compute D_{r_2} (8.6) we first substitute $dt = ((1 + \phi) - \beta(1 - \phi))x_2 dy$ and integrate from \hat{y}_0^h to \hat{y}_1^h . We then split this integration into (a) an integration from $\hat{y} = \hat{y}_0^h$ to $\hat{y} = 0$ and (b) an integration from $\hat{y} = 0$ to $\hat{y} = \hat{y}_1^h$. We then ignore the contribution from the region of regularization and simply set $\phi = \mp 1$ in the integrations (a) and (b), respectively. We apply the same approximation to the Hamiltonian $H(x_2, \hat{y})$ and obtain the value of \hat{y}_0^h and \hat{y}_1^h from the equation $H(0, \hat{y}) = h$. Combining this gives the following approximation of D_{r_2} :

$$D_{r_2} \approx \frac{2}{3\nu^3\beta\alpha} (\alpha(\eta^- + \beta\eta^+) + \beta(\zeta^- + \chi^- + \alpha(\zeta^+ + \chi^+))),$$

which is valid for ν small. Hence

$$D_{r_2} \approx \frac{\Delta_{II_2}}{\nu^3},$$

from (3.8). For D_{μ_2} , as defined in (8.7), we use (8.8) and approximate x_2 by the constant value ν^{-1} . This gives

$$D_{\mu_2} \approx \frac{2}{\nu}.$$

Hence, from (8.9), we have

$$\mu_2 \approx -\frac{\Delta_{II_2}}{2\nu^2} r_2,$$

which agrees with (8.22). We have not pursued a rigorous result of this kind.

8.3.2. Connecting limit cycles for case VI_3^ϵ . Krupa and Szmolyan [21] describe the classical canard explosion phenomenon, as observed in the van der Pol system. They prove that the periodic orbits within their chart κ_2 belong to a smooth and unique family of local periodic orbits that also includes $\mathcal{O}(1)$ periodic orbits that arise from their canard explosion. Their proof involves careful estimation on the dependency of the function $D(r_2, \mu_2, h)$, as defined in (8.4), on the distance to the singular canard (measured by the energy constant h). It seems plausible that a similar analysis could be performed to our system. However, the situation here is complicated by the fact that our Hamiltonian function H depends non-trivially on the regularization function ϕ . The statements in Theorem 8.8, case VI_3^ϵ , therefore summarize the previous results in Proposition 8.3 and Proposition 8.6. Instead we conjecture on the connection of small periodic orbits in Proposition 8.3 with the larger ones in Proposition 8.6 as follows:

CONJECTURE 1. *The two families of periodic orbits in VI_3^ϵ belong to the same family of locally unique periodic orbits.*

The limit cycles in Proposition 8.3 and Proposition 8.6 do not seem to be present in the PWS case VI_3 .

8.4. Saddle-node bifurcation. We conclude this section with the following main result

THEOREM 8.18. *Suppose (7.19) and (5.4). Then for ϵ sufficiently small:*

II_2^ϵ : *There exists an open set of regularization functions such that the periodic orbits in Theorem 8.8, case II_2^ϵ , undergo at least one saddle-node bifurcation.*

VI_3^ϵ : *Suppose, in addition, that Conjecture 1 holds. Then there exists an open set of regularization functions such that the periodic orbits in Theorem 8.8, case VI_3^ϵ , undergo at least one saddle-node bifurcation.*

Proof. A corollary of Theorem 7.6 is that we can always achieve $a_2\Delta_{II_2} < 0$ or $a_2\Delta_{VI_3} < 0$. The result therefore follows from the statements in Theorem 8.8 and Conjecture 1. \square

9. Numerics. In this section we illustrate the results in Theorem 8.18, and provide further support for Conjecture 1, by computing limit cycles for two model systems, for cases II_2^ϵ and VI_3^ϵ .

9.1. Case II_2^ϵ . In this section we consider the regularization of the following model system for case II_2 :

$$X^+(x, y) = \begin{pmatrix} -1 - 7x \\ x + 2x^2 \end{pmatrix}, \quad X^-(x, y, \mu) = \begin{pmatrix} 1 - 6x \\ (x - \mu) - 2(x - \mu)^2 \end{pmatrix}, \quad (9.1)$$

corresponding to the following parameters:

$$\delta = -1, \alpha = 1, \beta = -1, \zeta^+ = -7, \zeta^- = -6, \eta^\pm = \pm 2, \chi^\pm = 0, \Omega = 2,$$

in (2.12) and (2.13). The constant Δ_{II_2} given in (3.8) takes the value:

$$\Delta_{II_2} = -6.$$

According to Proposition 3.6 the limit cycles of the PWS system are therefore all stable. According to Theorem 8.8 the $\mathcal{O}(1)$ (with respect to ϵ) limit cycles of the regularized system are also stable.

We consider two regularization functions⁷:

$$\phi^l(\hat{y}) = \hat{y} \quad \text{for } \hat{y} \in (-1, 1), \quad (9.2)$$

and

$$\phi^c(\hat{y}) = \frac{3}{2}\hat{y} - \frac{1}{2}\hat{y}^3 \quad \text{for } \hat{y} \in (-1, 1). \quad (9.3)$$

From (7.13) we obtain $\hat{y}_0^* = 0$ in both cases. Inserting the corresponding values of $\phi_{1,H} = \phi'(0)$, $\phi_{2,H} = \phi''(0) = 0$, $\phi_{3,H} = \phi^{(3)}(0)$ into (7.14) and (7.15) gives the following values for $\mu_{2,H}$ and a_2 :

$$\begin{aligned} \mu_{2,H}^l &= 13r_2 + \mathcal{O}(r_2^2), \\ a_2^l &= \frac{1}{2}, \\ \mu_{2,H}^c &= \frac{26}{3}r_2 + \mathcal{O}(r_2^2) = \left(8 + \frac{2}{3}\right)r_2 + \mathcal{O}(r_2^2), \\ a_2^c &= -\frac{1}{2}. \end{aligned} \quad (9.4)$$

⁷The superscripts l and c refer to linear and cubic, respectively.

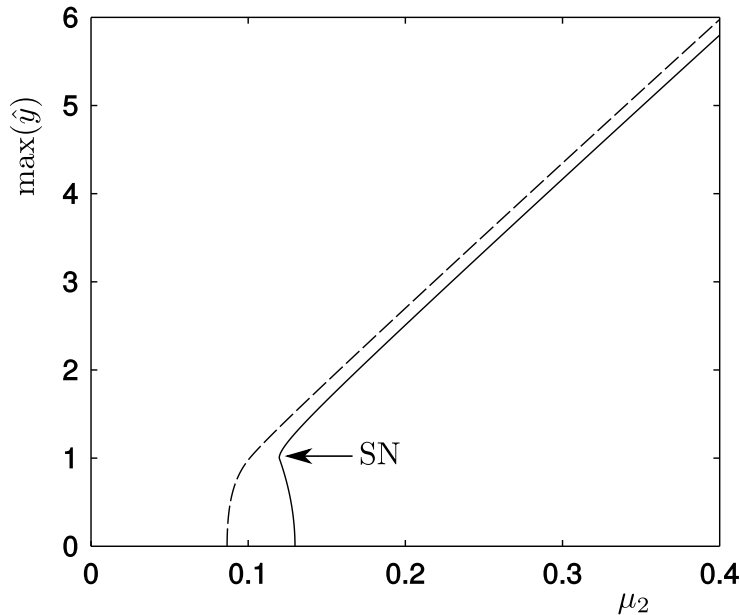


FIGURE 9.1. Periodic orbit amplitudes as a function of the parameter μ_2 for $r_2 = 0.01$. The full line shows the result of using the linear regularization function (9.2), the dotted line shows the result of using the cubic regularization function (9.3). As can be seen, the linear regularization function induces a saddle-node (SN) bifurcation, in agreement with Theorem 8.18.

Since $a_2^l \Delta_{II_2} < 0$ we have from Theorem 8.18 that the *linear* regularization function (9.2) introduces a saddle-node bifurcation. We demonstrate this as follows.

Using the numerical bifurcation software AUTO we continued the periodic orbits in the two regularizations of II_2 . In Fig. 9.1 we show the amplitude (measured as $\max(\hat{y})$) of the periodic orbits as a function of the parameter μ_2 for $r_2 = \sqrt{\epsilon} = 0.01$. The full line shows the result of using ϕ_l , as given in (9.2), while the dotted line shows the result of using ϕ_c , as given in (9.3). The linear regularization function introduces a saddle-node bifurcation, in agreement with Theorem 8.18. On the other hand, the *cubic* regularization function does not introduce any saddle-node bifurcation.

The Hopf bifurcations were numerically found to occur at

$$\mu_{2,H}^l \approx 0.1298, \quad \mu_{2,H}^c \approx 0.0866,$$

which are in good agreement with (9.4) for $r_2 = 0.01$. Also, in agreement with Proposition 8.5, we observed that the two family of limit cycles agree for larger values of μ_2 since the limit cycles for both regularizations must be $\mathcal{O}(\epsilon)$ -close to the limit cycles of the PWS system for $\mu = \mathcal{O}(1)$.

REMARK 9.1. We obtained system (9.1) by fixing (9.2) and (9.3) and the parameters δ, α, β and solving $a_2^l = -a_2^c$ for ζ^\pm and η^\pm setting $\chi^\pm = 0$ for simplicity.

9.2. Case VI_3^5 . In this section we consider the following model system for the case VI_3 :

$$X^+ = \begin{pmatrix} 1 + \frac{1}{2}x \\ x - x^3 \end{pmatrix}, \quad X^- = \begin{pmatrix} -1 \\ -2(x - \mu) + (x - \mu)^2 \end{pmatrix}. \quad (9.5)$$

Here

$$\delta = 1, \quad \alpha = -1, \quad \beta = 2, \quad \zeta^+ = \frac{1}{2}, \quad \zeta^- = 0, \quad \eta^+ = 0, \quad \eta^- = 1, \quad \chi^\pm = 0, \quad \Omega = 1.$$

We sketch the PWS system in Fig. 9.2 for $\mu = 0$. It is very similar to Fig. 12 in [22]. However, as opposed to [22] we have included the cubic term in X^+ which gives rise to an invisible tangency at $(x, y) = (1, 0)$ and a return mechanism from Σ^+ to Σ^- .

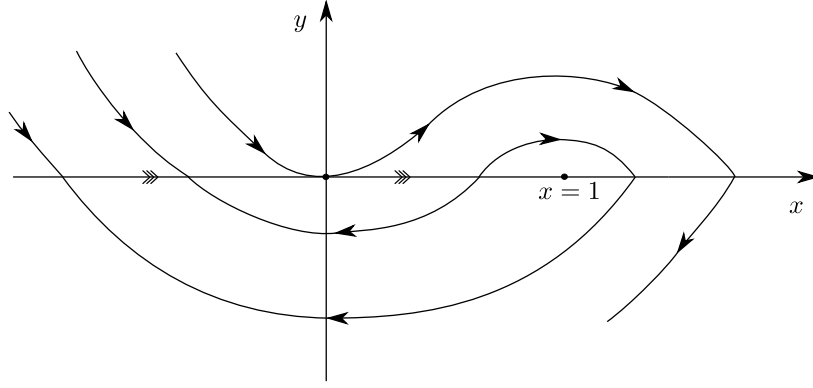


FIGURE 9.2. Sketch of the PWS system (9.5) for $\mu = 0$. The triple-headed arrows within Σ indicate the direction of the sliding vector field.

We then regularize X in (9.5) using the cubic function in (9.3). Since $\Omega = 1 > 0$, we can apply Proposition 7.3 to the regularized system and conclude that the system has an equilibrium (7.11) which undergoes a Hopf bifurcation at

$$\mu_2 = \mu_{2,H}^c \equiv -\frac{1}{12}r_2 + \mathcal{O}(r_2^2). \quad (9.6)$$

The first Lyapunov coefficient is obtained from (7.15):

$$a = -\frac{5}{64}r_2 + \mathcal{O}(r_2^2). \quad (9.7)$$

Since $a_2^c \equiv -\frac{5}{64} < 0$ we conclude that the periodic orbits are attracting for r_2 (and hence ϵ) sufficiently small and appear for $\mu_2 > \mu_{2,H}^c$.

This example also has a maximal canard (see Theorem 6.4). The parameter value at which it occurs is, from (6.22), given by

$$\mu_{2,c}^c = -\frac{1}{9\phi_{1,c}}r_2 + \mathcal{O}(r_2^2) \approx -0.07806r_2 + \mathcal{O}(r_2^2), \quad (9.8)$$

In the last expression we have used (6.10) to obtain

$$\phi_{1,c} \approx 1.4233.$$

There is a related example for the case VI_3 in [22] on p. 2169 (after reversing time and reflecting $x \mapsto -x$) with the same values of δ , α and β . The system in [22] has $\zeta^\pm = \mp 1$ as the only non-zero coefficients in (2.11). The reason for modifying the system given in [22] is that their system gives $a_2 = 0$ from (7.15), for all regularization functions ϕ . In fact a detailed calculation shows that $a \equiv 0$. The example in [22] is therefore codimension two for the regularization.

In Fig. 9.3 we have used the numerical bifurcation software AUTO to track the amplitudes of the limit cycles of (9.5) emanating from the equilibrium (7.2). We considered $r_2 = 0.1$. The amplitude of the limit cycles is now measured in Fig. 9.3 using $\max(x)$ instead of $\max(\hat{y})$ used above. This proved to be more illustrative in this case. A dramatic increase in amplitude is seen near $\mu_2 \approx -7.836574 \times 10^{-3}$. In Fig. 9.4 we have illustrated three different limit cycles within the original (x, y) -plane. The largest limit cycle looks like a *canard*. The three limit cycles occur for the following parameters:

$$\begin{aligned} \mu_2 &= -7.85 \times 10^{-3}, \\ \mu_2 &= -7.8365738 \times 10^{-3}, \\ \mu_2 &= -7.8365737 \times 10^{-3}. \end{aligned}$$

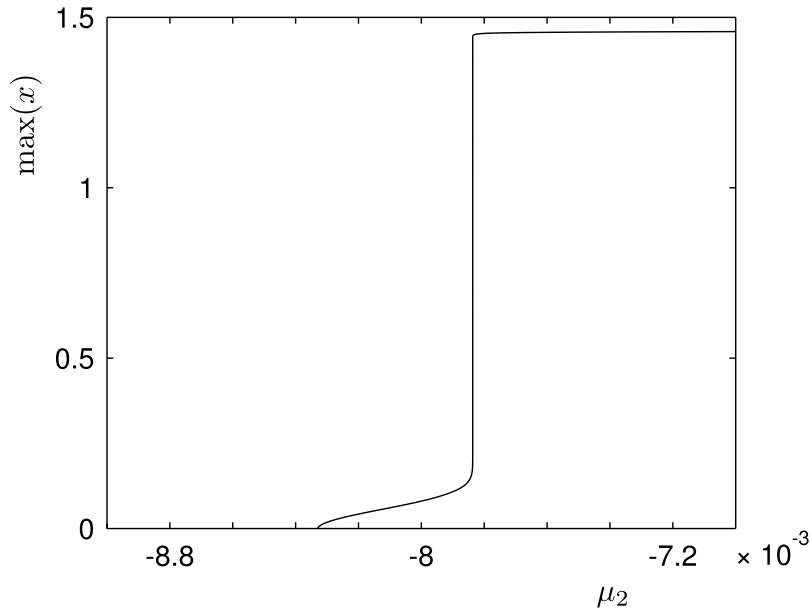


FIGURE 9.3. The amplitude of the limit cycles, measured in terms of $\max(x)$, as a function of μ_2 . The amplitude explodes due to the presence of a maximal canard around $\mu_2 \approx -7.8366 \times 10^{-3}$. The flat part beyond the canard explosion gives rise to the canard-like limit cycles similar the one shown in Fig. 9.4.

The difference between the last two parameters is 10^{-11} . The dramatic increase of amplitude is due to the canard explosion phenomenon described in Proposition 8.6. Numerically we found the following canard value

$$\mu_{2,c}^c = -7.8365738 \times 10^{-3}. \quad (9.9)$$

This value is in good agreement with (9.8) for $r_2 = 0.1$. Note that in comparison to the classical *canard* relaxation oscillation in the van der Pol system, the duck's head and chest are in our case, not due to motion along a curved slow manifold. Instead they are due to regular motion within Σ_{\pm} following the regular vector fields X^{\pm} , respectively. It is the motion along the slow manifold that creates the straight back of the duck. Also in the present case these different types of motions occur on an identical time-scale. There is a slow-fast behaviour but it is hidden and only visible through the scaling $\hat{y} = y/\epsilon$.

Now we replace the cubic regularization function in (9.3) by the following septic C^1 regularization function⁸:

$$\phi^s(\hat{y}) = -\frac{55}{54}\hat{y}^7 + \frac{83}{54}\hat{y}^5 - \frac{14}{27}\hat{y}^3 + \hat{y}, \quad \hat{y} \in (-1, 1). \quad (9.10)$$

This regularization function has been constructed so that a_2 , using (7.15), becomes

$$a_2^s = \frac{5}{64}.$$

This value is just the negative of the previous value a_2^c in (9.7). Hence periodic orbits emanating from the Hopf bifurcation are repelling and appear for $\mu < \mu_{2,H}$ where now

$$\mu_{2,H} = \mu_{2,H}^s \equiv -\frac{1}{8}\sqrt{\epsilon} + \mathcal{O}(\epsilon). \quad (9.11)$$

The canard value $\mu_{2,c}$ also changes and becomes

$$\mu_{2,c}^s \approx -0.12188\sqrt{\epsilon} + \mathcal{O}(\epsilon). \quad (9.12)$$

⁸The superscript s now stands for *septic*.

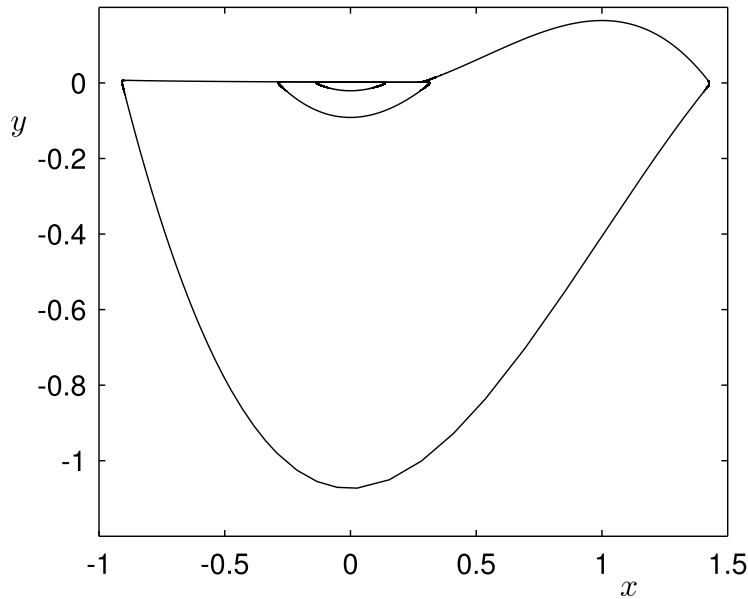


FIGURE 9.4. Three different limit cycles. Due to the canard explosion phenomenon (see Fig. 9.3) the difference in parameter between the largest and the second largest limit cycle is extremely small: 10^{-11} .

We again use AUTO with $r_2 = 0.1$ to continue periodic orbits from the Hopf bifurcation at $\mu = \mu_{2,H}^s$ (9.11). We obtain the bifurcation diagram in Fig. 9.5. As opposed to Fig. 9.3 we now observe a saddle-node (SN) bifurcation, which occurs before the canard explosion phenomenon.

REMARK 9.2. Fixing the values of δ , α and β it is straightforward to construct a family of model systems for VI_3 where the Lyapunov coefficients corresponding to regularization functions ϕ^l and ϕ^c (see (9.2) and (9.3)) have opposite signs: $a_2^l a_2^c < 0$. A simple example is the following:

$$X^+(x, y) = \begin{pmatrix} 1 + 7x \\ x + 8x^2 \end{pmatrix}, \quad X^-(x, y, \mu) = \begin{pmatrix} -1 + 6x \\ -\frac{3}{2}(x - \mu) + 8(x - \mu)^2 \end{pmatrix},$$

where

$$a_2^l = -\frac{5}{8}, \quad a_2^c = \frac{7}{32}.$$

However, we have not presented the details of this case since the saddle-node bifurcation occurs very close to the canard value and therefore it is not as clearly visible as the saddle-node in Fig. 9.5.

REMARK 9.3. This “duck” part in Fig. 9.4 is not covered by our results. However, it seems very plausible that the results in [21] can be extended to this case too.

10. Discussion and Conclusions. In this paper, we have considered the regularization of the codimension one two-fold bifurcation in planar PWS systems. The PWS two-fold bifurcation is dynamically very interesting as it may include singular canards, pseudo-equilibria and limit cycles. Using the blowup method of Krupa and Szmolyan [19], we continued these objects into the regularization and we related the PWS bifurcations to standard smooth bifurcations. Perhaps most interestingly, we were able to show that the regularization can induce saddle-node bifurcations of the limit cycles. The results were illustrated by numerical examples.

There are two questions that emerge from this work that we feel are worthy of further discussion. What light can regularization shed on the original PWS system? Is the introduction of saddle-node bifurcations a necessary consequence of regularization?

For the first question, it is clear that singular canards and pseudo-equilibria of the PWS system are limits of equivalent objects in the regularized system. Similarly, limit cycles in the PWS two-fold case II_2

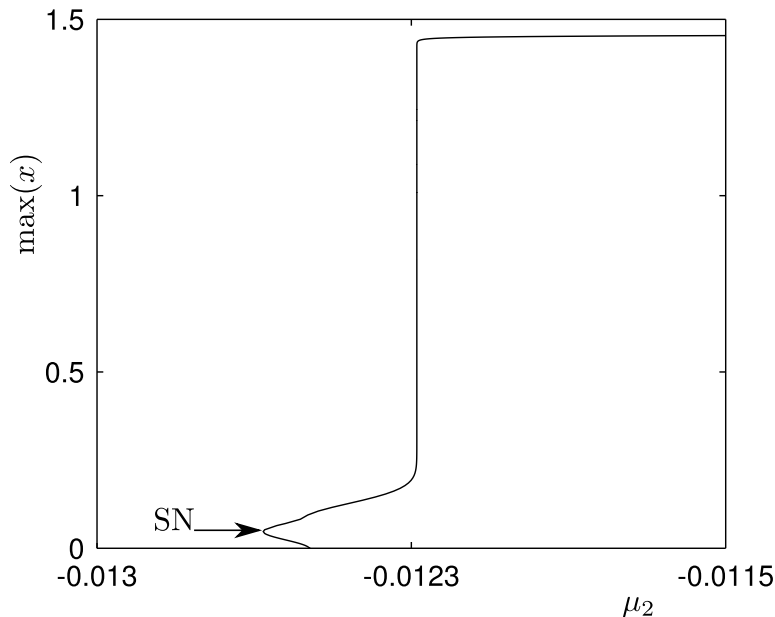


FIGURE 9.5. This diagram shows the amplitude of the limit cycles, measured in terms of $\max(x)$, as a function of μ_2 using the septic regularization function (9.10) to regularize the system (9.5). The amplitude explodes due to the presence of a maximal canard around $\mu_2 \approx -1.22369 \times 10^{-2}$.

are limits as $\epsilon \rightarrow 0$ of limit cycles in the regularized case II_2^{ϵ} , at least “macroscopically”; the saddle-node bifurcations occur “microscopically” within chart κ_2 . In comparison, the PWS case VI_3 is more singular. It possesses backwards and forwards non-uniqueness of orbits due to the presence of stable and unstable sliding. In particular, it is possible to identify closed “singular cycles”, reminiscent of singular cycles in slow-fast systems such as the van der Pol system (see Fig. 3.4). Our analysis showed that these singular cycles are limits of periodic orbits of the regularization. Interestingly, the quantity Δ_{VI_3} defined in (8.11) only depends on the PWS system, giving us an insight into the stability of a very singular object. The limit cycles of the regularization undergo a canard explosion phenomenon which gives rise to a very rapid amplitude increase of local periodic orbits. This can lead to global limit cycles as it was shown in section 9.2 and Fig. 9.4.

The second question is much broader. In this paper, we have considered planar two-folds, subject to the Sotomayor and Teixeira [30] regularization. We have shown that the criticality of Hopf bifurcations depends on the regularization function and generically it is possible to induce saddle-node bifurcations by varying the regularization function. But we have not shown how many saddle-node bifurcations may exist. Perhaps there are other PWS systems where the regularization does not induce bifurcations. Or there may be systems where other types of behaviour occur upon regularization. In addition there are other regularizations that could be considered.

REFERENCES

- [1] E. Benoît, J. L. Callot, F. Diener, and M. Diener. Chasse au canard. *Collect. Math.*, 31-32:37–119, 1981.
- [2] C. A. Buzzi, P. R. da Silva, and M. A. Teixeira. A singular approach to discontinuous vector fields on the plane. *J. Diff. Equations*, 231:633–655, 2006.
- [3] C. A. Buzzi, P. R. da Silva, and M. A. Teixeira. Slow-fast systems on algebraic varieties bordering piecewise-smooth dynamical systems. *Bulletin des Sciences Mathématiques*, 136(4):444–462, JUN 2012.
- [4] V. Carmona, F. Fernández-Sánchez, and A. E. Teruel. Existence of a reversible T-point heteroclinic cycle in a piecewise linear version of the Michelson system. *SIAM Journal on Applied Dynamical Systems*, 7:1032–1048, 2008.
- [5] J. Carr. *Applications of centre manifold theory*, volume 35. New York: Springer-Verlag, 1981.
- [6] T. de Carvalho and D. J. Tonon. Generic bifurcations of planar Filippov systems via geometric singular perturbations. *Bulletin of the Belgian Mathematical Society-Simon Stevin*, 18(5, S):861–881, 2011.
- [7] T. de Carvalho and D. J. Tonon. Normal forms for codimension one planar piecewise smooth vector fields. *Int. J. Bif. Chaos*, 24(7):1450090, 2014.

- [8] M. di Bernardo, C. J. Budd, A. R. Champneys, and P. Kowalczyk. *Piecewise-smooth Dynamical Systems: Theory and Applications*. Springer Verlag, 2008.
- [9] F. Dumortier. Local study of planar vector fields: Singularities and their unfoldings. In H. W. Broer et al, editor, *Structures in Dynamics, Finite Dimensional Deterministic Studies*, volume 2, pages 161–241. Springer Netherlands, 1991.
- [10] F. Dumortier. Techniques in the theory of local bifurcations: Blow-up, normal forms, nilpotent bifurcations, singular perturbations. In Dana Schlomiuk, editor, *Bifurcations and Periodic Orbits of Vector Fields*, volume 408 of *NATO ASI Series*, pages 19–73. Springer Netherlands, 1993.
- [11] F. Dumortier and R. Roussarie. Canard cycles and center manifolds. *Mem. Amer. Math. Soc.*, 121:1–96, 1996.
- [12] N. Fenichel. Persistence and smoothness of invariant manifolds for flows. *Indiana University Mathematics Journal*, 21:193–226, 1971.
- [13] N. Fenichel. Asymptotic stability with rate conditions. *Indiana University Mathematics Journal*, 23:1109–1137, 1974.
- [14] N. Fenichel. Geometric singular perturbation theory for ordinary differential equations. *J. Diff. Eq.*, 31:53–98, 1979.
- [15] A.F. Filippov. *Differential Equations with Discontinuous Righthand Sides*. Mathematics and its Applications. Kluwer Academic Publishers, 1988.
- [16] J. Guckenheimer and P. Holmes. *Nonlinear Oscillations, Dynamical Systems and Bifurcations of Vector Fields*. Springer Verlag, 5th edition, 1997.
- [17] C.K.R.T. Jones. *Geometric Singular Perturbation Theory, Lecture Notes in Mathematics, Dynamical Systems (Montecatini Terme)*. Springer, Berlin, 1995.
- [18] K. Uldall Kristiansen and S. J. Hogan. On the use of blowup to study regularizations of singularities of piecewise smooth dynamical systems in \mathbb{R}^3 . *SIAM Journal on Applied Dynamical Systems*, 14:382–422, 2015.
- [19] M. Krupa and P. Szmolyan. Extending geometric singular perturbation theory to nonhyperbolic points - fold and canard points in two dimensions. *SIAM Journal on Mathematical Analysis*, 33(2):286–314, 2001.
- [20] M. Krupa and P. Szmolyan. Extending slow manifolds near transcritical and pitchfork singularities. *Nonlinearity*, 14(6):1473, 2001.
- [21] M. Krupa and P. Szmolyan. Relaxation oscillation and canard explosion. *Journal of Differential Equations*, 174(2):312–368, 2001.
- [22] Yu. A. Kuznetsov, S. Rinaldi, and A. Gragnani. One parameter bifurcations in planar Filippov systems. *Int. J. Bif. Chaos*, 13:2157–2188, 2003.
- [23] J. Llibre, P. R. da Silva, and M. A. Teixeira. Regularization of discontinuous vector fields on \mathbb{R}^3 via singular perturbation. *J. Dyn. Diff. Eq.*, 19:309–331, 1997.
- [24] J. Llibre, P. R. da Silva, and M. A. Teixeira. Sliding vector fields via slow-fast systems. *Bulletin of the Belgian Mathematical Society-Simon Stevin*, 15(5):851–869, 2008.
- [25] J. Llibre, P. R. da Silva, and M. A. Teixeira. Study of singularities in nonsmooth dynamical systems via singular perturbation. *SIAM Journal on Applied Dynamical Systems*, 8(1):508–526, 2009.
- [26] J. Llibre and M. A. Teixeira. Regularization of discontinuous vector fields in dimension three. *Discr. Cont. Dyn. Sys.*, 3:235–241, 1997.
- [27] O. Makarenkov and J. S. W. Lamb. Dynamics and bifurcation of nonsmooth systems: A survey. *Physica D*, 241:1826–1844, 2012.
- [28] D. Michelson. Steady solutions of the Kuramoto-Sivashinsky equation. *Physica D*, 19:89–111, 1986.
- [29] C. B. Reves and T. M. Seara. Regularization of sliding global bifurcations derived from the local fold singularity of Filippov systems. *arXiv preprint arXiv:1402.5237*, 2014.
- [30] J. Sotomayor and M. A. Teixeira. Regularization of discontinuous vector fields. In *Proceedings of the International Conference on Differential Equations, Lisboa*, pages 207–223, 1996.
- [31] P. Szmolyan and M. Wechselberger. Canards in \mathbb{R}^3 . *J. Diff. Eq.*, 177(2):419–453, December 2001.
- [32] V. I. Utkin. Variable structure systems with sliding modes. *IEEE Trans. Automatic Control*, 22:212–222, 1977.